THE GEOLOGY OF THE UNKI PLATINUM-BASE METAL DEPOSIT, SELUKWE SUBCHAMBER, GREAT DYKE, ZIMBABWE.

By

CHARLEY ZVINAIYE MURAHWI

A Thesis submitted in partial fulfilment of the requirements for the degree of Master of Science in Economic Geology

Geology Department
Faculty of Science
Rhodes University
1995

FRONTISPIECE (Scale 1:244 000)

Landsat image of the Selukwe Sub-chamber of the Great Dyke. Features to note are as follow:

1. The impingement of the Shurugwi Greenstone Belt on the western flank.
2. The enhanced green and dark purplish areas of the Dyke representing norite and serpentinite, respectively.

ABSTRACT

This thesis focuses on platinum group element (PGE) mineralization in the Unki Section of the Selukwe Subchamber of the Great Dyke (Zimbabwe), and is based on drill hole intersections and underground and surface exposures of the Main Sulphide Zone (MSZ) which hosts significant concentrations of PGE. The petrological and geochemical data presented are part of a broader study currently underway and the present are restricted to the 2m section of the PGE-rich MSZ encountered in drill hole MR126.

The PGE-rich MSZ at Unki is unique in having a shear, locally referred to as the Footwall Shear, developed at or close to its base. It is however, similar to the other PGE occurrences on the Great Dyke (MSZ) in having its hanging-wall restricted to within 1m of the websterite/bronzitite contact. Slight axial tilting to the west is indicated by steeper dips on the eastern flank. The sulphide concentration within the MSZ can be used as a rough guide to the PGE-rich zone, but is not sufficiently precise to be used in stope control. The visual identification of the potentially mineable zone remains a problem that is unlikely to be solved.

Based on petrological evidence, the bulk of the sulphides with which the PGE are associated, are cumulus in status. This provides unequivocal evidence for an orthomagmatic origin of the MSZ. The dominant platinum group mineral (PGM) phase is the Arsenide/Sperrylite group which is most commonly found at the contact zones between base metal sulphides (BMS) and gangue. The PGM range up to 90 μm in length.

Geochemical evidence from the analyses of cumulate orthopyroxenes through the 2m PGE-rich MSZ interval at Unki reveals a trend of marked Fe enrichment upwards which corresponds to an enrichment in sulphide. This indicates that precipitation of sulphide was caused by fractionation with lowering of temperature in the magma. The Fe enrichment is followed by a reversal in Mg# of orthopyroxene which corresponds to the decrease in sulphide content, suggesting that

the termination of the PGE-rich MSZ was due to an increase in temperature associated with an influx of new magma. Coupled with these magmatic events are a complex interplay of chemical and physical processes occurring at a critical stage in the overall fractionation of the Great Dyke magma chamber.

The overall persistence and continuity of the PGE zone as observed in the Unki area is consistent with the inferred orthomagmatic origin of the mineralization.

The Dedication

To:

Anglo American Corporation Zimbabwe,

Prospecting Ventures Limited, (in particular JJ & MC)

The Pioneers of Great Dyke geology,

Those who blazed the trail in other layered intrusions world-wide,

and

Those who will follow the trail.

All that is long is not necessarily a banana
All that wriggles is not obviously a snake
But all that is long, wriggles and has a snake head,
is naturally the Great Dyke.

Chikuni, M. (1995)

That which proves too much proves nothing.
Were it not for that perhaps you could have made
this thesis more wriggling.

Jongwe, J. (1995)

Rome was not built in a day
And so will be my story on the Great Dyke

Murahwi, C. Z. (1995)

ACKNOWLEDGEMENTS

I am greatly indebted to:

1. Anglo American Corporation Zimbabwe for financing my studies at Rhodes and for granting me permission to use the Unki geological data in this thesis.

2. Dr H Gewald for supporting my application for financial assistance.

3. Professor A.H. Wilson for (a) the provision of XRF and microprobe analyses, (b) permission to use the Library facilities at the University of Natal Geology Department (Pietermaritzburg), and (c) for his attentiveness, advice and constructive comments, always willingly given.

4. Professor J. Moore for (a) reading the original drafts and offering constructive criticism and advice, (b) for many hours of discussion, and (c) his close interest and encouragement.

5. Dr M.D. Prendergast for useful general discussions on layered intrusions, in particular, the Great Dyke.

6. Dr C. Feather for providing useful general reading materials on electron microbeam techniques.

It is a pleasure to acknowledge the contributions of
Mrs Jane Jongwe and Ms Margaret Chikuni for doing all the typing and cartography drawing, respectively. A real 'big thank you' to you ladies. Messrs W. Mataranyika and C. Musa are thanked for helping in the graphics design.

Last but not least, a ' big thank you' to my wife Erica for giving me hope and inspiration, and for taking care of the kids during my long absence away from home at Rhodes.

CONTENTS

Page

Page

Page

LIST OF TABLES

LIST OF FIGURES

Page

Page

LIST OF APPENDICES

Chapter 1

INTRODUCTION

1.1 **Platinum Group Elements** (PGE)

1.1.1 *Brief History*

Platinum is unique in that it is a metal which has great applications as well as being precious. In the latter sense, it has been known to Man for centuries.

Platinum has been found in some artifacts from ancient Egypt, one example being the casket of precious metals given to the Egyptian princess Schipenweget in about 800 B.C. (Collender, 1987). The metal is likely to have come from the platinum bearing gravels of the White Nile in Ethiopia. Elsewhere in the Middle and Far East, inclusions of platinum have been discovered in occasional gold treasures. The use of platinum for ornamental purposes appears to have been confined to Colombia and Ecuador where bangles and ear and nose rings have been discovered in ancient burial grounds. It is unlikely that platinum group elements were recognized as separate metals by these early civilizations. The earliest known reference to the metal group was made in 1557 by an Italian scholar, Julius Scaliger, in a context where he criticized the earlier definition by Hieronimo Cardan of a metal as a substance that could be melted. Many years later, this metal which Scaliger had referred to as "a substance which it has not hitherto been possible to melt by fire or by any of the Spanish arts" became referred to variously as *papas de plata*, *smiris Hispanica* or *platina*m, meaning nuggets of platinum and silver (Spanish), respectively.

1.1.2 *The Elements*

The PGE comprise a family of six chemically similar siderophilic elements which together with gold and silver, constitute the precious or noble metals. They may be divided according to their relative densities into the heavy triad, consisting of platinum (Pt), iridium (Ir) and osmium (Os), and the lighter triad

comprising palladium (Pd), rhodium (Rh) and ruthenium (Ru). The PGE belong to the Group VIII transition metals, together with iron, nickel and cobalt. Their excellent catalytic qualities, resistance to corrosion, chemical inertness over a wide range of temperatures, and high melting points (in the range 1549 to 3050 degrees centigrade), render them indispensable for certain specialised applications. Their properties are further enhanced due to the fact that one element of the group may often be replaced by another when they are alloyed, but substitution by other metals is very difficult.

1.1.3 *Properties*

The heavy triad comprising Pt, Ir and Os have densities of 21,45 g/cm^3, 22,65 g/cm^3 and 22,58 g/cm^3, respectively. Iridium (Ir) is the densest terrestrial substance known, and along with platinum (Pt) and osmium (Os), is the least chemically active of all metals. The lighter triad of Ru, Rh and Pd have approximately the same densities in the region of 12 g/cm^3 to 12,45 g/cm^3. Excluding the densities, the rest of the other major physical properties of PGE permit their grouping into pairs as follows:

(i) the relatively soft and malleable elements: Pd and Pt with fairly low melting points of 1555°C and 1768°C, respectively;

(ii) elements with comparatively medium melting points and limited ductility: Rh - 1967°C, and Ir - 2454°C ; and

(iii) high melting point elements: Ru - 2334°C and Os - 3050°C. This pair forms the hardest and the most brittle of the PGE with the highest level of resistance to abrasion.

1.1.4 *Uses*

The current two main outlets of PGE are in the automobile emission control equipment (autocatalysts) and in the jewellery industry. In the automobile emission control equipment, PGE are used as catalytic convertors in the form of alloys Pt-Rh or Pt-Rh-Pd. These convertors reduce pollution from automobile exhausts by facilitating the reduction of nitrous oxide in hot exhaust gases to N and O, and by oxidizing hydrocarbons to CO_2 and H_2O (Buchanan, 1988). In the jewellery industry, platinum has gained market share at the expense of gold (Cowley, 1994). Another major use for PGE is the chemical industry where (i) platinum alloyed with 10% rhodium is used to oxidize ammonia in the production of nitrate fertilizers, and (ii) platinum catalysts are used to oxidize unpleasant pollutants in other industries, e.g. wire enamelling, in abattoirs, and in fish and meat processing.

Other uses of PGE are in laboratory equipment, catalysts for petroleum refining, thermocouples, electrical contacts, biomedical uses in anti-cancer drugs, dental alloys, fuel cells, and in high temperature vessels for the manufacture of glass. In addition, platinum is also used for investment purposes as bullion coins and in investment bars. The various uses of the major PGE for the Western world based on 1994 figures (Cowley, 1995) are summarized in Figure 1.1.

1.1.5 *Demand and Supply Factors*

The PGE are considered to be strategic minerals because of their extensive uses in the petroleum, chemical, and electronic industries and can thus be viewed as capital requirements for industry. The demand for these metals is therefore a sensitive barometer for the industrial climate. In periods of economic downturn, development of new industries and the expansion of existing ones are deferred and the demand falls rapidly; when the industrial climate becomes favourable, these are re-instated and the demand increases sharply.

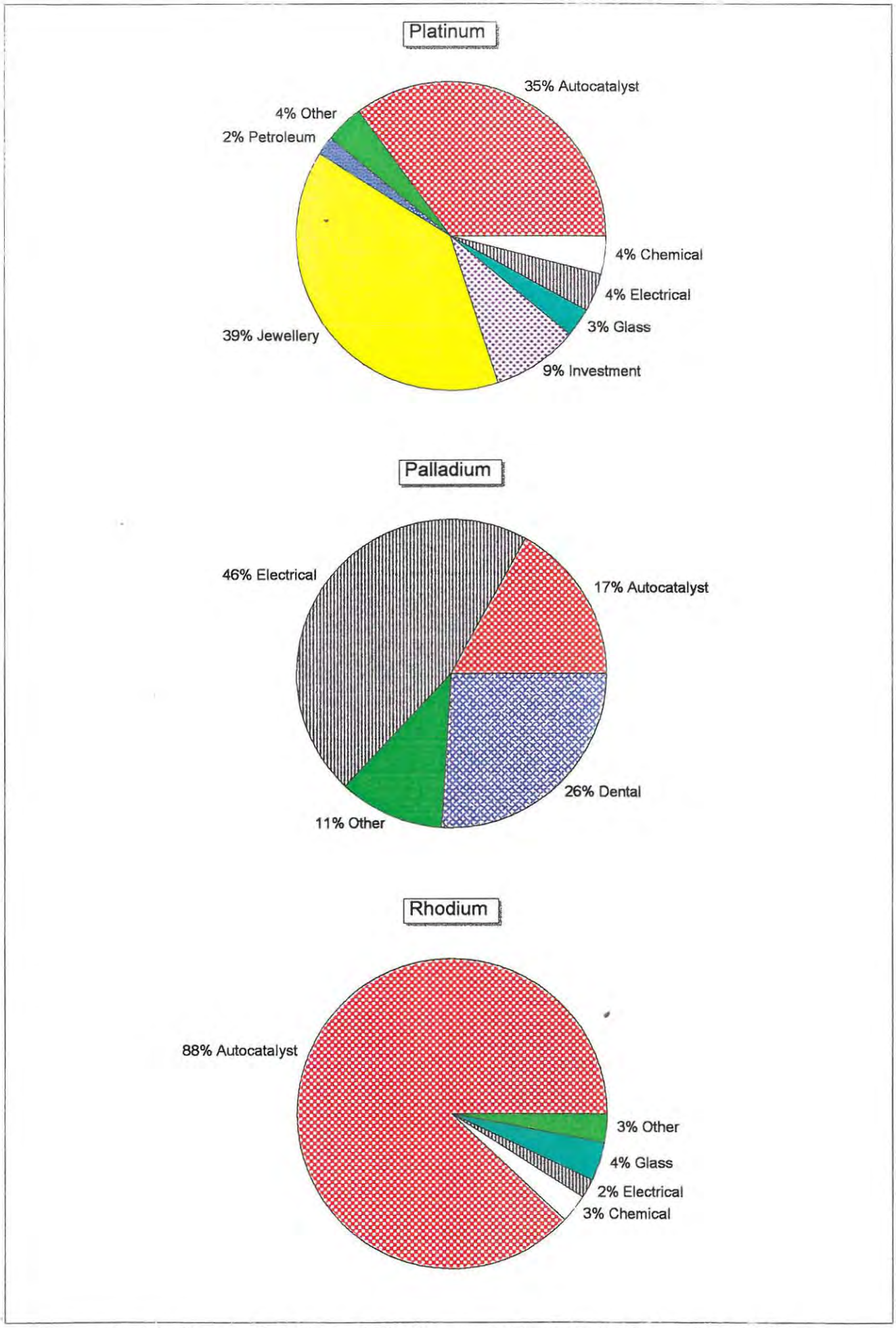

Fig 1.1 Platinum, Palladium and Rhodium demand by use in the Western World, 1994. (Source: Cowley, 1995)

1.2 PGE Deposits

1.2.1 *General*

The chemical similarity between PGE and iron, nickel and cobalt accounts for the fact that they tend to be naturally concentrated together. In the crust and upper mantle of the earth, PGE tend to be chalcophile in behaviour and this is related to S contents and oxygen fugacity. In the absence of chalcogens and other metalloids, their behaviour is siderophilic, i.e. they tend to alloy with metallic iron. In the early history of the earth, the siderophilic nature of these metals resulted in their partitioning into the molten iron which formed the core of the earth. The study of the occurrence of PGE in meteorites clearly strengthens the idea that these metals are very scarce in the lithosphere because of their dominant siderophile affinities. Thus, the platinum metals, from the evidence of meteorites, would tend to accumulate in the earth's nickel-iron core rather than the silicate crust. Based on all these facts, PGE should occur in association with magmatic chrome-bearing and titaniferous iron-ores, ferromagnesian silicates and magmatic iron, nickel and copper sulphides.

The PGE and other Group VIII transition metals only form economic concentrations in the crust as a result of the constant interchange of matter between the mantle and the crust (Naldrett, 1981). The genetic classification of PGE deposits as suggested by Macdonald (1987) comprises three classes, viz: orthomagmatic, alluvial and hydrothermal deposits (Table 1.1). The most economically significant deposits are those in the orthomagmatic class, but it should be noted that prior to the twentieth century, platinum was only recovered from alluvial deposits (Collender, 1987).

1.2.2 *Orthomagmatic Deposits*

The orthomagmatic class embraces all deposits formed solely within the magmatic environment. Macdonald (1987) further subdivides these into deposits resulting from (a) magma mixing,

Table 1.1 **A classification of PGE Deposits (after Macdonald, 1987)**

Table 1 A classification of PGE Deposits

Deposit Class		Examples
1. ORTHOMAGMATIC		
	1a) Magma Mixing	UG2+, Merensky Reef*, BIC J-M Reef*, SIC Great Dyke*, Zimbabwe Lac des lles*, Canada
	1b) Magma Contamination	Noril'sk#, USSR Sudbury#, Canada Kambalda#, Australia Thompson#, Canada
	1c) Deuteric	Dunite Pipes*, BIC
2. ALLUVIAL		
	2a) Placer	Choco*, Colombia Urals*, USSR
	2b) Paleoplacer	Witwatersrand#, South Africa
3. HYDROTHERMAL		New Rambler#, USA Rathbun Lake#, Canada Allard Stock #, USA Kupferschiefer#, Poland Coronation Hill+, Australia

BIC - Bushveld Igneous Complex, South Africa
SIC - Stillwater Igneous Complex, USA
* - Primary Product
\+ - Co-product
\# - Bi-product

(b) magma contamination, and (c) deuteric processes (Table 1.1). However, these subdivisions need to be reviewed in view of the several competing hypotheses which have been advanced to explain the mineralisation mechanisms in many different layered intrusions (see section 1.5).

1.2.3 *Alluvial Deposits*

Two subclasses of alluvial deposits are recognised; placer and paleoplacer deposits. PGE placer deposits are spatially associated with mafic-ultramafic complexes, most commonly of the 'Alaskan' or 'Alpine' type of mafic-ultramafic intrusions. They are recovered from river gravels that drain these areas. On a global scale, the most significant concentrations are in stream gravels in the Urals Mountains, Russia. In Zimbabwe, placers of sub-economic quantities occur on the west side of the Selukwe Subchamber of the Great Dyke.

Palaeoplacers are rare. The only known economic concentrations of PGE palaeoplacers are in the Witwatersrand Conglomerates (South Africa) where they are recovered as by-products during the extraction of gold from crushed ore. Their origin is subject to much debate but they may have resulted from greenstone-belt erosion (Macdonald, 1987).

1.2.4 *Hydrothermal Deposits*

Three distinct categories of hydrothermal PGE deposits are currently recognized Macdonald (1987): (a) those associated with epigenetic fluid flow in mafic-ultramafic rocks, e.g. the Rathburn Lake PGE-bearing Cu-Ni sulphide deposit located within the Wanapitei gabbronorite intrusion in Central Ontario, Canada, (b) precious metal-enriched (PGE, Au, Ag), porphyry copper deposits of alkaline affinity, e.g. the Allard Stock in the Colorado, USA; and (c) late diagenetic/epithermal deposits, e.g. the Kupferschiefer stratabound Cu-Ag (Pb-Zn) deposit, Poland. Zimbabwean sources of hydrothermal PGE deposits include the hydrothermal Au-Cu ores at Muriel and Athens Mines (Prendergast,

1988). In South Africa, the PGE found in veins and fissures in the dolomites of the Transvaal System are also of this type.

1.3 **Platinum Group (PG) Mineralogy**

1.3.1 *PG-minerals and unidentified PG-phases*

The naturally-occurring PG compounds are separated into two groups, viz. PG mineral species which are approved by the International Mineralogical Association (I.M.A.), and the unidentified PG phases which lack detailed characterization and remain unnamed, but for which quantitative analyses and qualitative chemical data are presented in the literature. There are 92 approved PG mineral species and almost 500 unidentified PG phases (Daltry and Wilson, in prep). In addition, over 20 non-platinum group minerals contain varying concentrations of one or more of the six platinum group elements.

1.3.2 *General Characteristics*

All PG- minerals and phases are non-silicates and a large proportion are sulphides, arsenides and tellurides. The PG-minerals most commonly have cubic symmetry and density values within the range 5 - 22 g/cm^3. Palladium-dominant compounds are the most abundant of the PG minerals and phases, whereas the Os-dominant compounds are the least abundant. Platinum exhibits the most sympathetic tendencies towards the other PGE whereas Pd exhibits the most pronounced antipathy.

1.4 **Magmatic Deposits**

1.4.1 *General statement*

Magmatic sulphide deposits are generally Ni-Cu rich with PGE as by-products (e.g. Sudbury and Noril'sk) or PGE-rich with Ni-Cu as by-products (e.g. Bushveld Complex). They are associated with a wide variety of mafic and ultramafic bodies as shown in Table 1.2 (Naldrett, 1989). These magmatic sulphide ores originate from droplets of an immiscible sulphide-oxide liquid forming

Table 1.2 Mafic and ultramafic bodies and related sulphide ores (after Naldrett, 1989)

Petro-tectonic setting	Ni-Cu ores	PGE ores
I. SYNVOLCANIC (largely Archaean)		
Komatiites	E. Goldfields, Australia; Zimbabwe; Abitibi, Ontario	
Tholeiites		
Picritic	Pechenga, USSR	
Anorthositic	Montcalm, Ontario	
II. RIFTED PLATE MARGINS & OCEAN BASINS		
Associated with Continental Crust	**Circum-Ungava Belt** Thompson Ni Camp; Ungava Ni Ores	**Kemi-Koilismaa Belt** Penikat Intrusion
Ophiolites (No continental crust)		**Unst Ophiolite** Cliffs deposit
III. CRATONIC AREAS		
Flood Basalt-related	**Siberian Traps** Noril'sk-Talnakh **Karoo** Insizwa-Ingeli Intrusion **Keweenawan** Duluth Complex Crystal Lake Gabbro	
Large Stratiform Complexes	**Sheet-like** Sudbury	**Sheet-like** Bushveld: Merensky Reef, UG-2 Chromitite Stillwater J-M Reef **Dyke-like** Great Dyke: Main sulphide zone
IV. EMPLACED DURING OROGENESIS		
Synorogenic	**Appalachia** Moxie & Katahdin Intrusion, Maine	
Late Orogenic		**Alaskan Type** Tulameen Complex

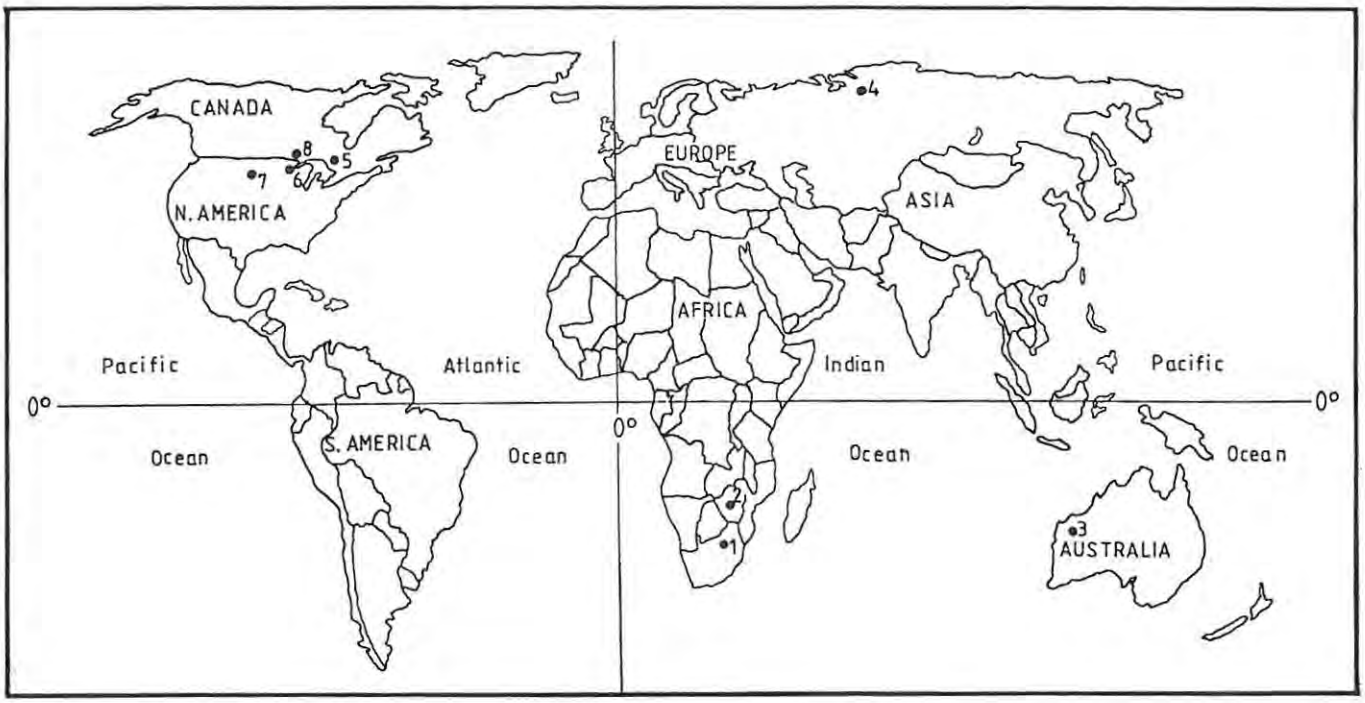

LEGEND

A. Magmatic S-rich PGE-Ni-Cu

1. Bushveld 2. Great Dyke 3. Munni Munni Prospect

B. Magmatic S-rich Ni-Cu-(PGE), Ni (PGE)

4. Norils'k 5. Sudbury 6. Duluth 7. Stillwater 8. Lacdes Iles

Fig.1.2 Distribution of major magmatic deposits around the world.

within silicate magma which then become concentrated in a specific location (Naldrett, 1989). The Group VIII transition metals, which include PGE, Fe, Co and Ni, partition strongly into the sulphide-oxide liquid, and become concentrated with it to form economically significant deposits. Thus sulphide precipitation is one of the most important phenomena in localizing and concentrating PGE and other related Ni-Cu deposits. The major known PGE deposits are associated with mafic-ultramafic layered complexes (Fig. 1.2). The layered complexes assume various geometrical forms ranging from dyke-like (Great Dyke, Zimbabwe), to funnel shaped (Kiglapait, Nain; and Skaergraard, Greenland), through to dipping sheet (Bushveld Complex, South Africa) and sill-like (Stillwater Complex, USA) models.

1.4.2 *Tectonic Setting*

Mafic and ultramafic bodies and their related sulphide ores occur in a variety of tectonic settings as depicted in Table 1.2 (Naldrett, 1989). Naldrett (1989) recognises four different tectonic settings as follows: Category I encompasses those mafic and ultramafic bodies of largely Archaean greenstone belts related to syn-volcanic activity. Category II groups together bodies associated with a rifted continental environment. Category III relates to bodies emplaced in a cratonic environment while Category IV has been created for bodies in an active orogenic belt. The third category, i.e. of intrusions in cratonic areas, comprises world class deposits of Ni-Cu-PGE (Noril'sk-Talnakh) and PGE dominant ores (Bushveld Complex and the Great Dyke).

1.4.3 *Classification of Magmatic PGE Deposits*

All the major known PGE deposits are associated with layered mafic-ultramafic intrusions. The PGE deposits associated with these intrusions can be classified into the stratabound and the non-stratabound groups (Naldrett, 1993). The stratabound group is further subdivided into those with a dominant association with sulphide and those with a dominant association with chromitite

Table 1.3 PGE Deposits in Layered Intrusions
(after Naldrett, pers. comm. 1993)

STRATABOUND

DOMINANT SULPHIDE ASSOCIATION

Associated with "Reef"

MR[1], J-M[2], AP-I[3], AP-II[3], SJs[3], PV[3]

Not associated with "Reef"

MSZ[4], LSZ[4]

DOMINANT CHROMITITE ASSOCIATION

UG-1[1], UG-2[1], SJc[3], A[2]

NON-STRATABOUND

Robie Zone[5], Platreef[1], Dunite Pipes.

Notes: 1 = Bushveld, 2 = Stillwater, 3 = Penikat,

4 = Great Dyke, 5 = Lac des Iles

MR = Merensky Reef, J-M = J-M reef,
AP-1 and AP-2 = Ala-Penikka, 1 & 2, Finland

SJs = Sompujararvi Sulphide Association, Finland

SJc = Sompujararvi Chromite Association, Finland

PR = Pasivaara, Finland

MSZ = Main Sulphide Zone (Great Dyke)
LSZ = Lower Sulphide Zone (Great Dyke)

A = A chromitite, Stillwater

(Table 1.3). Examples of the latter sub-group include the deposits of the Middle and Upper Group chromitites of the Bushveld Complex, in particular the UG-2 (von Gruenewaldt et al., 1986). In the sulphide related group, there are those occurrences which have a distinctive texture and/or mineralogy, e.g. the Merensky Reef (Vermaak, 1976), and those that show no such association, as represented by the Main and Lower Sulphide Zones of the Great Dyke which occur in uniform bronzitite that has no obvious characteristics other than sulphide distinguishing the mineralised zones (Prendergast, 1988a; Wilson and Tredoux, 1990).

The non-stratabound group is economically less significant than the stratabound group. The dunite pipes of the Bushveld Complex and the Robie Zone at Lac des Iles (Macdonald, 1988) in Ontario are examples of deposits that are not stratabound.

1.4.4 *Geological setting of PGE Deposits in Layered Intrusions*

The stratigraphic positions of PGE-enriched zones in layered intrusions mark the first significant appearance of sulphide development within these intrusions (Wilson and Tredoux, 1990). However, important differences with genetic implications exist with regard to the location of the PGE zones within the stratigraphic succession (Fig. 1.3). On this basis, the PGE-enriched zones in layered complexes are here informally categorised into two groups. The first group encompasses the J-M reef of the Stillwater Complex, and the Merensky and UG-2 reefs of the Bushveld Complex in which the PGE zones occur some 300 to 500m above the first significant appearance of cumulus plagioclase in the succession. The mineralised zone of the Penikat intrusion in Finland is underlain by up to 600m of plagioclase cumulates (Naldrett et al., 1987) and can also be included under this grouping. In the second group, the sulphide-hosted PGE zones are in pyroxenite, some distance below the first appearance cumulus plagioclase. Examples of this latter group include the Great Dyke (Fig. 1.3) and the Jimberlana intrusion (Keays and Campbell, 1981).

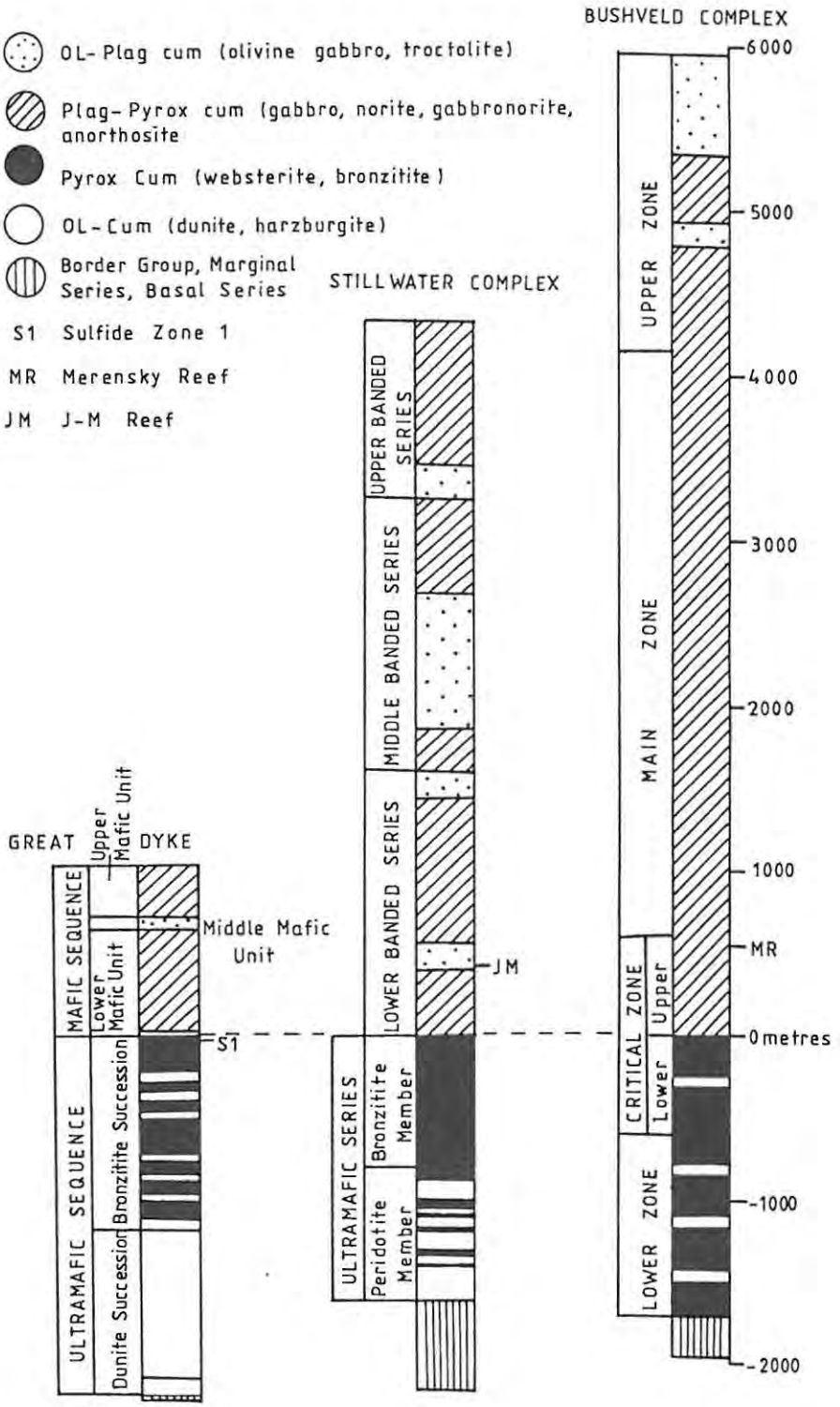

Fig .1.3 Stratigraphic sections of the Great Dyke (Darwendale Subchamber), Stillwater Complex and Bushveld Complex showing positions of Sulphide Zone S1, J-M Reef and Merensky Reef. All sections on the same vertical scale with the horizontal reference line drawn at the first appearance of plagioclase cumulates. Note the relatively small thickness of the Mafic Sequence in the Great Dyke.
[After Naldrett and Wilson, 1990]

1.5 Petrogenetic Models of Magmatic Sulphide Deposits

1.5.1 *Basic Concepts*

Current models on the origin of magmatic sulphide ores are viewed in terms of the magma replenishment history and the evolution of the magma body. Naldrett (1989) has shown that these deposit types are characterized by sulphides with unusually high PGE tenor, but with normal tenors of Ni, Cu and Co. This finding is based on the ranges of chondrite-normalized average PGE concentrations in 100% sulphides of a number of important types of magmatic ores.

Campbell and Naldrett (1979) have shown that, in the case of magmatic sulphide deposits, the tenor of a low abundance trace element such as a PGE in sulphide (Y) is dependent on: (a) its original concentration in the host magma (X); (b) the partition coefficient (D) and (c) the ratio of the mass of silicate magma to sulphide involved in the equilibration (R). The function R is governed by the equation $Y = \frac{X.D\ (R + 1)}{(R + D)}$

Based on the variable R, the same initial magma composition can account for "normal" Ni-Cu sulphide and PGE-enriched Merensky-type sulphide compositions. The difference in behaviour between the PGE on the one hand, and Ni, Cu and Co on the other between the two deposit types, is due to a difference in their partition coefficients. What is required without the need to call on different magmas is to explain how different R values have developed in different geologic situations.

1.5.2 *Existing Models*

The geological processes necessary for the formation of an economic magmatic sulphide deposit involve enrichment factors in the order of about one thousand (Macdonald, 1987). As mentioned earlier (section 1.4), sulphide liquation is among the most important factors in localizing and concentrating PGE and other related Ni-Cu deposits. For this sulphide precipitation to

occur, the silicate liquid must become sulphide-saturated and this is dependent upon the following factors:

(a) temperature
(b) oxygen fugacity
(c) magma composition - FeO, SiO_2 and S content
(d) magma mixing as a result of repetitive inputs of magma.

Under point (d) above, it is generally accepted (Campbell and Turner, 1986) that layered intrusions have formed through repetitive inputs of magma. These inputs are likely to have been turbulent and thus to have involved significant entrainment and mixing of resident magma within the input. The resulting hybrid would also spread out at the appropriate density level to give rise to turbulently convecting layers. If sulphides formed in the hybrid at this stage, the turbulent mixing and convection would have provided the ideal environment in which they could have developed a high R-factor, and thus have become enriched in PGE.

Sulphide saturation may be achieved in one of three ways as proposed by Naldrett et al. (1990):

(i) **Fractional segregation** where sulphide saturation is attained through fractionation;
(ii) **Batch segregation** where batch segregation of sulphide is achieved through mixing of a primitive magma with an evolved resident magma that is close to crystallizing plagioclase.
(iii) **Constitutional zone refining** where sulphide saturation is preceded by volatile-induced partial melting and remobilization of cumulates and sulphides.

The above three processes lead to the formation of different types of deposits as illustrated in Figure 1.4. Subsolidus and deuteric processes are responsible for the modification of the original primary textures in these deposits.

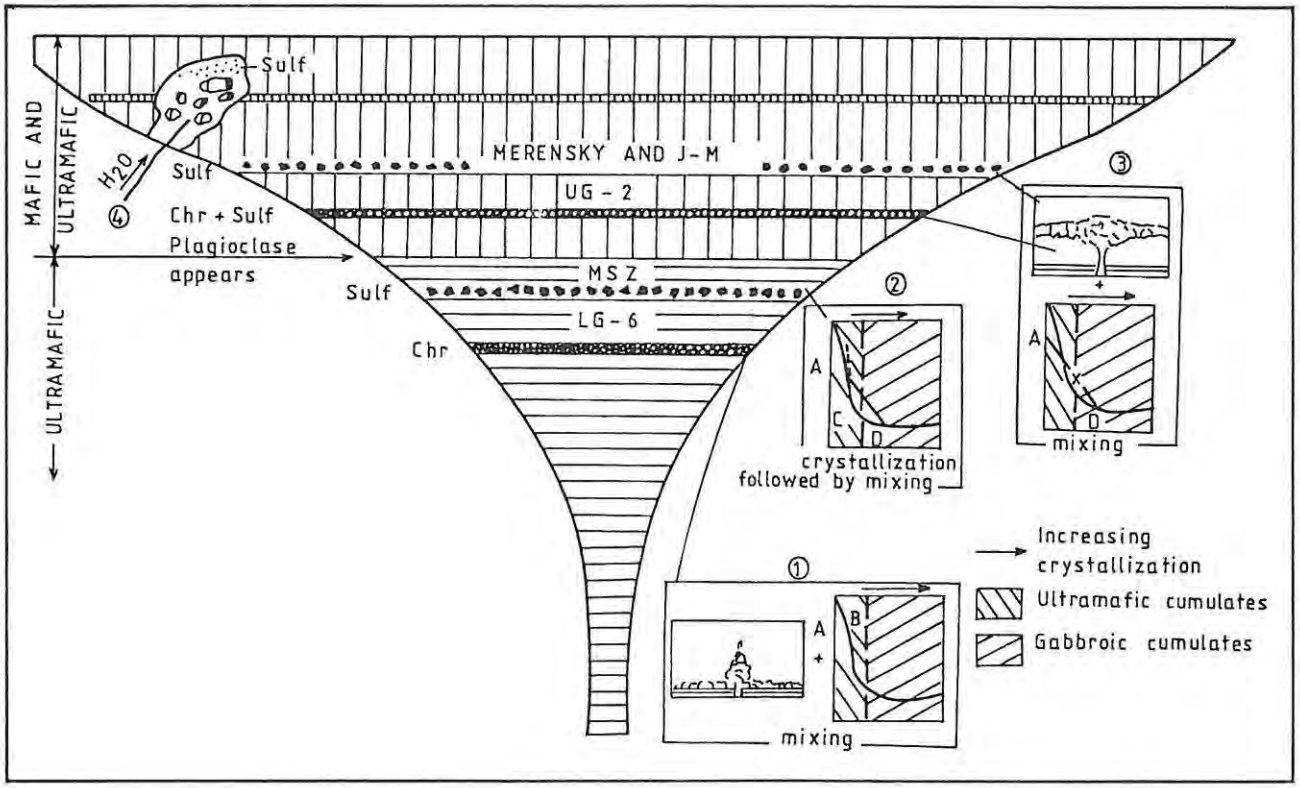

Fig .1.4 Cross-section through a hypothetical layered intrusion, showing the types of chromitite and PGE-enriched sulphide deposits that can result from fractional crystallization, magma mixing and constitutional zone refining. Mixing of resident with primitive magma before plagioclase has appeared on the liquidus of the former is likely to produce sulphide- and, therefore, PGE- poor chromitite (Example 1); fractional crystallization may give rise to a PGE-rich sulphide layer not associated with the base of a cyclic unit (Example 2); mixing of resident with more primitive magma after plagioclase is crystallizing from the former may give rise to sulphide- and, therefore, PGE- enriched chromitites or PGE-rich sulphide layers (Example 3). Volatile-induced partial melting of cumulates can give rise to constitutional zone refining and the concentration of PGE at the point at which the partial melt becomes saturated in sulphide (Example 4). [After Naldrett, Brugmann and Wilson, 1990]

Example 1: Applicable to BIC chromitites and most of Stillwater.
Example 2: Applicable to Zones 2 and 3 Great Dyke (Unki).
Example 3: Applicable to Merensky Reef.

1.6. PGE Resource Development on the Great Dyke.

The Main Sulphide Zone (MSZ) of the Great Dyke contains the world's second largest PGE resource after the Bushveld Complex. The first recognition of PGE within the MSZ was in 1925 in the Makwiro area near Selous (Lightfoot, 1926, 1927). Following this discovery, the MSZ was soon traced throughout most areas of the Great Dyke in the Darwendale, Sebakwe, Selukwe and Wedza Subchambers (Fig.2.1). Initial interest focused on the near surface, oxidised zone but later shifted to the deeper sulphide ore. However, since its discovery in 1925 to date, no viable platinum mine has ever been established due to a variety of reasons.

The first major attempt at producing platinum from the MSZ was by the Grainger brothers at Wedza Mine near Mimosa (Fig. 2.1) during the period early 1926 to late 1928. A relatively sophisticated reduction plant with 600 ton per month capacity was erected. PGE grades were estimated at 4,5 g/t over 1m. The concentrates produced from the plant were sent to the United Kingdom for refining. The eventual failure of this operation was largely due to low plant recoveries at less than 50% of head grade and a fall in platinum price, i.e. £7 per ounce in 1928 (Bowen, 1994). It became apparent that the fine-grained platinum minerals could not be economically recovered from the oxidised ore with the existing wet gravity or froth flotation methods (Wagner, 1929).

The next major phase of activity was in the 1950s. Between 1951 and 1953, the Great Dyke Wedza Syndicate investigated the oxidised ore in the Wedza area (Morrison, 1974) and established that the PGE could be economically recovered in ferronickel by smelting the ore in an electric arc furnace.

Despite this metallurgical success, nothing came out of this project. It was, however, realised that the high cost of electric smelting could partly be offset by cheap surface mining and by savings in crushing the relatively soft friable ore without the need for subsequent grinding (Prendergast, 1988a).

Table 1.4 Global resource estimates for the MSZ.

Subchamber	Resource ($x10^6$)		Total
	Sulphides	Oxides	
Musengezi	166	24	190
Darwendale/Sebakwe	3 288	186	3 475
Selukwe	389	122	511
Wedza	170	56	226
Total	4 012	389	4 401

Notes: 1. Assuming an economic stoping width of 180cm

2. Oxide resource within ~ 250m of outcrop. (After Prendergast, 1988).

Seven years later in 1960, Ben G. Worst compiled Geological Survey Bulletin No. 47 - "The Great Dyke of Southern Rhodesia" which had tremendous impact in reviving interest on the MSZ. Several mining companies, notably Anglo American Corporation, Union Carbide and Rio Tinto began serious exploration on the Great Dyke. Although the initial interest was on chrome it soon changed to focus on the MSZ. Between 1960 and 1983, these three companies independently conducted deep diamond drilling which proved a huge tonnage of potential ore (Table 1.4) in a widely persistent MSZ up to 1,8m thick beneath the remnants of the upper mafic sequence of the Great Dyke. The main target areas established were Wedza - Mimosa in the Wedza Subchamber (Union Carbide), Middleridge in the Selukwe Subchamber (Anglo American), Zinca in the Sebakwe Subchamber (Rio Tinto), and Selous in the Darwendale Subchamber (Union Carbide) (Fig.2.1). Union Carbide and Rio Tinto set up trial mining and plant-scale metallurgical extraction projects at their respective targets while Anglo American sunk an exploration shaft at Unki in the Middleridge area. All these pilot projects investigated and proved the technical feasibility of appropriate mining schemes and extraction processes. Despite these successes in exploration and evaluation efforts, a producing mine could not be developed, and by 1984, all the Great Dyke platinum projects had become dormant.

The main reasons for this disappointing result have been listed by Prendergast (1988b) as follows:

1. the relatively marginal grade which could only be offset by cost-efficient mining and extraction, and by higher metal prices than prevailed at the time;

2. the high capital investment required to develop a mine of the optimum economic size, and

3. the poor market perception of the local investment climate.

Other contributory technical problems are the poor ground conditions encountered at Selous and Zinca, and the lack of distinct petrographic markers for miners to follow. Dilution

was, and remains, the critical problem to successful mining (Prendergast, 1988b).

The fourth and current phase on the Great Dyke PGE projects was initiated in 1987 when Delta Gold NL obtained an exploration lease over the Selous ground which had been abandoned by Union Carbide in the early 1980s. A significant capital injection as a result of the joint-venture partnership with Broken Hill Proprietary (BHP) in 1990 resulted in Delta becoming the leader in a new exploration thrust. The joint venture partners, now known as Hartley Platinum, have completed a detailed feasibility study at Selous and are set to establish the first platinum mine in Zimbabwe by mid 1996. Delta's recent acquisition of mining rights over the ground previously owned by Rio Tinto and Anglo American in the Sebakwe Subchamber in 1994 has enhanced its position in terms of output potential. Meanwhile Union Carbide (now Zimbabwe Mining and Smelting Company) and Anglo American have re-appraised their properties at Wedza-Mimosa and Unki, respectively. In July 1993 Union Carbide announced that after an expenditure of Z$85 million since 1975, they intend to open a US$400 million mine at Mimosa. Since 1993, Anglo American Corporation have been busy with trial mining and associated testwork at Unki. Cluff Mineral Resources (Zimbabwe) Limited have also recently entered the platinum field and have begun an intensive evaluation of the Snakes Head area in the Musengezi Subchamber (Fig. 2.1).

Factors in favour of the MSZ as a potential future world source of PGE as first noted by Prendergast (1988b) are; (i) the large proven resources of potential ore in an essentially continuous mineralised zone, with relatively uniform grades over wide areas, (ii) the absence of major technical obstacles, (iii) the continuing rise in demand for, and the strategic status of PGE for industrial use, and (iv) special unprecedented problems which may affect future supplies from each of the current major producers (Buchanan, 1979) for example, Canada, although a current major world producer of PGE, has its production closely-linked to the nickel market that cannot be increased for its own sake; the same applies to the Russian supply.

1.7 Objectives of this investigation

The present study focuses on the Unki Section of the Selukwe Subchamber and is based on drill hole intersections, and underground and surface exposures of the MSZ. The purpose of the study is threefold:

1. To present a comprehensive account of the main geological characteristics of the Unki PGE deposit, which, it is hoped, will provide a sound geological background to any future mining venture at Unki and its environs. Of particular interest is the visual identification of the PGE-rich zone and the distribution patterns of the metals.
2. To augment the data base on the Selukwe Subchamber.
3. To develop a scenario for the magmatic events that led to the formation of the PGE deposits at Unki and to relate the applicability of this model to the Great Dyke as a whole.

To achieve these objectives, an overview of the current ideas and knowledge on the Great Dyke is first presented. This is followed by a chapter on the Selukwe Subchamber geology, with emphasis on the Unki area. The ore deposit model is discussed in Chapter 7 and is based mainly on petrological and geochemical evidence presented in Chapters 5 and 6, respectively.

Chapter 2

GENERAL GEOLOGY OF THE GREAT DYKE

2.1 General/Background information

The Unki platinum-base metal prospect is one of three major recent mining projects located on the Great Dyke, Zimbabwe. The other two are the Hartley and the Mimosa prospects (Fig. 2.1).

The Great Dyke is a unique early Proterozoic (2,47 GA; Hamilton, 1977) layered mafic-ultramafic intrusion which dominates the geological map of Zimbabwe. It occurs as a linear feature averaging 8 km in width and cuts Archaean granitoids and greenstone belts of the Zimbabwe craton for 550km in a NNE direction. Its lower ultramafic sequence is renowned world-wide for high grade metallurgical chromite seams which have been actively mined for over 80 years. The uppermost pyroxenite layer contains a major resource of platinum group elements (PGE), Au and base metals. The PGE resource of the Great Dyke represents the world's second largest known deposit after the Bushveld Complex.

A number of satellite dykes are genetically related to the Great Dyke based on palaeomagnetic evidence. These are the Umvimeela and East Dykes parallel to the Great Dyke to the west and east, respectively, and the Main Swarm satellite dykes to the south.

Although the Great Dyke was first recognised as a geological entity by the explorer Carl Mauch as early as 1872, the first comprehensive account on its geology, structure and mode emplacement is that published by B.G. Worst in 1960. Worst (1960) recognised that the Dyke is not a true dyke but is an assemblage of four contiguous lopolithic layered complexes which differ in the number of layers and thickness. He termed the four complexes, from north to south, the Musengezi (43 km long), Hartley (321 km) Selukwe (96km) and Wedza (80 km) complexes

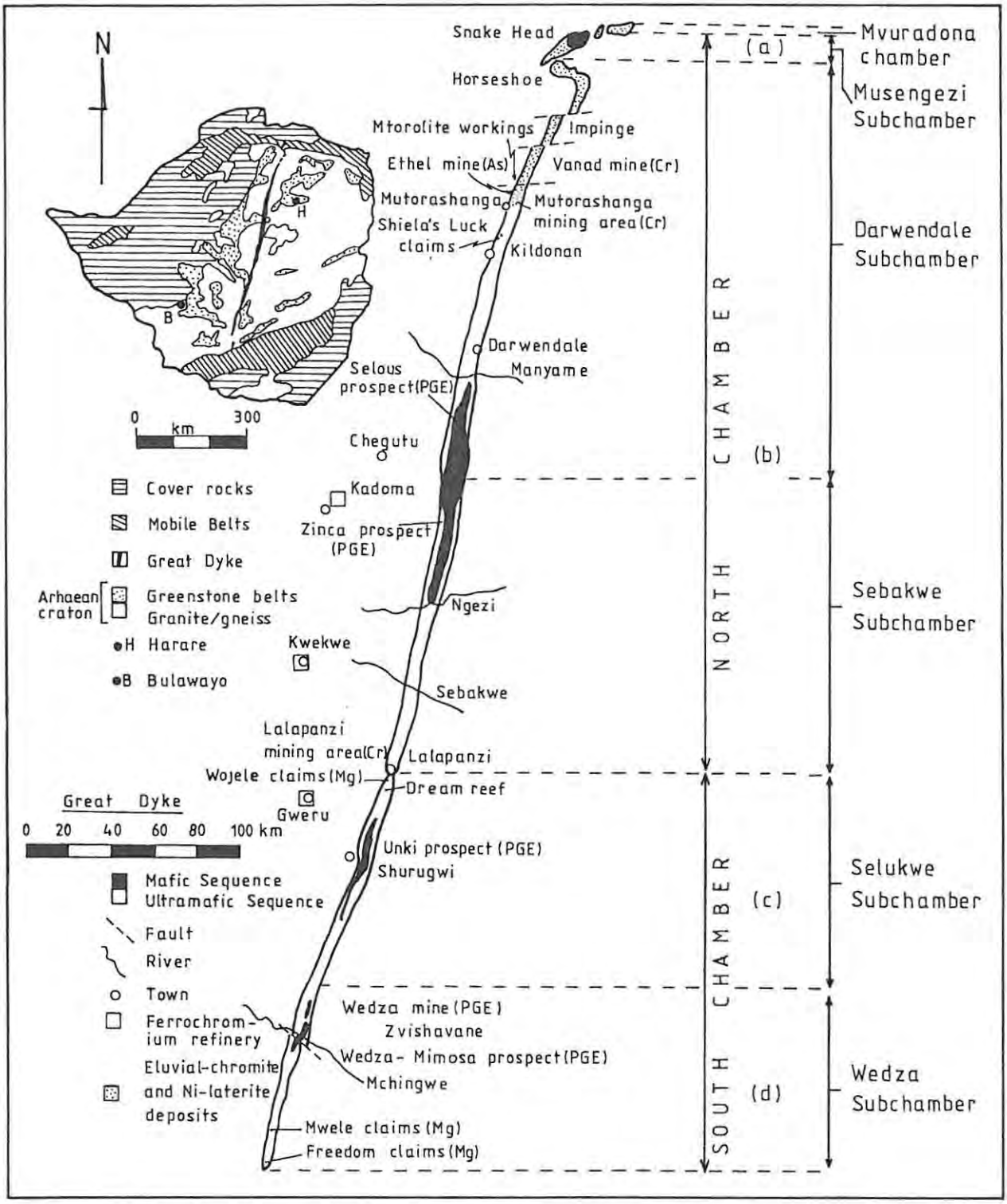

Worst's (1960) subdivisions of the Magma Chambers are shown as follows:
(a) Musengezi Complex (b) Hartley Complex (c) Selukwe Complex
(d) Wedza Complex

Fig. 2.1 Simplified geological map of Great Dyke showing major stratigraphic divisions. Also shown are locations of principal mineral deposits, mines and prospects (As,asbestos; Cr,chromite; Mg,magnesite; PGE, platinum-group elements) and ferrochromium refineries, as well as other localities referred to in text. Upper inset, tectonic setting of Great Dyke.
[Modified after Prendergast and Wilson, 1989]

(Fig. 2.1). These lopoliths are preserved in a graben fault structure trending NNE.

The geometry of each complex as described by Worst (1960) was essentially a shallow boat-like structure with the constituent rock layers forming a syncline in transverse section, and plunging gently towards the centre of each complex. The dip of the stratification varies between 10° and 45°. In general, the upper layers have shallower dips than the lower layers. Hess (1950) considered that magma intruded through a primary fissure in each complex giving rise to successive horizontal layers. Worst (1958, 1960) expanded on Hess's ideas. He envisaged magma to have intruded through fissures at the centres of the complexes as a series of pulses. Each pulse is thought to have crystallised but did not cool completely before the inflow of the next pulse, resulting in the sharp contacts between the layers. He further suggested that the magmas ranged from mafic to ultramafic as a consequence of a primary differentiation process at depth. Bichan (1969) advocated a similar mechanism and also recognised that not all pulses crystallised completely before further injection of magma took place. Worst (1960) considered the present synclinal attitude of the layering and the shallow plunge of the longitudinal axis towards the centre of each complex to be due to progressive overloading of the floor of the magma chambers, greatest near the feeder sites and augmented by graben subsidence and down faulting along the present inward-dipping margins of the Dyke. Consequently, the upper mafic units are only preserved near the centres of the complexes at the present erosion level.

Each complex of the Great Dyke consists of an upper mafic succession of gabbro and norite and a lower sequence of ultramafic rocks of pyroxenite, dunite and chromite as essentially mono-mineralic cumulates.

2.2 Recent developments on the knowledge of the Great Dyke

2.2.1 *General statement*

Since the 1970s, growing academic and industrial interest has culminated in a steady accumulation of structural, stratigraphic, petrological and geochemical data on the Great Dyke. Some of Worst's (1960) ideas about the structure of the Great Dyke and its mode of emplacement have subsequently been modified.

For about 90% of its length, the Great Dyke is flanked on its margins by granitic rocks. The remaining 10% is flanked by greenstone belts and it is in these areas that the PGE-rich pyroxenite layer has been preserved. This coincidence together with the tectonic control over and structural setting prior to the Great Dyke event, remain some of the most intriguing problems of Great Dyke geology.

2.2.2 *Tectonic setting*

The Zimbabwe craton is dominated by a suite of predominantly NNE-trending fractures one of which is occupied by the Great Dyke (Wilson et al., 1987). Examples of other representatives of this craton-wide suite include those occupied by the Umvimeela and East satellite dykes, and a number of sinistral wrench faults further to the east. The same fracture trend is noticeable in some of the major greenstone belts and older gneisses of the craton and is indicative of tectonically unstable conditions during the Archaean, i.e. prior to the Great Dyke emplacement event. By 2500 Ma, the Zimbabwe craton had finally stabilised with the emplacement of the late Archaean granites (i.e Chilimanzi granite suite) and had become sufficiently brittle to produce major fractures to develop what were exploited by the Great Dyke magmatic event.

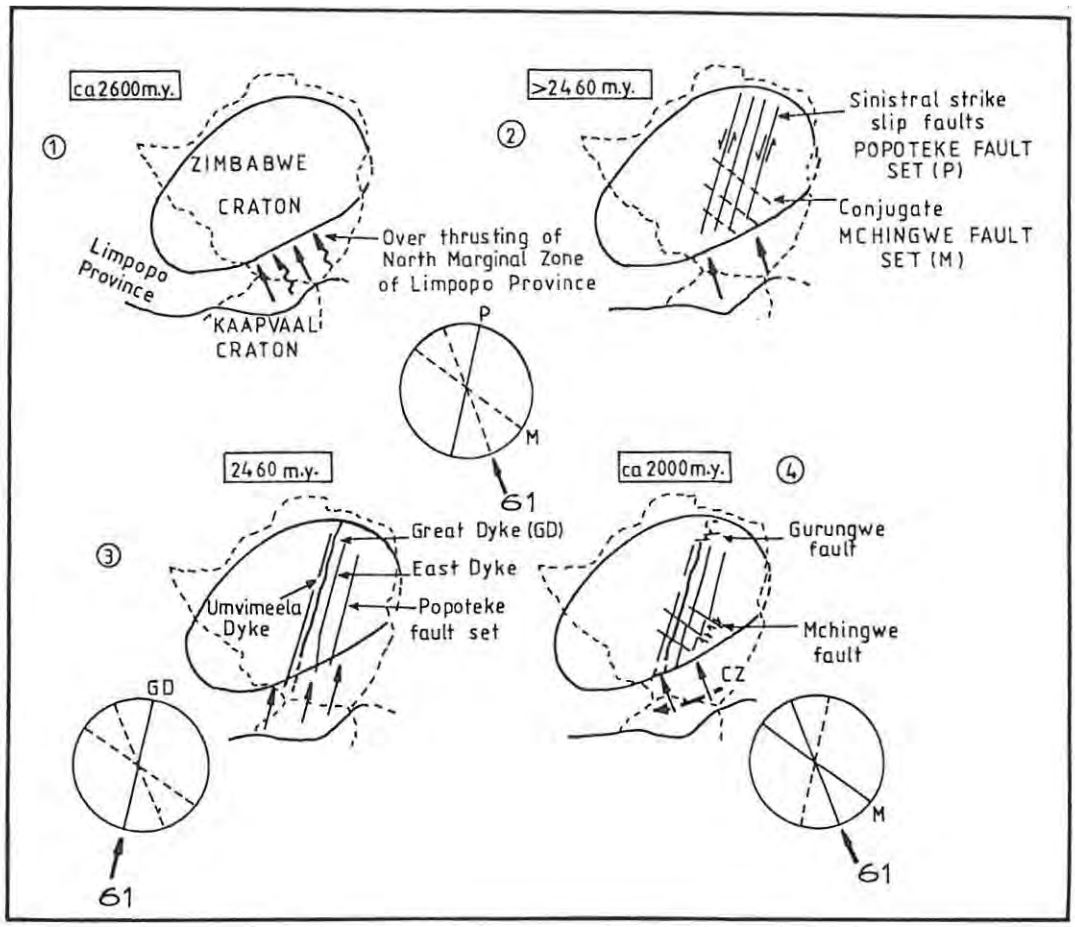

Fig.2.2 Schematic interpretation of events leading to development of fracture patterns in Zimbabwe Craton and subsequent emplacement of Great Dyke. (1) collision of Zimbabwe and Kaapvaal Cratons and northward overthrusting of North Marginal Zone of Limpopo Province; (2) development of sinistral strike-slip faults of Popoteke Fault Set together with conjugate Mchingwe Fault Set; (3) rotation of maximum compressive stress causing extensional conditions and emplacement of Great Dyke and satellites; (4) post-Great Dyke reactivation of Mchingwe Fault Set resulting in dextral movement. Dextral movement in Central Zone (CZ) of Limpopo Province indicated. Gurungwe Fault at north end of Great Dyke shown for reference purposes.
[After Wilson and Prendergast, 1989]

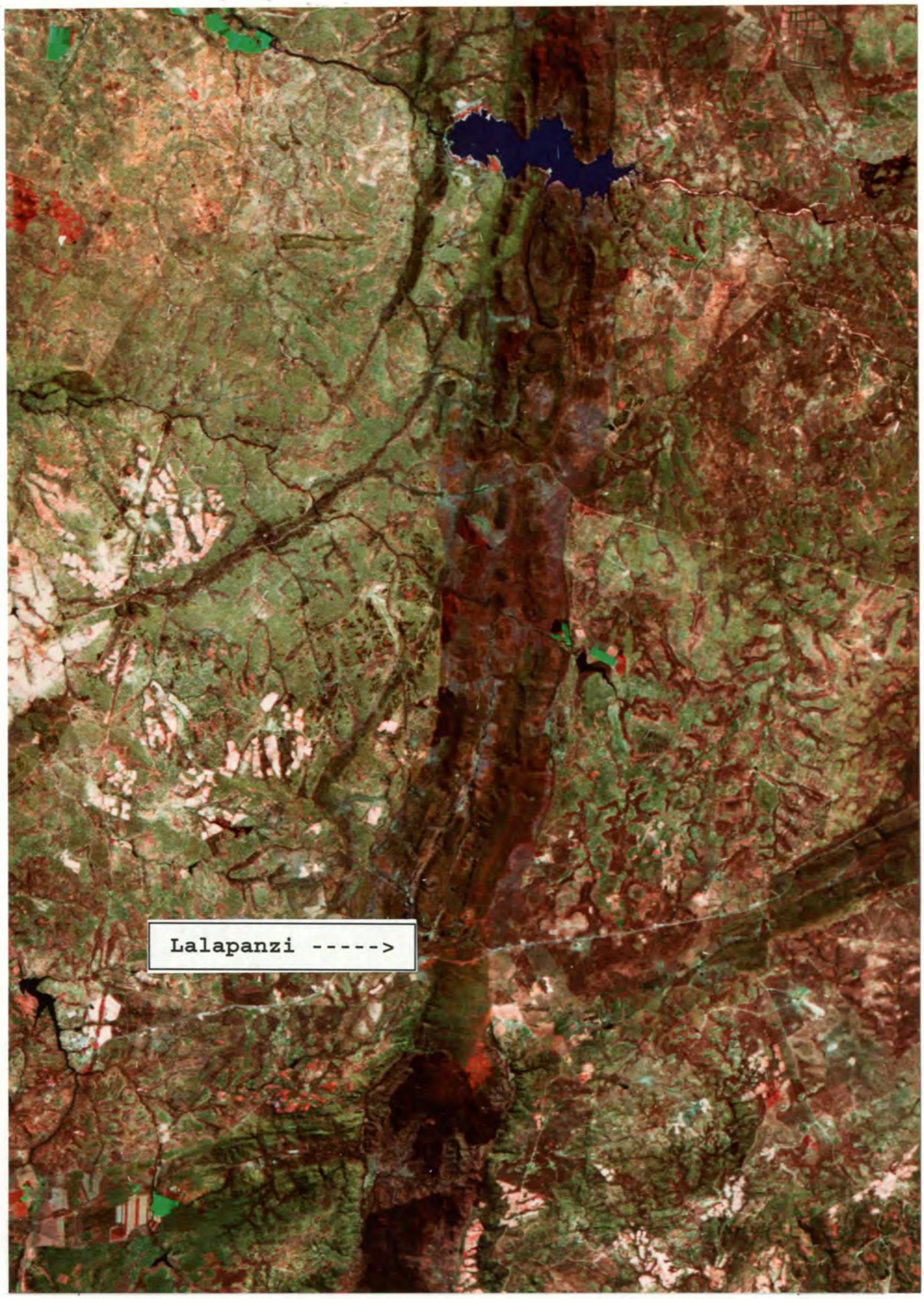

Fig 2.3 Landsat image of the Great Dyke showing the only major structural break along its length at Lalapanzi.

Stowe (1980) points out that the fractures related to the Great Dyke event are mainly normal faults with overall crustal tension indicated to be roughly E-W with the maximum compressive stress in the horizontal plane oriented N14°E. Wilson and Prendergast (1989) reviewed several models proposed to explain the origin of the Great Dyke fracture system. The most favoured model relates the Great Dyke emplacement event as resulting from extensional tectonics following a period of collision between the Kaapvaal and Zimbabwe cratons which imposed a craton-wide fracture pattern. The whole sequence of events is summarized in Figure 2.2.

The internal structure of the magma chamber and later deformation of the craton are responsible for two large-scale structural features of the Great Dyke: (1) the marked sinuosity as evidenced by a change in direction of approximately 10° between the North and South Chambers; (2) major east-west dextral movement within the Zambezi province which culminated in the rotation, tilting and severe faulting in the extreme northern portion of the Great Dyke (Wilson and Prendergast, 1989).

2.2.3 *Subdivisions and structure of the Magma Chamber*

The four complexes as originally defined by Worst (1960) were discriminated on the basis of stratigraphic variations and the disposition of the upper mafic rocks. They were regarded as fault-bounded remnants of four lopoliths. The mafic centres were thought to overlie downwarped feeder sites.

Evidence for large-scale graben faulting is lacking although sheared margins are observed in certain parts of the Great Dyke, for instance near Mtorashanga (Prendergast, 1988b). In other areas such as Sebakwe (Hughes, 1970), marginal faults are absent. Furthermore, the graben model as implied by the marginal faults, is not necessary to explain the narrow width of the Great Dyke in any area. Prendergast (1988b) noted that for the entire length of the Great Dyke, the only unequivocal structural and

stratigraphic break occurs at Lalapanzi between the Selukwe and Hartley complexes. On this basis, Wilson and Prendergast (1989) introduced the idea of two main magma chambers, i.e. the North Chamber and the South Chamber (Fig. 2.1). The present author has examined landsat images of the Great Dyke noting that indeed the only major structural break is at Lalapanzi (Fig. 2.3). The North and South Chambers have been subdivided into a number of compartments designated as subchambers (Wilson and Prendergast, 1989). These are the Musengezi, Darwendale and Sebakwe Subchambers for the North Chamber, and the Selukwe and Wedza Subchambers for the South Chamber (Fig. 2.1). Wilson and Prendergast (1989) further noted that the isolated east segment of the Musengezi Subchamber has a different stratigraphic sequence from the Western segment, with no evidence that this was caused by structural dislocation. They thus considered it to be a distinct separate entity from the North Chamber and suggested the name Mvuradona Chamber. No subdivision of the Mvuradona Chamber is recognised at present.

The overall transverse shape of the Great Dyke, including the nature of the deep zone below the layered sequence has been interpreted by Podmore and Wilson (1987), using 18 gravity profiles measured across the Great Dyke at approximately 25km-intervals between the southern tip of the Wedza Subchamber and Mtorashanga in the northern half of the Darwendale Subchamber. All gravity profiles show a bell-shaped Bouger anomaly and have been fitted to the geological model of densities and thickness of layers using an interactive computer model (Podmore and Wilson 1987). The most important facts from the interpretation are as noted below:

(a) A clearly dyke-like deep structure averaging about 1km in width exists at depths of between 4km and 10km along almost the entire length of the Great Dyke. The deep structure is less evident at Lalapanzi than elsewhere and this is taken as supporting evidence for the boundary between the North and South Chambers (Fig. 2.4).

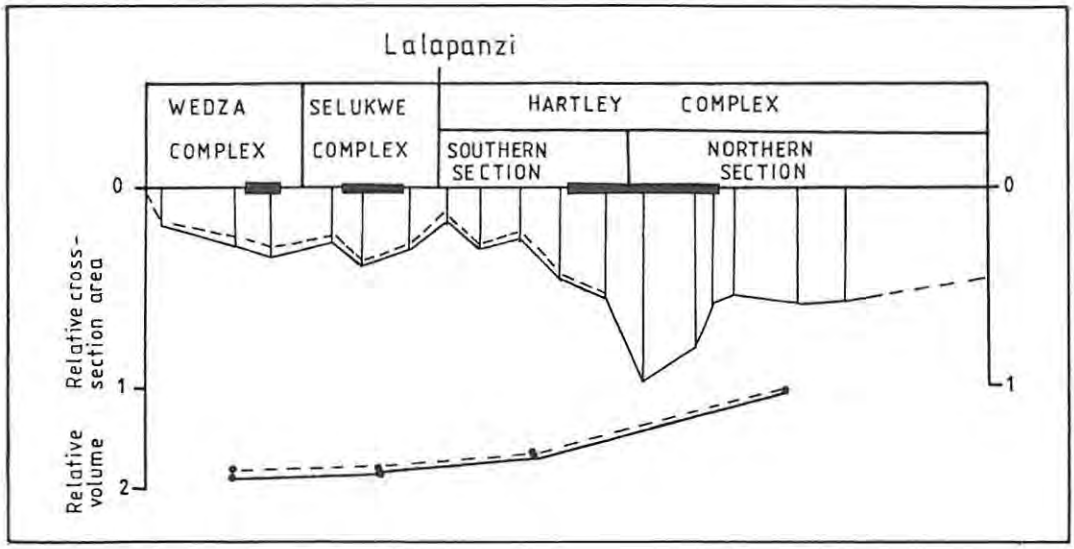

Fig.2.4 Relative cross-sectional area for 18 gravity traverses (positions identified by vertical lines) across Great Dyke with relative volumes of Wedza and Selukwe Complexes, and southern and northern sections of Hartley Complex. Lalapanzi, situated at boundary of Hartley and Selukwe Complexes, shown. Dashed line represents direct measurements and solid line is that corrected for elevation difference from north to south (650m). Black horizontal bars represent positions of gabbro remnants.
[After Podmore and Wilson, 1987]

(b) The Great Dyke magma chamber was a Y-shaped cross section in contrast to Worst's (1960) conjecture of shallow boat-like complexes with feeders at the centres (Fig. 2.5). Nonetheless, the original structural concept is incorporated to the extent that the axial feeder dyke may have been broader and discharged larger volumes of magma in the centres of the Selukwe and Wedza Subchambers (Prendergast, 1988b). Discrete central feeders are not recognised.

(c) Overall, the magnitude of the Great Dyke structure increases steadily from south to north with the largest anomalies occurring near the gabbroic remnants in each subchamber (Fig. 2.4). The coincidence of mafic (gabbroic) remnants with greenstone belts in the adjacent host rocks is taken to imply competency contrasts culminating in greater volume development of the Great Dyke at these points (Wilson and Prendergast, 1989).

(d) The noticeable asymmetry of certain gravity profiles is attributable to either local tilting of the Great Dyke or the irregular development of the deep structure. The inferred tilt to the east is consistent with the proposed uplift of the craton in the east relative to the west (Podmore and Wilson, 1987). This does not, however explain the asymmetry of the synclinal structure in some areas (Prendergast, 1988b).

(e) A number of profiles indicate the existence of a substantial lower magma chamber at about 5km depth parallel to the length of the Dyke with an approximate width of 2,5km (Podmore and Wilson, 1987).

The observed longitudinal symmetrical inward plunge and boat-like outcrop of each of the Subchambers are attributed to the larger volume of the magma chamber in the vicinity of the gabbro-norite remnants (Fig. 2.1) culminating in greater subsidence of

supporting crust in these areas (Wilson and Prendergast, 1989).

Prendergast (1988b) noted that the inward dip of the walls of the intrusion observed at present erosion levels corroborates the gravity shape of the Ultramafic Sequence as revealed by the gravity profiles. An example is the inward-dipping granite contact (45°) east of Unki Farm, Shurugwi. Nowhere have roof rocks to the Great Dyke been preserved. The possible original transverse shape of the now eroded uppermost Mafic Sequence has been reconstructed indirectly by extraction modelling on the basis of the vertical variation in pyroxene composition through the Mafic Sequence (Podmore and Wilson, 1987). This approach has limitations dependent on fluid dynamic processes within the chamber. However, the modelled rate of differentiation for the Lower Mafic Unit is consistent with the existence of several major sill-like lateral extensions of which the topmost is now removed by erosion and the lower one now seen as the remnant gabbroic caps. This model is supported on the west side of the Darwendale subchamber where the gabbro is in direct contact with granite wallrocks (Wilson and Prendergast, 1989).

Further evidence for a narrow Great Dyke magma chamber and its transverse structure comes from field observations. The Border Group (Fig. 2.5A) which has been recognised at several different localities, and structural and stratigraphic levels suggests a high degree of undercooling at the margin resulting in a high rate of nucleation followed by rapid cooling below the stable subsolidus temperature (Wilson and Prendergast, 1989).

2.2.4 *Lithology and cyclic units*

The Great Dyke comprises a lower Ultramafic Sequence overlain by an upper Mafic Sequence (Fig. 2.6). The Mafic Sequence is preserved as remnants in each of the subchambers and is divided into three subunits, i.e. Lower, Middle and Upper Mafic units as shown in Figure 2.6. The Ultramafic sequence consists of a lower Dunite Succession and an upper Bronzitite Succession (Fig. 2.6).

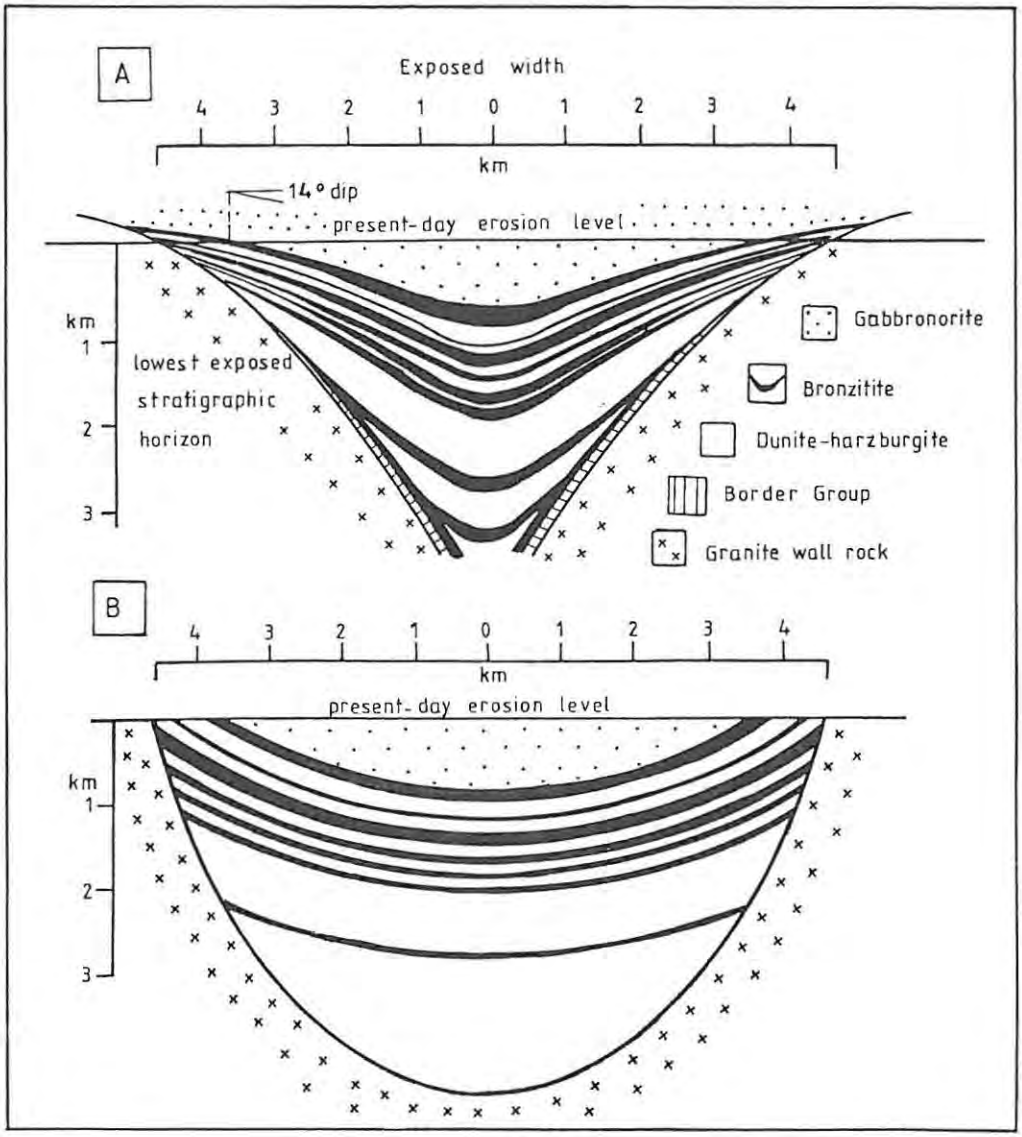

Fig.2.5 Proposed transverse sections of layered sequence of Great Dyke. *A*, revised transverse section based on field observations, layering dip angles and gravity studies showing attitude of layering and its relationship to wallrocks (Wilson and Prendergast, 1989). *B*, previously proposed semi-circular section of Great Dyke (Worst, 1960).

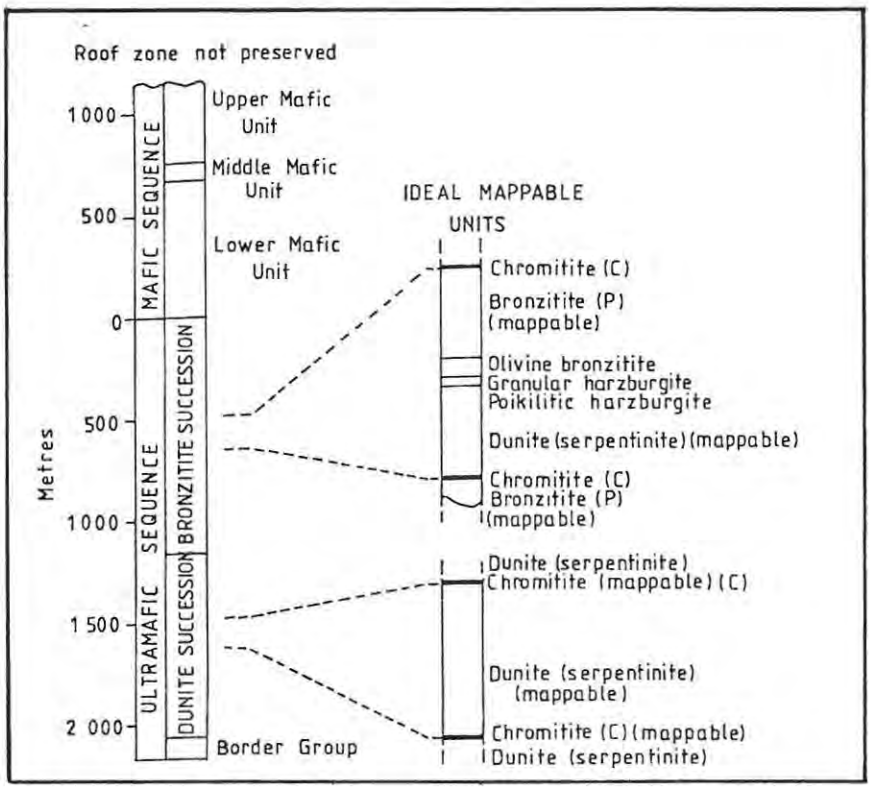

Fig.2.6 General subdivision of Mafic and Ultramafic Sequences of Great Dyke with details of cyclic units in Bronzitite and Dunite Successions. Chromitite layers generally mappable on basis of extensive trenching. [After Wilson and Prendergast, 1989]

Cyclic units in the Dunite Succession are defined by repeated occurrences of dunite or harzburgite separated by narrow chromitite layers while the cyclic units in the Bronzitite Succession show a complete progression from a basal chromitite or a marked chromite concentration, through dunite, harzburgite and olivine bronzitite to a well-developed bronzitite layer at the top. Similar patterns of lithologies are noted in the Stillwater Complex (Jackson, 1970) and Jimberlana Intrusion (Campbell et al., 1970).

Wilson (1982) noted the restricted mineral assemblages found in the ultramafic rocks of the Great Dyke and recommended that they be named on a modal basis according to the IUGS (Streckeisen, 1973). Table 2.1 summarizes the Great Dyke rock names and cumulus status of the minerals, and also the lithological sequence encountered in an ideal macro-unit.

Although the stratigraphy in all the Great Dyke chambers is broadly similar to each other, important differences exist in the nature of the cyclic units within the Bronzitite Succession (Fig. 2.7). In the North Chamber, six cyclic units (each approximately 200m thick) are recognised whereas sixteen units (each approximately 80m thick) are developed in the South Chamber (Wilson and Prendergast, 1989). Only one lithological sequence is clearly identified as common to all the three chambers,i.e. the topmost bronzitite passing upwards into the websterite which, in turn, is overlain by the mafic succession. The cyclic units are thought to have been produced by repeated injections of primary magma followed by fractionation and differentiation (Wilson, 1982).

In the earliest subdivision of the Great Dyke stratigraphy (Worst, 1958, 1960), each lithology was considered to represent a different magma type and cyclic units that comprised several lithologies were not recognised. The lithologically distinct layers were numbered sequentially downwards from the top of the Ultramafic Sequence-i.e. Pyroxenites Nos. 1 to 7 and chromite

Table 2.1 Major rock-types of the ultramafic zone of the Great Dyke

Rock-type and sub-unit	Cumulus minerals	Postcumulus minerals*
Bronzite (br)	Opx (95-100)+	Cpx (0-5), Plag (0-2)
Olivine bronzitite (ol br)	Ol (0-50), Opx (50-100)	Cpx (0-1), Plag (0-1)
Harzburgite (hz)	Ol (70-90), Chr (0-5)	Opx (2-15), Cpx (2-15), Plag (0-5)
Dunite (du)	Ol (94-100), Chr (2-5)	Opx (0-5), Cpx (0-5), Plag (0-2)
Chromitite (chr)	Chr (90-100) Ol (0-10)	Opx (0-20)

*Postcumulus overgrowth on cumulus phases is not taken into account.

+Numbers in parentheses refer to the range of modal proportions of individual mineral. (After Wilson, 1982).

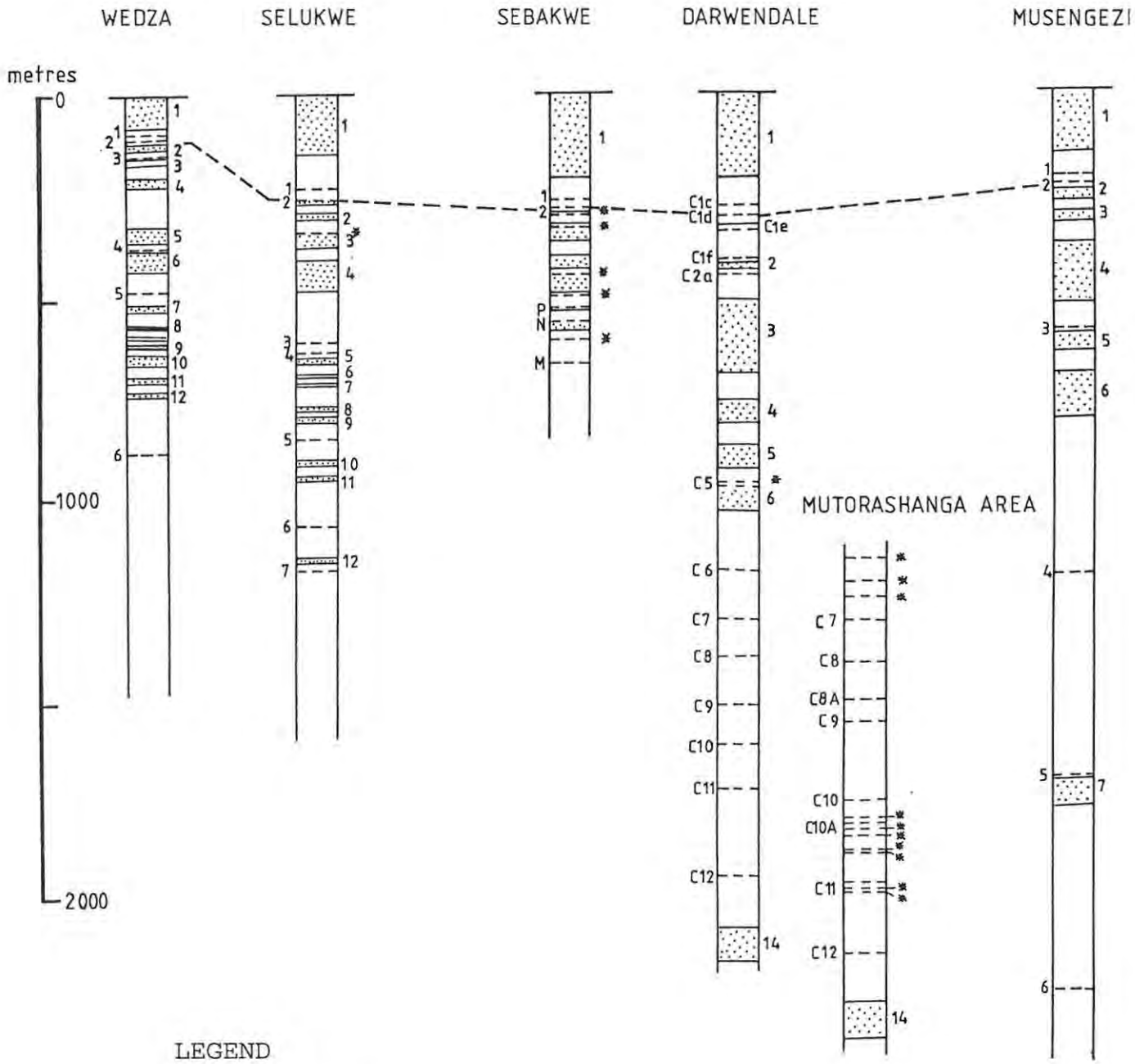

Fig.2.7 Stratigraphic distribution of chromitite and pyroxenite layers in five subchambers of Great Dyke. Compare very similar stratigraphic successions in all subchambers from chromitite C1d (broken line) upwards with different successions below this level. Chromitite-dunite succession in Mutorashanga mining area accurately constrained by borehole information. (N.B. new numbering system (Wilson, 1982) applied here only to layers in Darwendale Subchamber.)
[After Prendergast and Wilson, 1989]

seams Nos. 1 to 11. This system of numbering disregards the importance of linking lithologies in the same cyclic unit and lacks provision for additional lithologies, as for example, the poorly developed chromitite layers which were not previously recognised. The current system of numbering (Wilson, 1982) takes into account petrological criteria and the major subdivision of the stratigraphy into cyclic units (Wilson and Prendergast, 1989). The rules of the current numbering system are listed as follows;

(i) Cyclic units in the ultramafic sequence are numbered from the mafic-ultramafic contact downwards whereas units in the mafic sequence are numbered upwards from this horizon .

(ii) Cyclic units are defined on the basis of major phase changes observed on a mappable scale, such as pyroxenites and chromitites

(iii) Contrary to Worst (1960), individual mappable layers within the cyclic units are numbered according to the unit in which they occur, e.g. P1, P2, P3, etc., for bronzitites, and C1, C2, etc., for the chromitites. In this way the bronzitites (P1-P6) retain the traditional numbers (Worst, 1960), while the chromite layers are allocated new numbers.

(iv) Further subdivisions of layers and cyclic units can be accommodated on the basis of petrological criteria and should be identified by the use of lower case letters (e.g. chromitite layers defining subunits within cyclic unit 1 would be C1a, C1b, C1c, etc.). Consequently, important chromite seams such as Nos. 1,2 and 4,5,6,7 and 9 are now referred to as chromitites C1c, C1d, C5, C6, C7, C8 and C10, respectively.

2.2.5 *Mineral chemistry*

The mineral compositions of the Great Dyke succession have been fully investigated and documented only in the Darwendale area of the North Chamber (Wilson and Wilson, 1981; Wilson, 1982). The most important facts from these investigations are listed as follows:

(1) There is a systematic upward decrease in Mg contents through the Ultramafic Sequence from Cyclic Unit 10 to 1 (Fig. 2.8). This is interpreted as reflecting the fractionation of high - Mg basaltic magma (15,6% MgO initial magma composition (Wilson, 1982)).

(2) In the lowest part of the Ultramafic Sequence, chromite and olivine compositions become higher in Cr and Mg, respectively (i.e. increasingly primitive upwards) followed by a slight but steady decline. These mineral compositions become more strongly evolved from the upper part of Cyclic Unit 1 upwards (Fig. 2.8).

(3) The mineral compositions of chromite and in particular the parameter $Fe^{3+}/(Cr+Al+Fe^{3+})$, which increases upwards from Cyclic Unit 9 in both layered and disseminated chromite, reflects increasing oxygen fugacity of the magma which may have a bearing on the precipitation of chromitite layers (Wilson and Prendergast, 1989). The mineral compositions are indicative of a gradually evolving liquid repeatedly modified to more primitive compositions by mixing of the resident and new magmas (Fig. 2.8).

2.2.6 *Magma emplacement and crystallization*

The cyclical layering of the Great Dyke Ultramafic Sequence is explained by repeated injections of primitive magma of identical composition while the major compositional reversals at bases of the cyclic units are explained by slow mixing of new parental

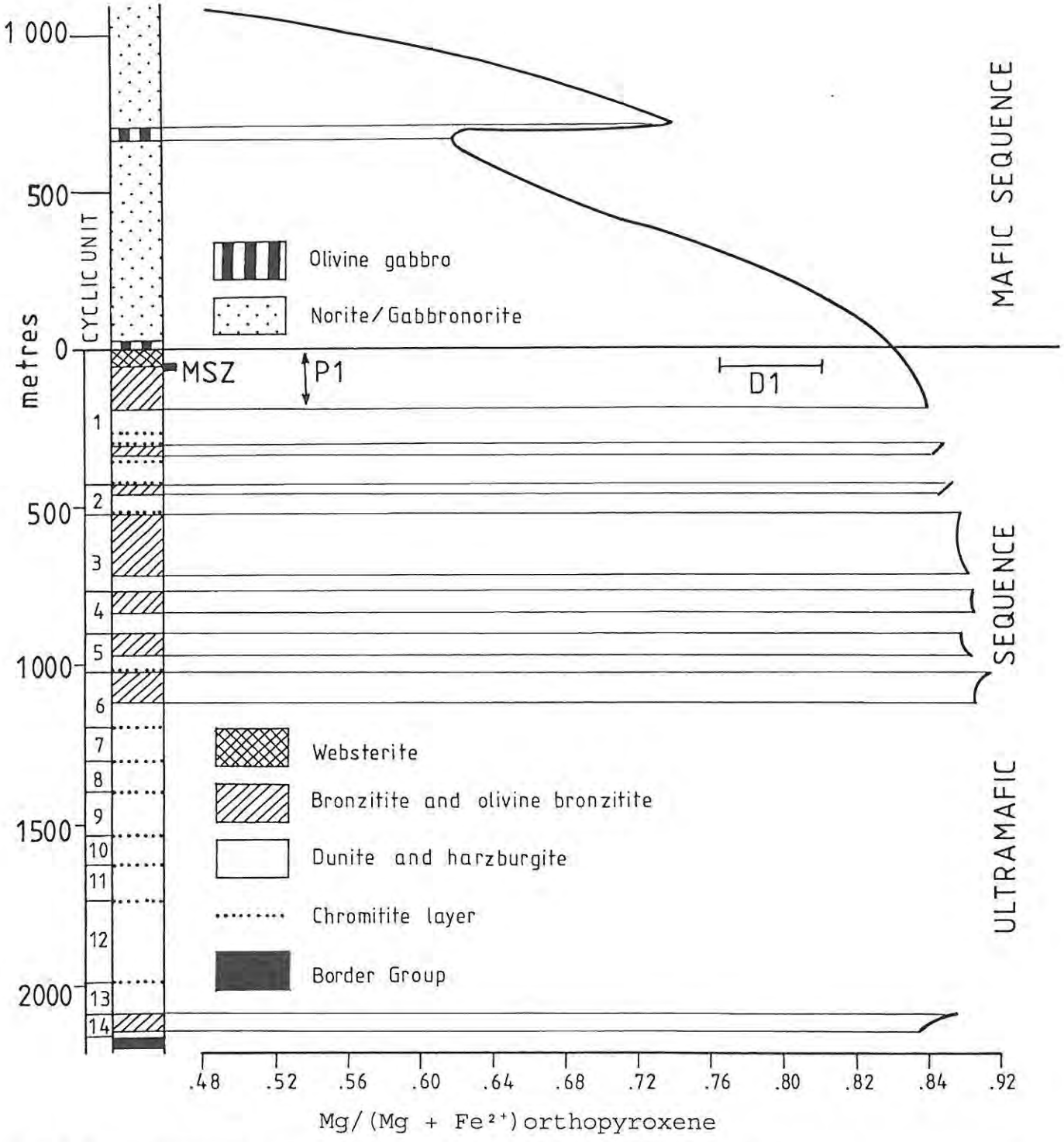

Fig.2.8 Schematic stratigraphic column of Great Dyke igneous sequence in Sebakwe and Darwendale Subchambers. Mg/(Mg + Fe^{2+}) ratios of cumulus orthopyroxene from pyroxenite and norites illustrate limited fractionation in Ultramafic Sequence followed by marked fractionation in mafic sequence. Position of P1 pyroxenite layer and MSZ are indicated at top of Ultramafic Sequence. [After Podmore and Wilson, 1987]

magma with the older, more evolved magma at the zone of crystallization (Wilson, 1982; Wilson and Prendergast, 1989). It is envisaged that each new injection of hot dense primitive magma would either spread out below the cooler, lighter and more evolved resident magma (Huppert and Sparks, 1980) or would mix turbulently to varying degrees with the resident magma by fountaining (Turner and Campbell, 1986; Campbell and Turner, 1986). Prendergast and Wilson (1989) argue that fountaining and mixing were probably the dominant replenishment processes as a consequence of a high velocity of each pulse as dictated by the relatively large width of the axial feeder.

The magma chamber is thought to have been an open system in its early stages represented by the crystallization of the Ultramafic Sequence (Wilson, 1982; Wilson and Prendergast, 1989). This is evidenced by the rate of compositional change with stratigraphic height in the upper parts of the Ultramafic Sequence and in the Mafic Sequence. The occurrence of the chromitite layers at the bases of the cyclic units is supportive of the injection process. The presence of chromite-bearing harzburgite below certain chromitite layers implies some degree of mixing between resident and primitive magmas prior to the precipitation of chromite, but this may also be partly due to entrapment of residual magma, or to upward streaming of interstitial liquid by compaction of underlying cumulates (Wilson and Prendergast, 1989).

The largest magma compartments (i.e. subchambers) are developed in the north and this may imply that the emplacement took place progressively from north to south (Wilson and Prendergast, 1989). In the initial stages, the subchambers were filled separately with magma and produced different patterns of cyclic layering at lower levels. Coalescence gradually occurred at high levels from the level of Cyclic Unit 2 upwards. At this stage a single continuous chamber became apparent as indicated by the similarity of the layering pattern of Cyclic Unit 1. Save for one minor influx in the Mafic Sequence responsible for a reversal in orthopyroxene composition (Podmore and Wilson, 1987), no major

injections of primitive magma occurred after the crystallization of Cyclic Unit 1. The PGE sulphide mineralisation associated with the P1 pyroxenite has been linked to one of the last injections of magma (Prendergast and Wilson, 1989; Prendergast and Keays, 1989) followed by fractionation.

The crystallization sequence of the Ultramafic Succession has been deduced from a projection of the liquid line of descent into the low- pressure system Ol-Cpx-Plag-Qtz (Irvine, 1979). Plots of chemical analyses and CIPW norms of the East Great Dyke chill together with modelled derivative liquids show good agreement with the observed crystallization sequence in the Darwendale Subchamber (Wilson, 1982). As can be deduced from Fig. 2.8, the cyclic units below Unit 1 can be envisaged as migrations from the olivine field towards and slightly overlapping the orthopyroxene field, followed by a rapid return to the olivine field, signifying a new magma pulse.

In the Mafic Sequence, extreme overall iron enrichment occurs with no development of cyclic units. The rate of orthopyroxene differentiation was more rapid than in the Ultramafic Sequence as a result of the magma chamber becoming sealed. The fact that major impulses of magma occurred in the Ultramafic Sequence, where hot dense new magma was injected into lighter and cooler evolved resident magma, implies that the crystallization may have been mediated by a double-diffusive convection process (Wilson, 1982). On the other hand, large-scale convection processes are likely to have been dominant in the more differentiated magma crystallising the Mafic Sequence, due to it being feldspar-saturated and hence, near the density minimum.

Although gravity settling of olivine or orthopyroxene in the Great Dyke cannot be ruled out completely, the mineral chemistry data indicate *in situ* crystallization at or near the floor of the magma chamber (Wilson, 1982). Prendergast (1988b) pointed out that the fine-scale layering of some of the disseminated olivine

chromitites of the upper group chromitites is also best explained by in situ crystallization.

2.3 Mineralisation and mineral deposits

The Great Dyke hosts vast mineral deposits of which the prominent ones include chrome, asbestos, PGE, nickel, copper and gold. The locations of the principal mineral deposits are shown in Figure 2.1. Presently chromite is the only mineral mined on the Great Dyke.

2.3.1. *Chromitite Layers*

The main chromitite layers of the Great Dyke have been informally divided into the upper group chromitites (C1c, C1d and C2a) and the lower group chromitites (C5-C12) (Slatter, 1981). This subdivision is based principally on the contrasting bulk chemical compositions between them. The two groups are separated from each other by a zone of pyroxenite-dominant cyclic units devoid of significant chromite concentrations (Fig. 2.7). Only chromitites C1c and C1d of the upper group can be correlated at the same stratigraphic level in all the subchambers.

The upper group chromitites are chemical-grade ores with low Cr/Fe ratios of around 2:1. The lower group chromitites are high or metallurgical grade ores with high Cr/Fe ratios in the order of 3:1.

2.3.2 *Origin of Chromitites*

The stratigraphic location of chromitite layers at the bases of cyclic units is evidence that their origin is related to the process of multiple replenishment of the magma chamber with primitive magma (Prendergast and Wilson, 1989). With mixing between primitive and evolved magmas, the hybrid was driven into the primary chromite phase volume with chromite crystallizing as the sole phase (Irvine, 1977). The massive nature of the chromitites with sharp footwall and gradational hanging-wall

contacts is indicative of continued fractionation and Cr depletion shifting the magma composition back to the olivine-chromite cotectic.

The Great Dyke chromitites are generally characterized by high chromite Fe^{3+} content relative to chromite in the adjacent dunites (Wilson, 1982; Wilson and Prendergast, 1989). This is interpreted as evidence of chromite precipitation by mixing of an evolved, low fO_2 magma, with a primitive magma with relatively high fO_2 (Wilson, 1982). However, there is a possibility of postcumulus modification of chromite by trapped liquid in the dunites (Roeder and Campbell, 1987) which makes it difficult to evaluate the precise role of fO_2.

2.3.3 *PGE Mineralisation*

The potentially economic concentrations of PGE sulphide mineralisation are hosted by the Pyroxenite No.1 (P1) Layer at the top of Cyclic Unit 1. This P1 Layer (± 200m thick) is only preserved directly beneath the central mafic remnants in the Wedza, Selukwe, Sebakwe, Darwendale and Musengezi Subchambers (Fig. 2.1). It consists of a thick bronzitite and a thin overlying websterite (between 7 and 33m thick), both varying in thickness between and across each subchamber.

Three subunits are recognised within the P1 Layer, and are numbered from top to bottom. Subunit 1 contains a broad zone of sulphide mineralisation and is made up of three sublayers, viz: sublayer 1a which consists of a 10m thick websterite, and sublayers 1b and 1c comprised of the uppermost bronzitites with a combined thickness of between 2.5m and 5m. The PGE-rich Main Sulphide Zone (MSZ) occurs just below the base of the Main Websterite. Within this subunit the pyroxene compositions become progressively Fe-enriched and Cr-depleted up section.

Subunit 2 with an average thickness of between 20 and 30m is characterised by a bronzitite with very low sulphide content. The pyroxene compositions become more primitive upwards.

Subunit 3 comprises bronzitites containing a broad zone of between 50 and 60m of weakly disseminated sulphide mineralisation. The sub-economic PGE zone termed the Lower Sulphide Zone (LSZ) is located here. The pyroxene compositions are marked by an overall upward Fe-enrichment trend. The lower portions of Bronzitite No.1 do not contain any significant sulphide mineralisation.

2.3.4 *The Origin of the LSZ and MSZ*

Two important common features suggesting a broadly similar origin for the sulphide zones of subunits 1 and 3 are (a) stratigraphic locations within a bronzitite host rock, and (b) PGE-enrichments at the bases of the sulphide zones and with identical vertical metal distributions (Prendergast, 1988a).

Current ideas on the origin of the PGE deposits (Prendergast, 1988a; Wilson and Tredoux, 1990) are closely linked to the magma replenishment history and evolution of the magma body. The layered pyroxenite which hosts the MSZ can be viewed in terms of bottom crystallization from a system of double diffusive liquid layers emanating from a major influx of hot, dense parental magma, at the level of C1c chromitite at the base of the cyclic unit (Huppert and Sparks, 1980; Sparks and Huppert, 1984; Turner and Campbell, 1986; Prendergast and Wilson, 1989; Prendergast and Keays, 1989). The principal factors that culminated in the formation of the PGE-enriched LSZ and MSZ have been summarized by Prendergast and Wilson (1989) as follows:

(a) repeated replenishment of primitive magma and silicate fractionation enriching the resident magma in sulphur and PGE.

(b) sulphur saturation largely as a result of overall cooling of the magma combined with depletion of iron by the extensive fractionation of olivine and orthopyroxene.

(c) sulphide precipitation/extraction of PGE from the magma.

(d) control of sulphur saturation and sulphide precipitation by fractionation and cooling following the last major magma replenishment (chromitite C1c), and enhanced by further minor replenishments during the formation of the pyroxenites. The different development of the LSZ and MSZ has been attributed to the nature of the intervening minor replenishment, and the fractionating rate in the magma chamber.

Chapter 3

GEOLOGY OF THE SELUKWE SUBCHAMBER

3.1 Location and Access

The Selukwe Subchamber constitutes the northern portion of the South Chamber of the Great Dyke (Fig. 2.1) and lies 20km due east of Shurugwi town. The area with potential for platinoid mineralisation is approximately 230km², and is held by Anglo American Corporation (AAC) under the New Middleridge claims (Fig. 3.1). AAC has subdivided the New Middleridge claims into five targets. These are (from north to south) Paarl, Unki, Helvetia, Bougai and Kironde (Fig. 3.1).

The Unki deposit is located close to the northern margin of the subchamber. Access is via the Shurugwi-Zvishavane road. At the bottom of Wolfshall Pass, a dirt road runs north-eastwards across the claims area.

A 33 kv power line services the Unki shaft area (Fig. 3.1). A possible source of additional power could be from the 88 kv line from Lalapanzi to Mashava. Water supplies would be available from boreholes or by pumping from the Umtebekwe River upon which a dam site is reserved. There is a railhead at Shurugwi which services the Zimbabwe Mining and Smelting Company's chromite mines in the vicinity.

3.2. History of Exploration

The earliest reference to platinum occurrence in the Selukwe Subchamber was made by Zeally (1918) who reported the presence of disseminated sulphides on Helvetia Farm, near Shurugwi town. However, serious exploration for PGE only began in 1963 under Anglo's Exclusive Prospecting Order number 127. Between 1966 and 1981, 84 vertical surface diamond drill holes were sunk. In

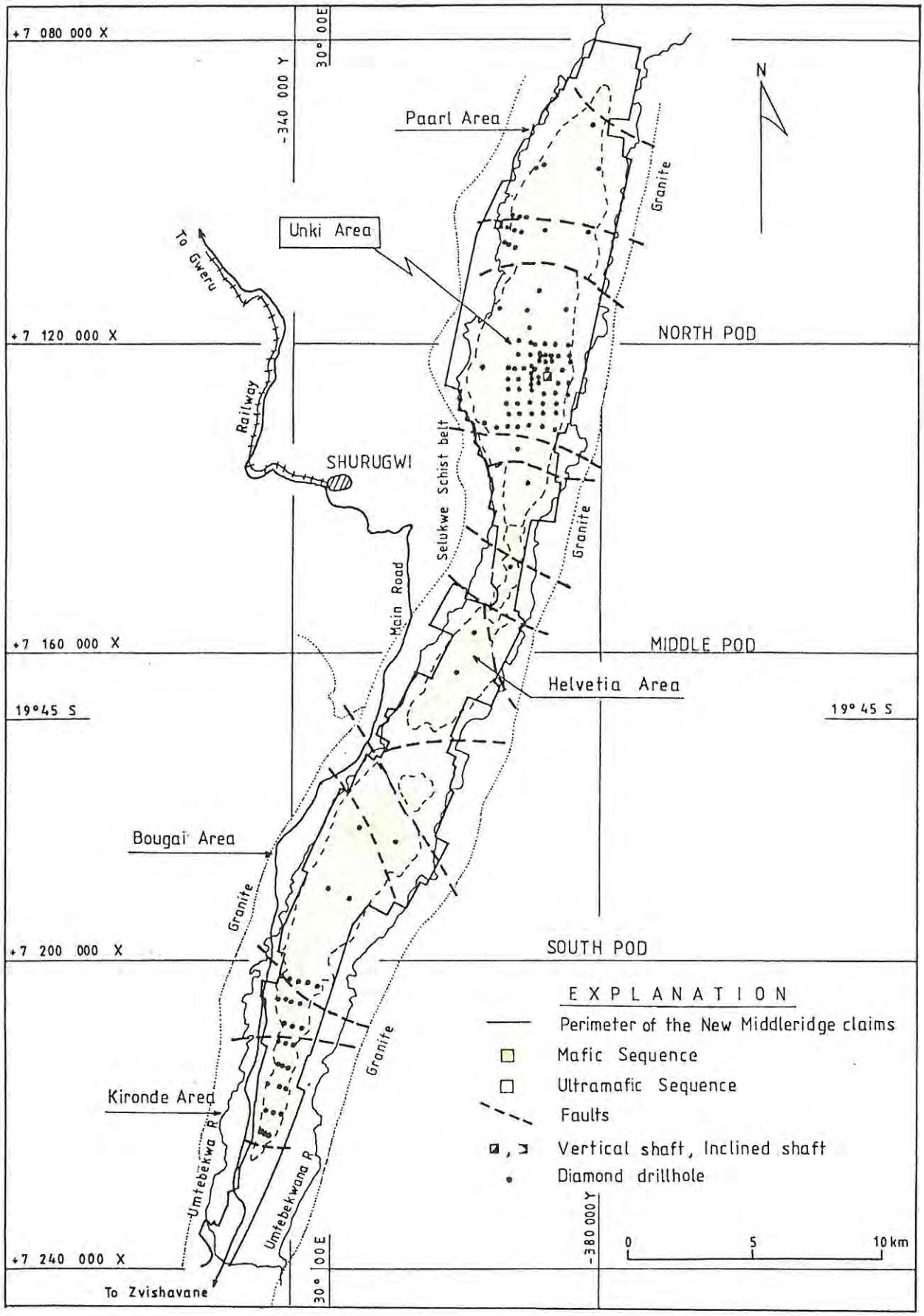

Fig.3.1 Simplified geological map of the Middleridge Claims, Selukwe Subchamber.

addition to surface diamond drilling, underground exploration and trial mining were carried out at Paarl and Unki (Fig. 3.1) in 1968 and 1972, respectively. This exploratory work proved a huge tonnage of potential ore within a widely persistent zone of up to 1,8m thick. Despite this success, an economically viable mine could not be developed mainly due to (1) the difficulty in visually establishing the zone to be mined after efforts with phosphomolybdate to delineate a bright blue zone on the stoping faces proved unsuccessful, (2) the low metal prices arising from severe surplus as a result of the expansion of Rustenburg's operations in 1971 and a general economic recession, (3) the marginal grade and high capital investment required to develop a mine of the optimum economic size, and (4) the poor investment climate caused by the Rhodesian war.

The late 1980s saw a dramatic recovery in the price of nickel and sustained values of precious metals. Consequently in 1989, Anglo American resuscitated its interest in the Main Sulphide Zone and focused upon Unki where the tonnage/grade potential was greatest.

3.3 Regional Geology

The Selukwe Subchamber, as is characteristic of the other Great Dyke subchambers, comprises a gently dipping synclinal sequence of layered dunites, harzburgites, chromitites, pyroxenites and gabbroic rocks. It however, differs from subchambers of the North Chamber in having (i) a greater number of cyclic units (Fig.2.7), and (ii) narrower cyclic units. The generalized stratigraphic succession is shown on Figure 3.2.A.

The eastern margin of the Selukwe Subchamber is in contact with granite for almost its entire length. Biotite diorite and other hybrid rocks are common as a result of the intermingling of granite and Dyke rocks. On aerial photographs, the granite areas are clearly seen to differ from the Dyke in tone and texture. The distinctive banding and differential erosion of the latter are absent from the granite. The granite - Dyke contact can be

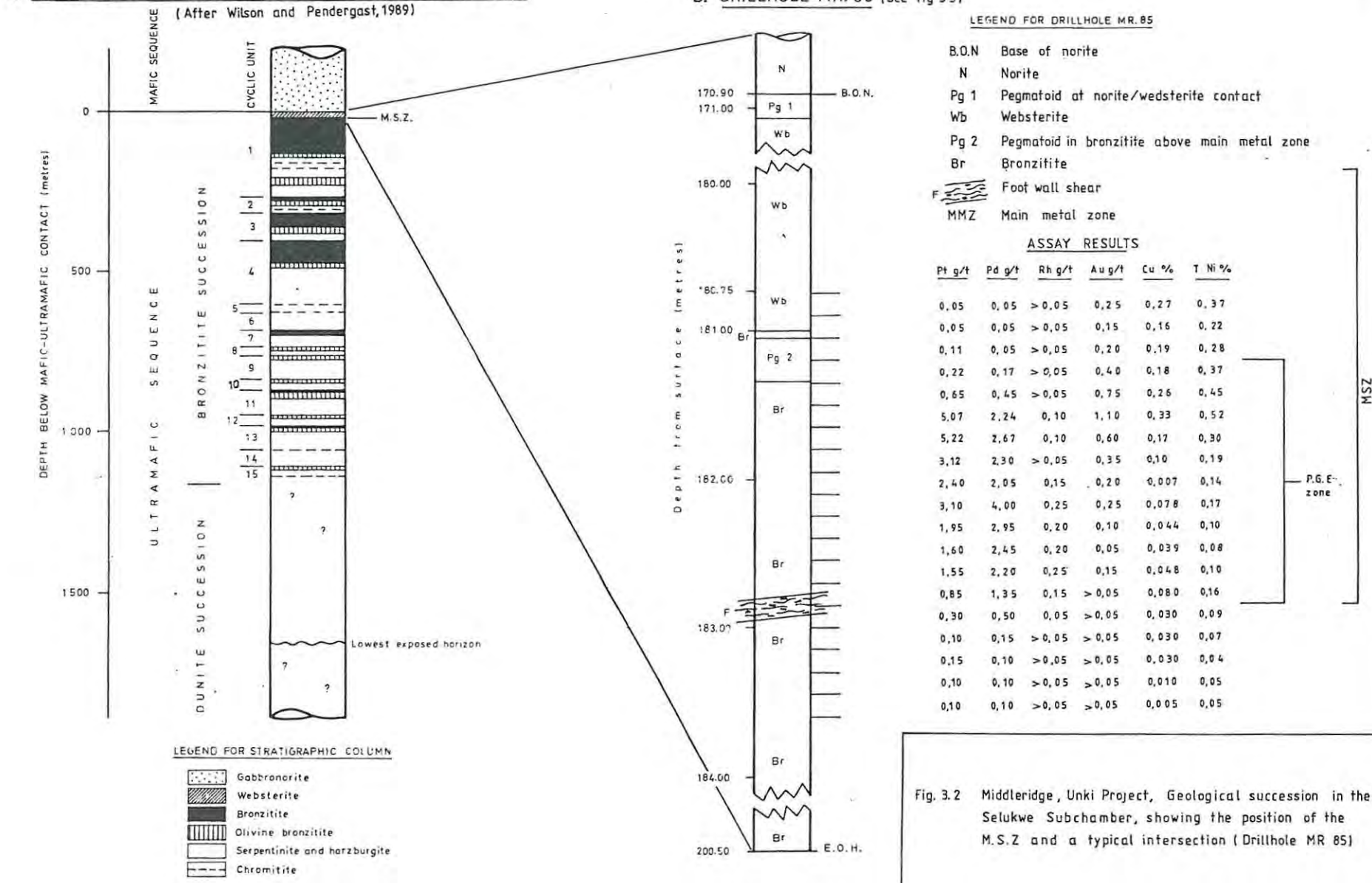

Fig. 3.2 Middleridge, Unki Project, Geological succession in the Selukwe Subchamber, showing the position of the M.S.Z and a typical intersection (Drillhole MR 85)

determined on the photographs for much of the subchamber, but there are areas where the spread of granitic sand on to the Dyke has obscured the contact. Within the Dyke rocks, interlayering and lensing of serpentinites, harzburgites and olivine bronzitites, on a variety of scales as described by Coghill and Wilson (pers. comm., 1992), are sporadically developed in the strike direction of the eastern margin.

The greater part of the western margin of the Selukwe Subchamber is in contact with epidiorites, phyllites, micaceous grits and serpentines of the Selukwe Schist Belt. The Schist Belt rocks exhibit another fairly distinctive pattern on aerial photographs. These areas are darker than the Dyke. Much of the Schist has a finer photographic texture caused by smaller trees, more stunted and more closely spaced than those on the Dyke. The rocks of the Schist Belt form more broken country, lacking the linearity of the bands (layers) of the Dyke.

The ultramafic rocks of the Schist Belt contain lenticular bodies of chromite which are older than, but not directly related to, the chromite deposits of the Great Dyke. Small, isolated roof pendants of Schist Belt rocks occur in the norite of the Mafic Sequence of the Dyke. At the extreme northern end of the Middleridge claims, small chrome pods believed to belong to the Shurugwe podiform chrome deposits, have been observed within the Dyke rocks.

The mafic (gabbronorite) rocks overlying the PGE mineralization have a strike extent of 45km (Fig. 3.1) and average about 270m in vertical thickness. At Selous in the North Chamber (Fig. 2.1), up to 1200m of mafic rocks overlie the PGE zone (Wilson, 1982).

Well developed cyclic layering characterizes the Ultramafic Sequence. The stratigraphic succession (Fig. 3.2) is dominated by the P1 layer which hosts the MSZ. The MSZ is a thin (up to 5m thick) stratiform zone of high sulphide enrichment and is

developed close to the top of the P1 layer of the uppermost cyclic unit (Fig. 3.2). The PGE-rich zone is at the base of the MSZ. Some 30-40m below the MSZ, is a broader zone of disseminated sulphide, which is referred to as the LSZ. The sulphide content of the LSZ is much lower, than that of the MSZ (Wilson and Prendergast, 1989). The MSZ in the Selukwe Subchamber is typically located at 10m below the base of the norite of the Mafic Sequence, whereas in the Darwendale and Sebakwe Subchambers (North Chamber), the MSZ is at an average distance of 35m below the base of the norite (Wilson, 1992).

Below the P1 layer, the dominant rock types are olivine bronzitites, harzburgites and chromitites. Chromitite CU1 is 100m below the base of the MSZ.

Younger dykes of granite - pegmatite, granite, aplite, dolerite and quartz dolerite have intruded the Great Dyke locally. They are steeply dipping and normally occupy a fracture for only part of its length.

3.4 Regional Structure

The layers of the Dyke within the Selukwe Subchamber are similar in form to the other subchambers (Worst, 1960; Wilson, 1976 & 1982; Prendergast, 1988b). The layers are arranged in a synclinal form and crop out as bands, which dip inwards towards the centre of the subchamber. The dips become steeper in bands nearer the margins of the dyke. A maximum average dip of 15° is indicated around the periphery of the subchamber, but in general, the average dip on the eastern margin is 1-2° steeper than on the western margin. This indicates some slight axial tilting to the west.

The syncline has a shallow plunge towards the middle of the subchamber; this direction is reversed in some structural blocks as a result of faulting. The continuity of layers across the Dyke from exposures on the eastern and western sides, is

demonstrated by the fact that some layers at the northern and southern extremities of the subchamber can be seen to cross the axis at surface.

A number of major transverse steeply dipping faults interrupt the overall continuity of the Selukwe Subchamber, so that three major pods, with PGE potential, remain with barren ground between them (Fig. 3.1), as a result of erosion. These are informally recognized as the North, Middle and South pods (Fig. 3.1). Other numerous NE-SW and NW-SE fracture systems can be observed from aerial photographs but relatively few of these cause any significant off-setting of the Dyke margins.

3.5 Details of the Unki area geology

3.5.1 *Surface exposures*

The Unki area comprises the southern half of the North Pod and covers an area of approximately 15 km². It is bounded to the north and to the south by faults of several tens of metres of throw, and to the east and west by the Umtebekwana and Umtebekwe rivers, respectively (Fig. 3.3). A maximum average dip of 15° is indicated on the eastern flank of the Unki basin, decreasing gradually down dip to horizontal or nearly so, in the centre of the basin. The average dip on the western side is slightly less at 13°.

The P1 layer which is host to the MSZ, is rarely exposed along the edges of the eastern and western margins except where gulleys occur. Interdigitating bronzitite and websterite as seen in marginal drill hole intersections, is largely obscured by weathering. Wherever the MSZ is exposed in gulleys and streams, it is characterized by nodules of optically continuous plagioclase oikocrysts enclosing bronzite crystals. This nodular pyroxenite, often referred to as the "potato reef" (Wilson 1976), is characterized by a sulphide-rich matrix which is very prone to weathering. The contact between the P1 layer and the

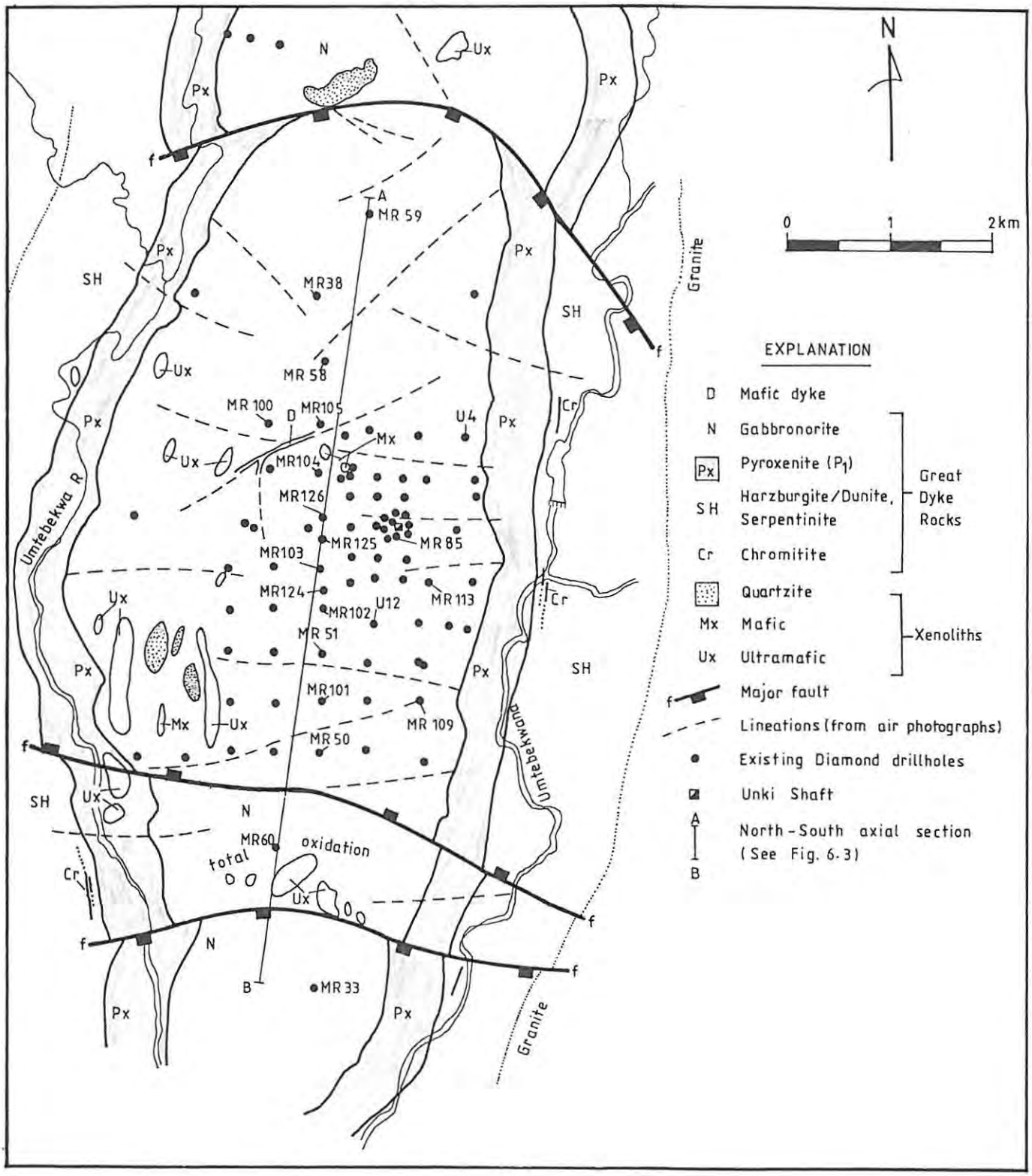

Fig.3.3 MIDDLERIDGE : Simplified geological map of the Unki Area.

overlying gabbronorite is sharp and is marked by a pegmatoidal pyroxenitic layer with blebs of sulphide. These sulphides are devoid of PGE. Large vleis occur over the gabbronorite at the centre of the Unki area and bailing tests have shown water accumulating at shallow depth below surface. It is, however, anticipated that this water will not be a major problem during mine development as the pyroxenite beneath the norite is impervious.

The PGE-rich MSZ is located in the uppermost (P1) pyroxenite band, about 10m below the base of the norite. It lies at or near the contact between two pyroxenite types: an upper websterite consisting of cumulus augite (>50%) with subordinate bronzite, and a lower almost monomineralic layer of bronzitite. Augite oikocrysts occur through much of the bronzitite and are not necessarily confined to the MSZ. The PGE-rich section of the MSZ is not visually identifiable.
The MSZ is approximately 916m above sea level in the deepest part of the Unki basin. This represents a vertical depth of about 275m below surface. Exposures of the dunite/harzburgite succession below the P1 layer appear to be confined to the banks of the Umtebekwana River on the eastern flank (Fig. 3.4). Chromitite seams, C1a and C1c are discontinuously exposed along both the eastern and western flanks of the Dyke (Fig. 3.3).

Xenoliths of various compositions occur within the Unki area, particularly on the western flank (Fig. 3.5). These have been categorized into 3 types (Wilson, 1992 internal report) as follows:

(a) rocks which have been derived from material extraneous to the Great Dyke;

(b) rocks which are part of the low pressure assemblage of the Great Dyke but which crystallised at some point other than their present position; and

Fig.3.4 Spheroidal weathering of heavily jointed poikilitic harzburgites giving rise to "core stones" (Umtebekwana River on the eastern flank of Unki).

Fig.3.5 Checking for field relationships between xenoliths and the Great Dyke Rocks (Unki area, western flank).

(c) rocks which are part of a primitive sequence of differentiates referred to as autoliths.

There is no evidence to suggest a stratigraphic control in the distribution of the xenoliths and no reason to believe that these fragments will be concentrated in the MSZ. However, in two drill holes from the axial region, the MSZ is partly disrupted by xenolithic fragments.

Mafic dykes and sills are not common as has been observed in the Darwendale and Sebakwe Subchambers (Worst, 1960). Only one major dolerite dyke transects the Unki area. This dyke occupies part of a major NE-SW fracture zone to the north of Unki shaft (Fig. 3.3).

3.5.2 *The MSZ and identification of the PGE zone*

The MSZ in the Unki area was tested by 74 vertical surface diamond drillholes. The PGE-rich section of the MSZ zone consistently occurs at $\pm$ 1m below the websterite/bronzitite contact. It averages about 2,2m in width. The contact between the websterite and bronzitite is often gradational and is characterised by the presence of relatively smaller augite oikocrysts than those in the main bronzitite. The restriction of the metal zone to within 1m of the websterite/bronzitite contact suggests a geological control, possibly associated with a clear-cut magmatic event or process.

Visible sulphide in varying quantities is identifiable through the MSZ and the websterite into the base of the norite. The PGE-rich zone is located at the base of the sulphide zone, but base-metal sulphides extend beyond the upper limit of the PGE zone. The sulphide minerals associated with the MSZ are dominated by pyrrhotite, with lesser chalcopyrite and pentlandite, occurring as disseminations and clusters between pyroxenes. Base metal sulphide concentration generally appears highest at or close to the top of the PGE zone, but varies from drill core to drill

core. The PGE-rich zone cannot be precisely identified on the basis of sulphide concentration. As a general rule, the lithological contacts between norite and websterite and between websterite and bronzitite are characterized by clusters of sulphide blebs. The fact that the PGE-rich zone cannot be precisely identified on the basis of sulphide concentration may indicate that some platinum group minerals are not sulphide related.

The main morphological features identifiable from diamond drill core logging are a pegmatoid in the hanging wall and a narrow shear called the Footwall Shear (Fig.3.2B). The PGE zone is sandwiched between these two features. However, the persistence of the hanging wall pegmatoid has not been consistently established in all the drill cores.

The hanging wall pegmatoid occurs at a distance of between 20cm and 60cm above the top of the PGE zone and varies between 2cm and 60cm in thickness. It is rich in sulphides and can contain up to 0,35% Ni but is not enriched in PGE. Characteristically, the pegmatoid is coarse grained with up to 15mm-sized grains of pyroxene, feldspar, quartz, phlogopite and minor amounts of amphibole. It is important to note that a similar pegmatoid is developed at the contact between norite and websterite.

The writer considers that the pegmatoids at the base of the norite and in the hanging-wall of the MSZ are indicative of hydrothermal stages of the crystallization process. The base of the norite is an adcumulate with an anorthositic texture. Hence, this rock acted as a barrier to the upward movement of late residual liquids of low-melting-temperature silicates and water culminating in the formation of a pegmatoid. The same hypothesis holds for the pegmatoid at the base of the mono-mineralic websterite in the hanging-wall of the MSZ.

The Footwall Shear demarcates the base of the main metal zone and in 30% of the drill hole intersections coincides with the $\pm$ 1 g/t

Pt cut-off in the footwall. For the remainder of the intersections, the base of the shear coincides with a natural cut-off of ± 0,4 g/t Pt in the footwall. The thickness of the Footwall Shear varies between 5mm and 60cm with an average of 30cm. The shear infilling material consists of slickensided mylonite with gouge and breccia often accompanied by magnesite and chrysotile veining giving rise to imbricate structures (Fig. 3.7). The base is a smooth, sub-horizontal planar surface. A system of sub-parallel joints occurs in a zone 0.5m above and below the shear.

The Footwall Shear is a later feature than the pegmatoids. Its position at the base of the main metal zone is enigmatic but it is evident that this position marks the boundary between contrasting rock types, i.e. a mineralised amphibolitic bronzitite above it and an unmineralised bronzitite below it. Based on this observation, the development of the shear may have been due crustal loading which took advantage of a plane of weakness between contrasting rock types.

3.5.3 *Mine Geology*

The layout of underground workings at Unki Shaft as at end of October, 1995, is as shown in Figure 3.6. Detailed underground mapping was carried out along the drives, raises, cross-cuts and the stopes. The aim of this exercise was three-fold:

1. to establish the visual characteristics of the PGE-rich zone of the MSZ for the miners to follow;
2. to investigate the existence of potholes or washout channels, and
3. to establish the geomechanical properties of the stopes.

Visual characteristics of PGE Zone

The same features as seen in drill hole intersections were seen on underground exposures; these are the hanging-wall pegmatoid and the Footwall Shear (Figs. 3.7 and 3.8). As far as could be

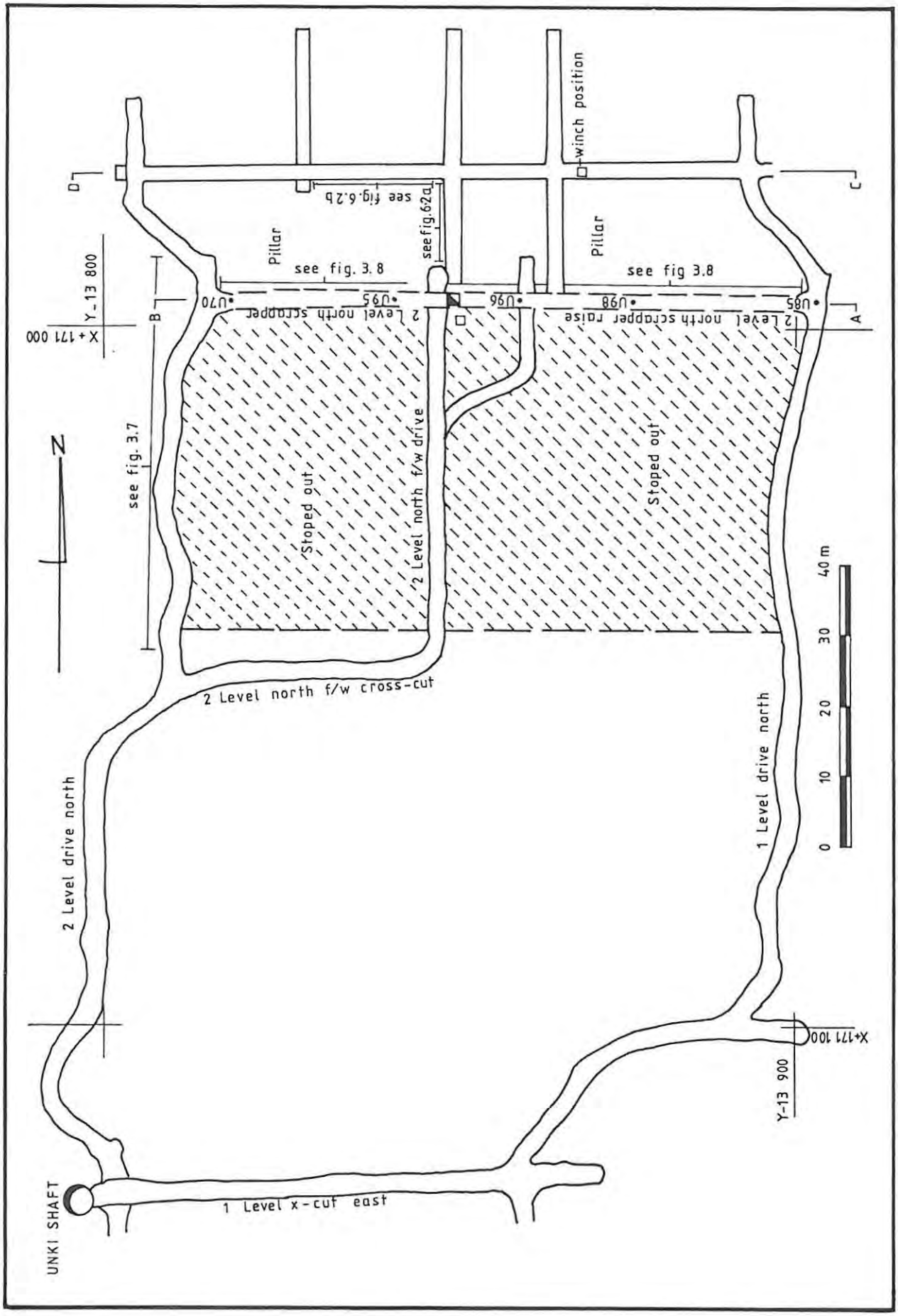

Fig. 3·6 Unki Mine Level Plan, trial stoping 1994/5

established, both features are persistent throughout the Unki workings. The hanging-wall pegmatoid is occasionally transgressive but does not seem to affect the PGE-rich zone. Its adverse effects, if any, can only be determined when full-scale mining begins.

The Footwall Shear undulates along strike and down dip (Figs. 3.7 and 3.8). The undulations appear to be more pronounced along strike where amplitudes of up to 75cm can occur over a distance of 30-50m. The undulations are not apparent from the contour plots of the elevations of the base of the Footwall Shear as observed in drill hole intersections (Fig. 3.9). There is evidence of two phases of movement along the plane of the Footwall Shear. The major displacement of 1.5m is sinistral in the N - S direction (Fig. 3.10). The second but minor phase of movement is in the E - W direction (Fig. 3.11). A system of sub-parallel joints occurs in a zone ± 50cm above and below the shear (Fig. 3.7).

The PGE zone is characterized by the presence of visible sulphides but in varying concentrations. There are three cases noted:

(i) Peak sulphide zone lying 20-40cm above peak PGE zone;
(ii) Peak sulphide zone coinciding with the peak PGE zone; and
(iii) Peak sulphide zone lying ± 20cm below the peak PGE zone.

These distributions correlate well with the three different metal profiles discussed in Chapter 6. The latter case is less common than the other two. However, in all the three cases, the base of the PGE zone corresponds to the base of visible sulphide. In some cases, it is extremely difficult to deduce the zone of maximum sulphide concentration.

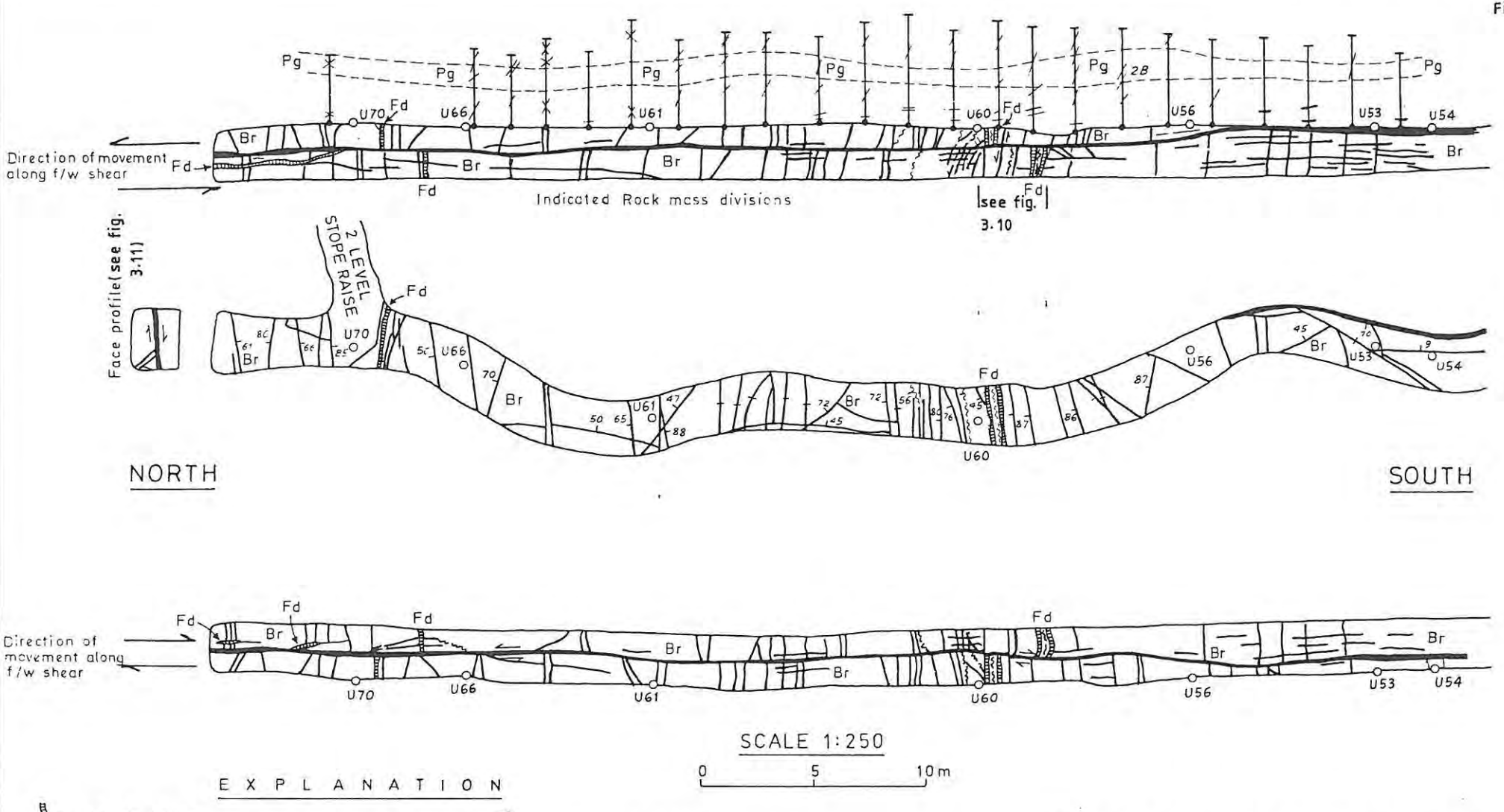

SCALE 1:250

0 5 10 m

EXPLANATION

- Fd Felsic dykes
- Pg Pegmatoid
- Br Bronzitite
- 80 Dip, amount in degrees
- Joints
- Fault gouge with imbricate structures (F/W shear)
- Shear
- Diamond drillhole
- U660 Survey peg

MIDDLERIDGE–UNKI SHAFT

2 LEVEL DRIVE NORTH

Geology — roof and sidewalls

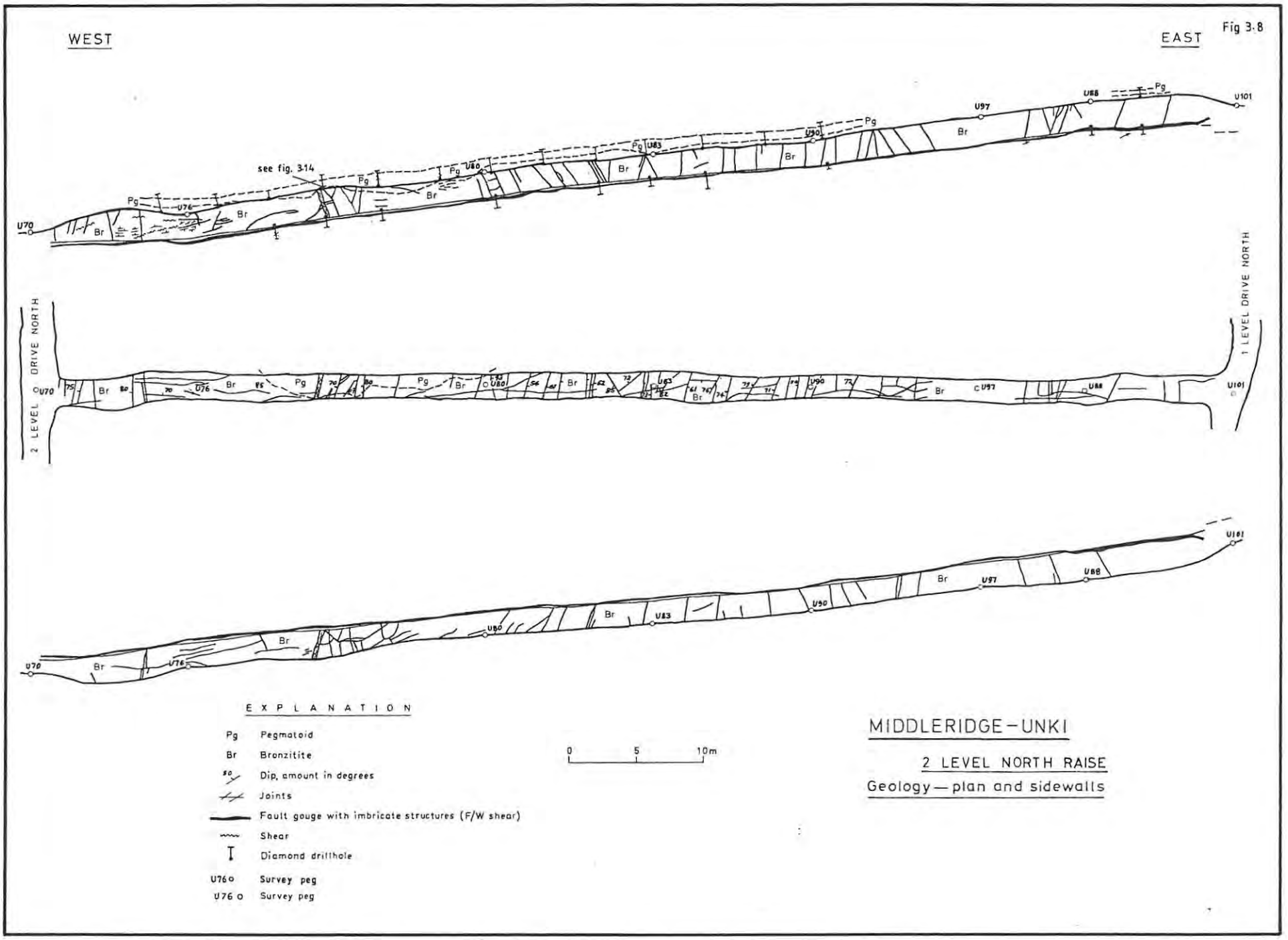
WEST
EAST
Fig 3.8
see fig. 3.14
U70
U76
U80
U83
U90
U97
U88
U101
Pg
Br
2 LEVEL DRIVE NORTH
1 LEVEL DRIVE NORTH
EXPLANATION
Pg Pegmatoid
Br Bronzitite
50 Dip, amount in degrees
Joints
Fault gouge with imbricate structures (F/W shear)
Shear
Diamond drillhole
U76 o Survey peg
U76 o Survey peg
0 5 10m
MIDDLERIDGE – UNKI
2 LEVEL NORTH RAISE
Geology — plan and sidewalls

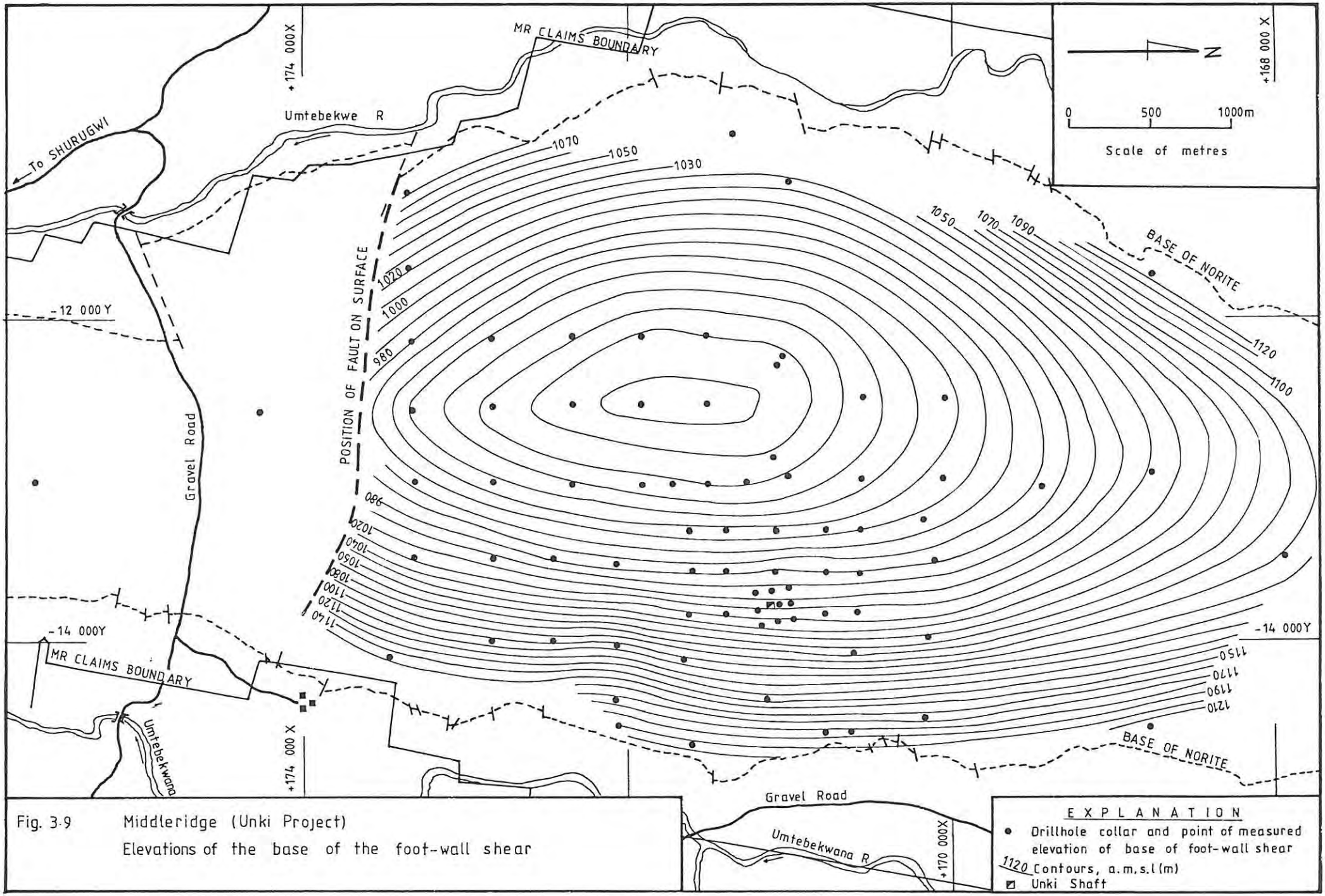

Fig. 3.9 Middleridge (Unki Project)
Elevations of the base of the foot-wall shear

Augite oikocrysts are seen macroscopically as dark blue-green or emerald green, coarse-grained plates on the stope faces. Although these are not restricted to the MSZ, they tend to decrease in size towards the top of the PGE-rich zone. This gradational change is however, not equally manifested on all stope faces. Thus, other than sulphide distinguishing mineralized bronzitite from unmineralized bronzitite, there is no other visible petrographic marker for the miners to follow.

Potholes/washout channels

No potholes or washout channels such as those cited at Mimosa (Prendergast, 1988b) have been encountered in the Unki workings. This does not however, prove their non-existence as the current (1995) underground workings are very limited in extent.

The geomechanical properties of the stopes are discussed separately under section 3.5.4 below.

3.5.4 *Structure and Geomechanics*

Two major E-W subvertical faults form natural boundaries to the north and the south of the Unki area (Fig. 3.3). The area lying in between these two faults is relatively free of major structural disruptions as evidenced by the smooth contour plots of the hanging wall elevations of the top of the PGE zone (Fig. 3.12). However, on a local scale, aerial photographic interpretation combined with underground geochemical mapping, identified three major joint systems, i.e. E-W, N-S and NE-SW. The predominant fracture system is E-W (Fig. 3.13). Tardy felsic dykes ± 15 cm wide, occur as infilling material in some of the major E-W discontinuities (Fig. 3.13). The N-S fracture systems often give rise to step faults with negligible vertical displacements of up to 15 cm (Fig. 3.14). As these step faults are generally spaced at 12 m apart, the possibility of toppling failure from the roof is highly unlikely.

Fig.3.10 Unki stope. Footwall Shear showing sinistral displacement (horizontally) of felsic dykes (fd). [2 level drive north, looking east].

Fig.3.11 Unki stope. Footwall Shear showing drag movement to the east as indicated by arrow. [2 level drive north, face].

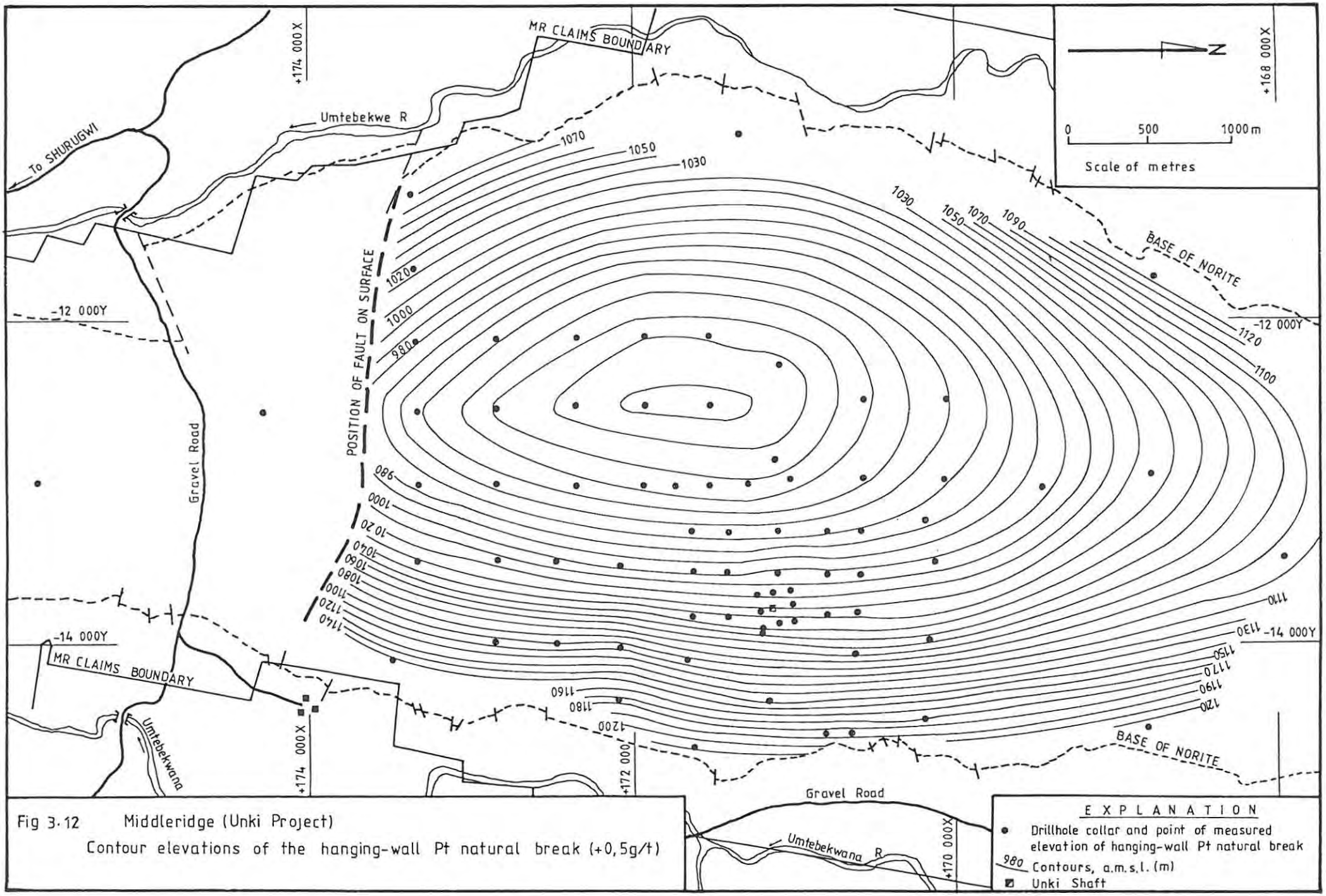

Fig 3.12 Middleridge (Unki Project)
Contour elevations of the hanging-wall Pt natural break (+0,5g/t)

An evaluation of the geotechnical data from underground mapping in the stope (Fig. 3.13) shows three significant poles associated with these joint sets (Fig. 3.15a). The three planes corresponding to the poles are shown on Figure 3.15b and are as follows:

(i) Plane 1 - representing E-W discontinuities which are steeply dipping (+75°) to the north.

(ii) Plane 2 - representing N-S discontinuities dipping east at ± 50°.

(iii) Plane 3 - representing NE-SW discontinuities dipping north-west at ± 70°.

Wedge failure is likely to occur where all three sets of discontinuities combine to form a wedge in the roof. The frequency with which this type of failure will occur is enhanced if the spacing between joints is very close in all three directions. In this regard, it is worth noting that the major N-S and NE-SW discontinuity sets at Unki are widely spaced at > 15 m, and hence, fairly stable conditions should be expected underground. Similar conditions have been observed at Mimosa in the Wedza Subchamber (Prendergast, pers. comm., 1994), whereas at Zinca and Selous in the Darwendale Subchamber, extremely poor ground conditions prevail as a consequence of numerous faults, dykes and sills.

The Footwall Shear at or close to the base of the PGE zone does not pose any safety hazard. Its significance in mining terms is discussed in chapter 6.

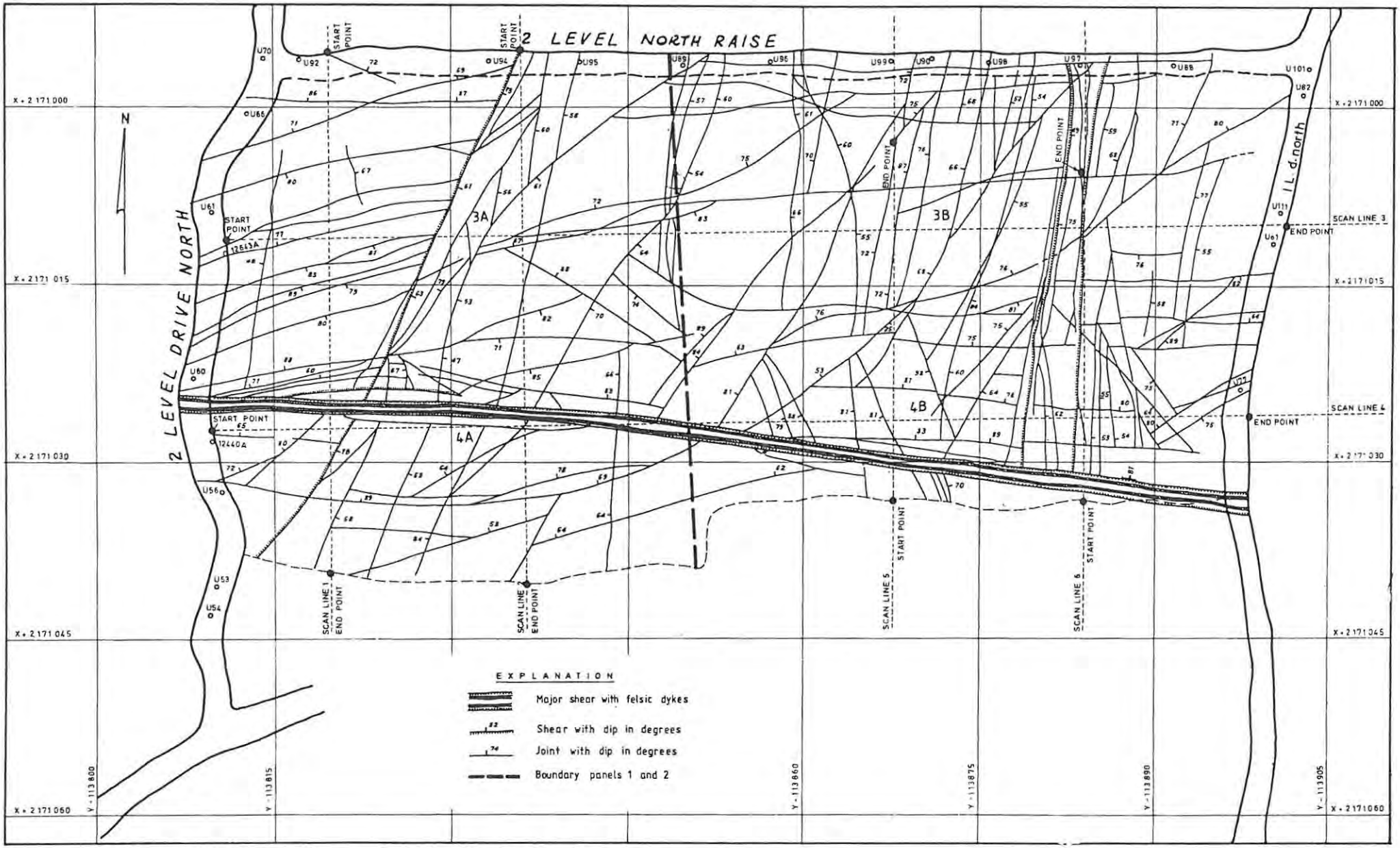

Fig 3.13 Middleridge (Unki Project), Unki stope diagrammatic joint pattern and scanlines

Fig 3.14 Unki stope. Step fault in 2 level north-raise (looking south).

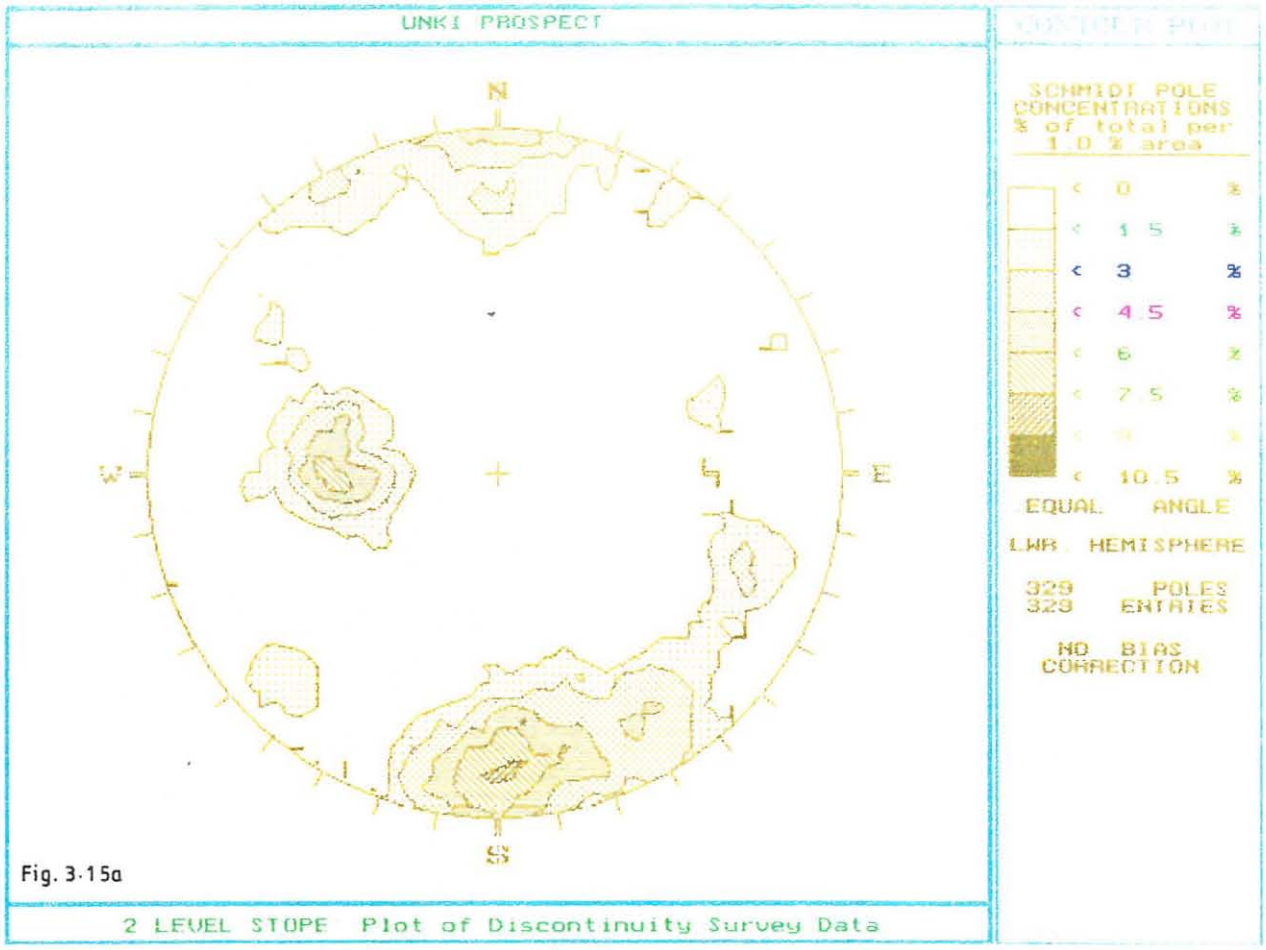

Fig. 3.15a

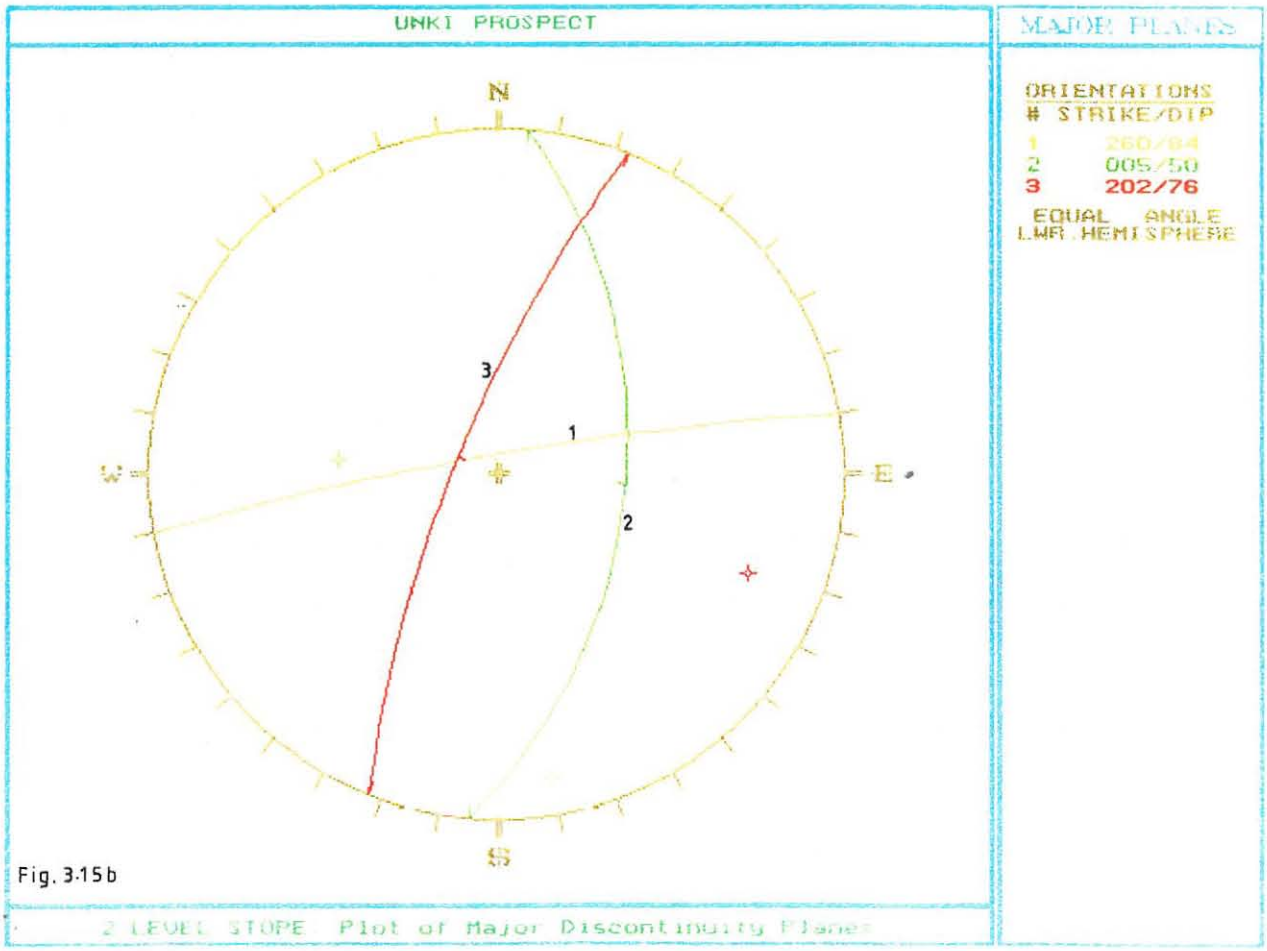

Fig. 3.15b

Chapter 4

PETROGRAPHY AND PETROLOGY OF THE MSZ

4.1 Mineral Assemblage and Textures

The lithology in which the MSZ is hosted is a bronzitite. A modal analysis by point counting (Appendix 1) shows that it consists of between 70 to 98% cumulus bronzite, with subordinate to minor postcumulus augite, plagioclase, quartz, biotite, opaque oxides, and sulphides (Table 4.1). Accessory minerals include apatite, sphene and zircon. The transition from bronzitite to the overlying websterite is relatively gradational over about 30cm and is marked by the appearance of augite as a distinct cumulus phase.

Throughout the MSZ and the whole bronzitite unit in general, augite occurs as postcumulus oikocrysts, often with well-developed crystal faces. The enclosed bronzite crystals are characteristically highly irregular, embayed, and rounded because of reaction (Fig. 4.1). This reflects that the orthopyroxene and clinopyroxene are not in equilibrium. Embayed and rounded orthopyroxene crystals are not observed outside the oikocrysts. Similar textures have been noted in the Stillwater Complex (Jackson, 1961).

Plagioclase is an important postcumulus phase and occurs as irregular grains up to 60mm in diameter enclosing several bronzite grains including some of the augite oikocrysts. These plagioclase oikocrysts are responsible for the formation of the nodular pyroxenite which is informally referred to as the "potato reef". A single plagioclase oikocryst may form a nodule but in most cases a cluster of several oikocrysts constitute a single nodule. Plagioclase oikocrysts are restricted to near the boundary of the bronzitite and websterite of the P1 layer, in the uppermost section of the MSZ. The plagioclase is weakly zoned

TABLE 4.1 Modal Analysis of MSZ profile in Drill hole MR126 by Point Counting

SAMPLE NO	Opx	Cpx	Pl	Alt	Bi	Sd	Mt	Tot %
MR126/38	74	4	10	2	3	4	3	100
MR126/39	73	5	8	5	2	5	2	100
MR126/40	75	5	6	4	1	7	2	100
MR126/41	73	7	5	4	2	6	3	100
MR126/42	74	4	5	7	3	4	3	100
MR126/43	72	4	5	11	2	4	2	100
MR126/44	69	5	3	15	3	2	3	100
MR126/45	73	5	5	8	5	2	2	100
MR126/46	75	5	6	9	2	1	2	100
MR126/47	81	3	5	6	3	Tr	2	100
MR126/48	83	4	7	3	2	Tr	11	100

Abbreviations:

Opx orthopyroxene
Cpx clinopyroxene
Pl plagioclase
Alt alteration
Bi biotite
Sd sulphide
Mt magnetite
Tot total
Tr trace

N.B. Sample numbers are in descending order from 40cm above PGE-rich zone to its base.

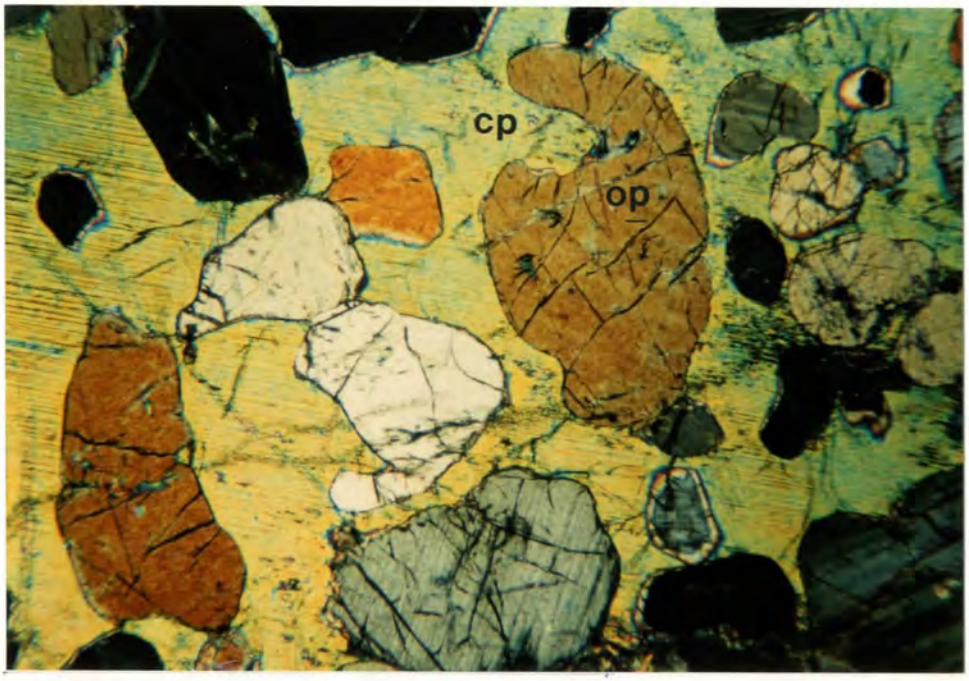

Fig.4.1 Augite oikocryst (cp) showing reacted and corroded bronzite (op) [Crossed polars, objective 2,5]

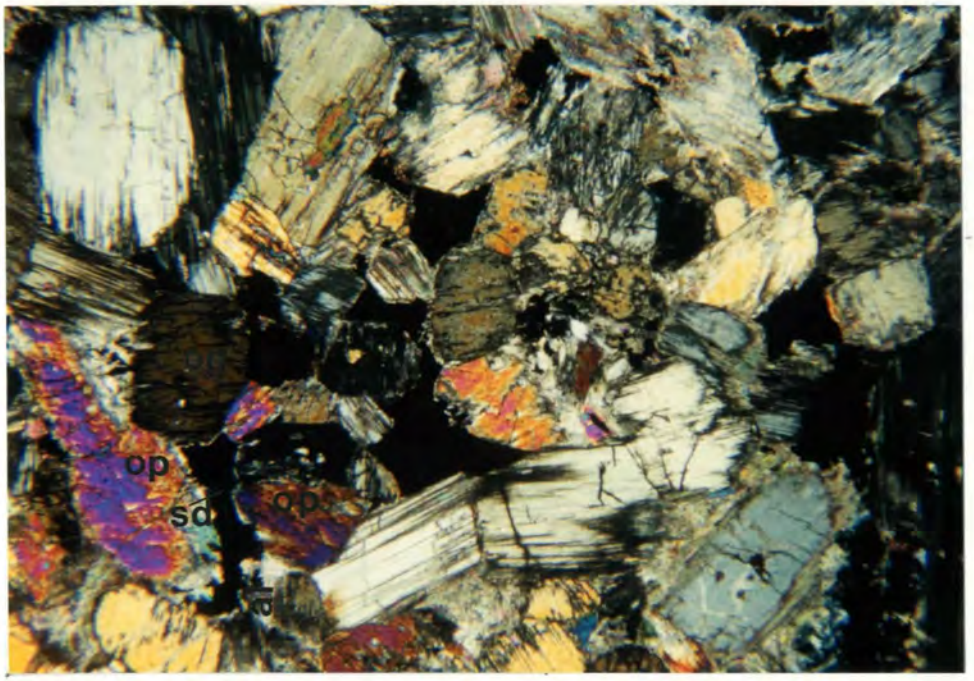

Fig.4.2 Cumulus bronzite (op) forming a local mesostasis with sulphide (sd) and alteration (al) as discussed in text. [Crossed polars, objective 2,5]

towards the contact with enclosed cumulus orthopyroxene grains, but the zoning becomes progressively more pronounced towards the margins of the plagioclase crystals. This indicates that in the central part of the nodules, the plagioclase was close to the primary liquidus composition, whereas towards the margins, crystallization was largely controlled by the evolved trapped liquid (Wilson, 1992). The margins of the nodules appear prone to weathering due to the strongly zoned plagioclase and the assemblage of late-stage minerals including sulphide. Weathering gives rise to subspherical structures which result in the characteristic nodular appearance of this rock type.

Wilson (1992) has drawn attention to the fact that the zoning pattern in the plagioclase and the distribution of the clinopyroxene oikocrysts indicates that these postcumulus crystals may not have formed entirely by crystallization of the trapped intercumulus liquid, but instead largely in an open system linked to the parent magma body (i.e.,as heteradcumulus phases). The eventual enlargement of the oikocrysts would have resulted from the trapped liquid which also gave rise to the assemblage of low-temperature minerals.

Sulphides occur throughout the MSZ with modal proportions varying between 7% and less than 0,1% (at least in the type section represented by drill hole MR126 - see Fig. 3.3). The sulphide grains are relatively large (0,15 - 3mm in diameter) where the modal proportions are between 1 and 7%, giving rise to a net texture. There is evidence of a strong association of sulphide with alteration (Fig. 4.2). The interstitial nature of the sulphides suggests that they may have displaced trapped liquid. In some zones there is evidence of remobilisation of sulphide on a micro-scale culminating in the inclusion of sulphide particles within altered pyroxene and along cleavages (Figs. 4.3 and 4.4). However in other zones, limited amounts of sulphide with lobate to cuspate shapes are enclosed within unaltered cumulus pyroxene and in the unzoned portions of the plagioclase and clinopyroxene oikocrysts. This is indicative of early sulphide liquation and entrapment (Wilson, pers.comm., 1995).

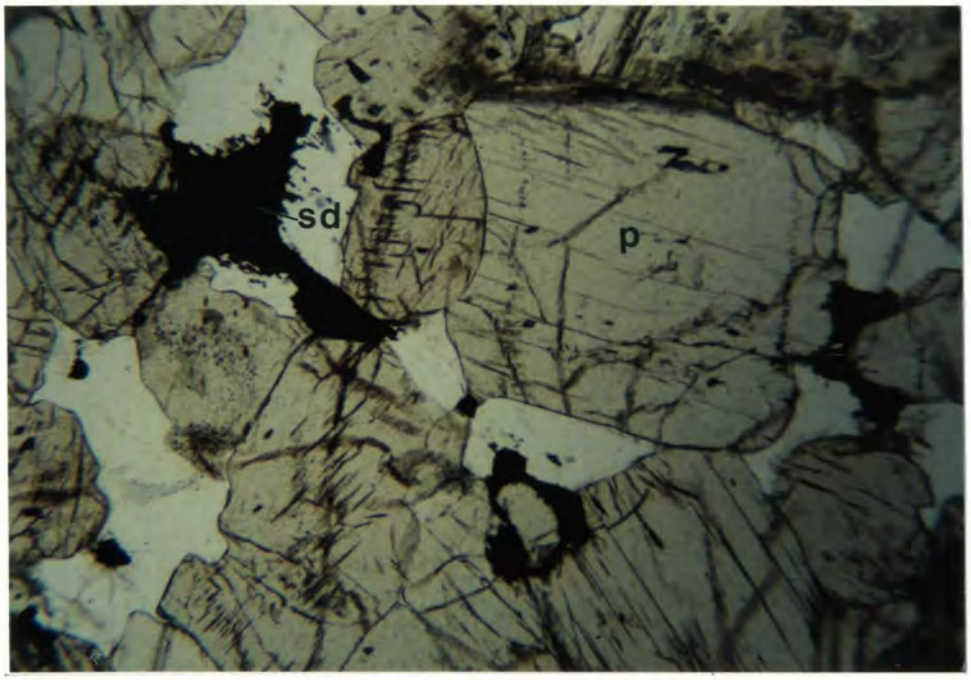

Fig.4.3 Interstitial sulphides (sd) and sulphide inclusions (seen as black specks) within altered pyroxene (p) as discussed in text.
[Plane polarised light, objective 2,5]

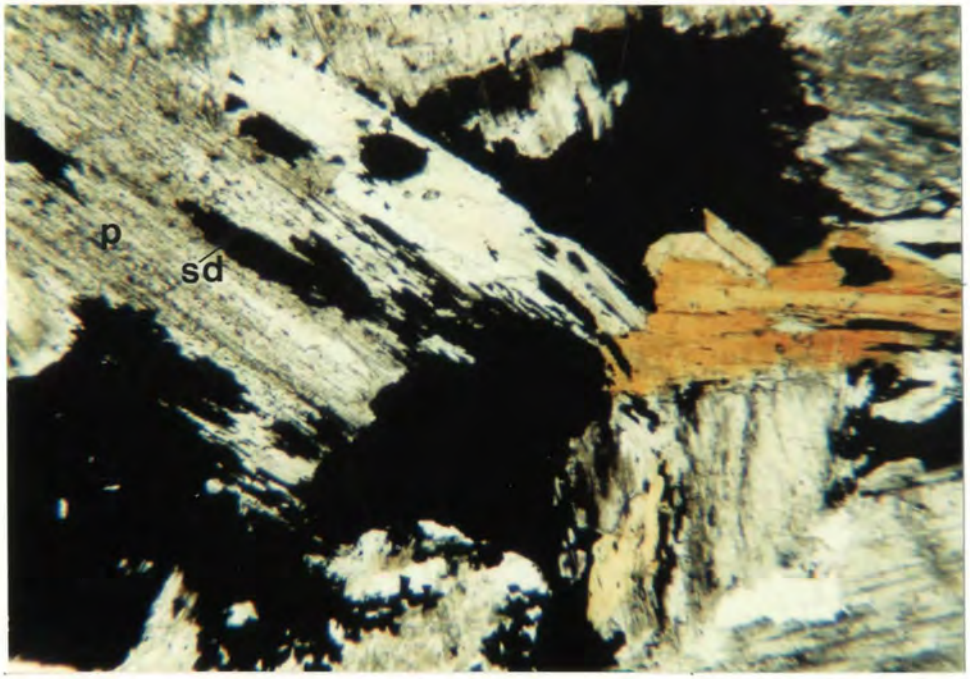

Fig.4.4 Redistribution of sulphide (sd) within altered pyroxene (p) as discussed in text.
[Plane polarised light, objective 6,3]

The minor postcumulus minerals which include quartz, alkali feldspar, albite, iron oxides, phlogopite and apatite, are thought to have crystallized from trapped late-stage liquid (Wilson, 1992) and appear to be more prevalent in the MSZ than lower down in the P1 layer. Some of these minerals have skeletal to micrographic intergrowth textures. These forms are depicted in Figures 4.5 to 4.8.

4.2 Origin of Primary Textures

The primary textures discussed here are those that relate largely to the distinction and status of cumulus and intercumulus phases.

4.2.1 *Cumulus phases*

The cumulus texture throughout the MSZ is orthocumulate to mesocumulate with an intercumulus volume varying between 10 and 30%. The main cumulus phase is bronzite which takes different forms according to the minerals with which it is in contact. Cumulus bronzite crystals which are in contact with plagioclase have euhedral shapes (Fig. 4.9). The contact relationships between bronzite and postcumulus augite vary from embayed to irregular and interfingering (Fig. 4.10). Based on these textural relationships, the sequence of crystallization for the main mineral phases are deduced as follows:

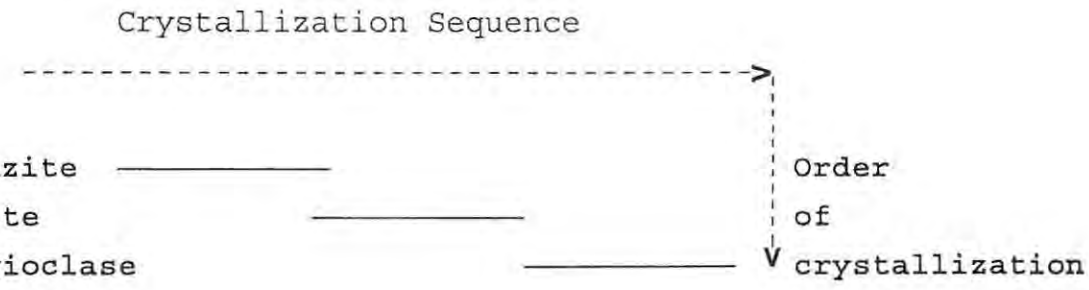

Reaction replacement is reflected by embayed, sutured or irregular contact relationship between two different minerals

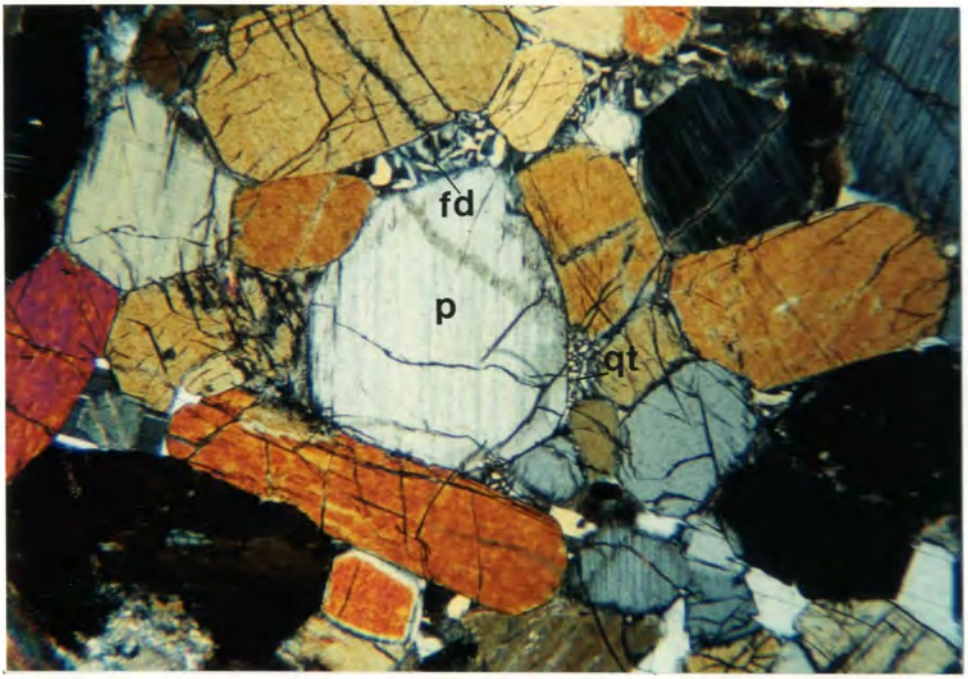

Fig.4.5 Pocket of postcumulus quartz (qt) and K feldspar (fd) surrounding a rounded pyroxene (p) crystal.
[Crossed polars, objective 2,5]

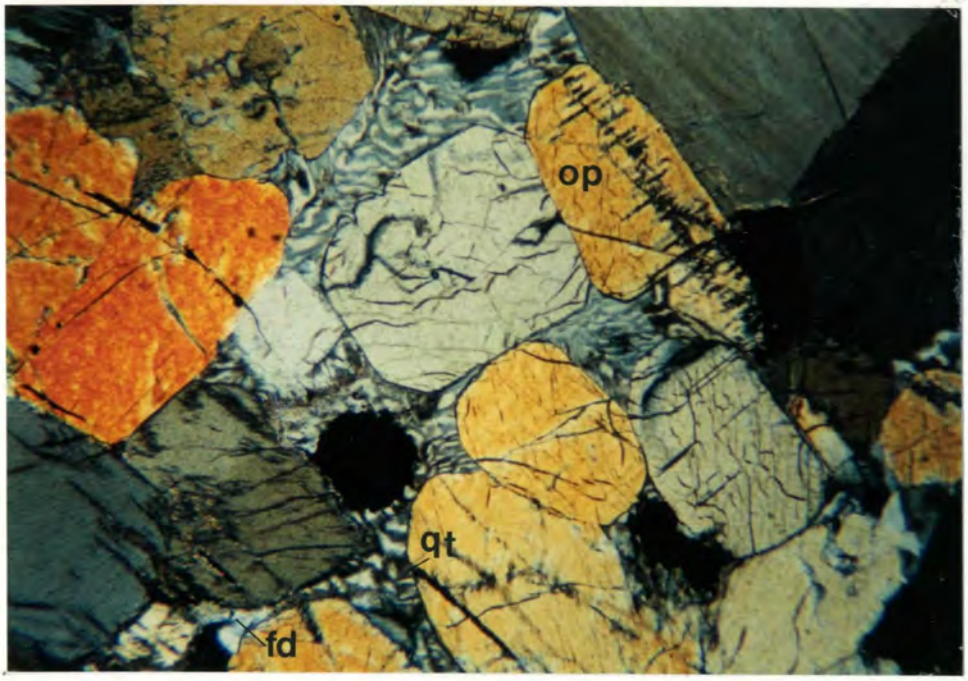

Fig.4.6 Interstitial micrographic quartz (qt) with fluid inclusions and minor altered feldspar (fd). Note exsolution lamellae in bronzite (op) as described in text.
[Crossed polars, objective 2,5]

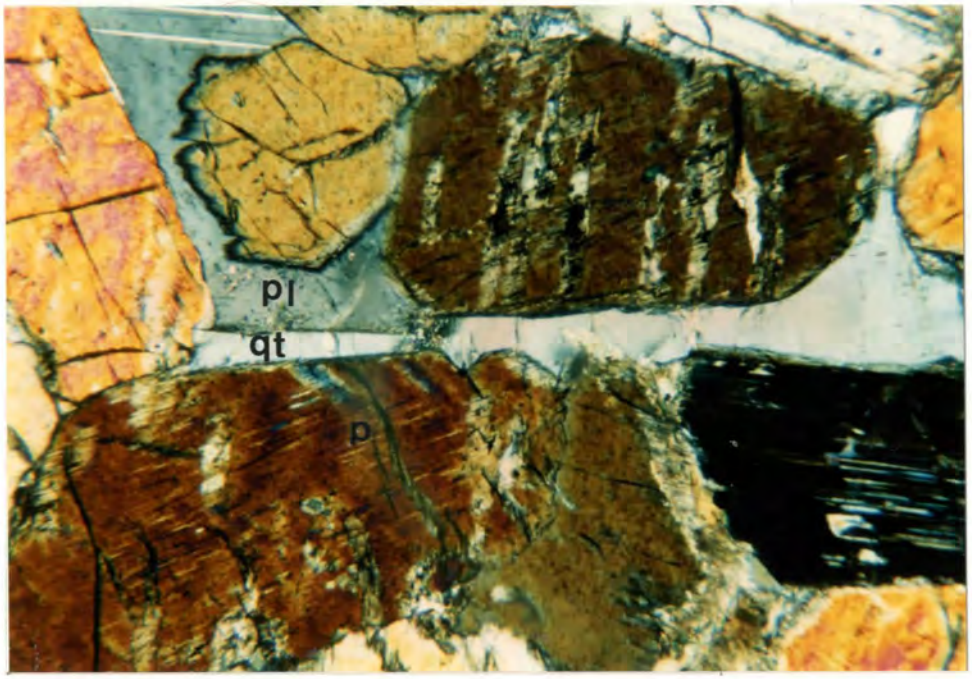

Fig.4.7 A sliver of quartz (qt) between plagioclase (pl) and pyroxene (p). [Crossed polars, objective 2,5]

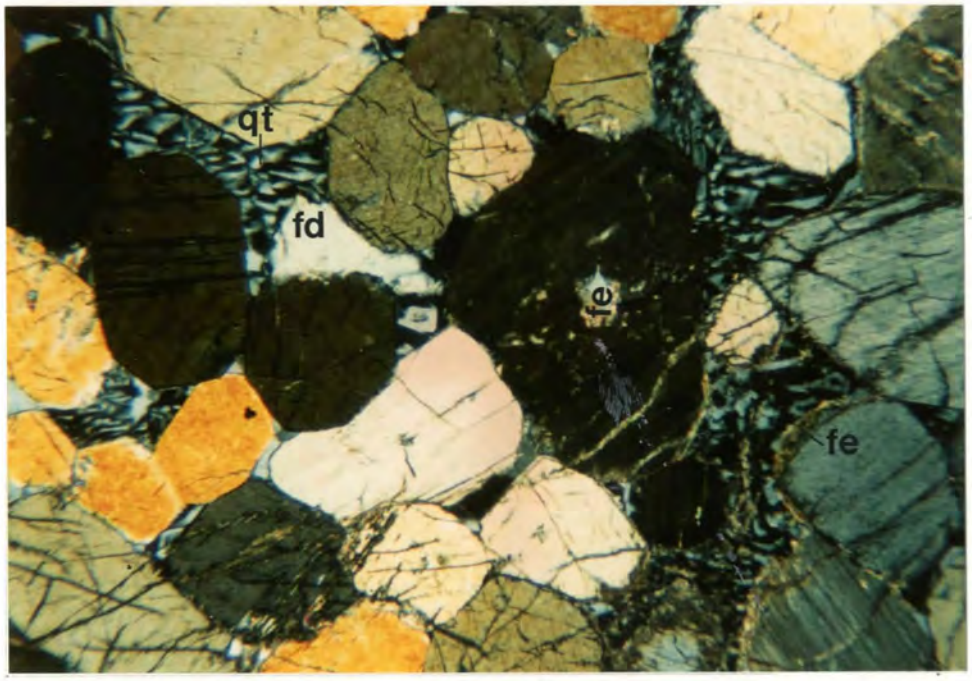

Fig.4.8 Micrographic intergrowth textures comprising quartz (qt), feldspar (fd) and iron oxides (fe)
[Crossed polars, objective 2,5]

(Fig. 4.1). However, the same structures may also exist between two grains of the same mineral species, indicating mutual interference during crystallization .

Exsolution of augite is not common in the cumulus bronzite crystals but does occur as fine lamellae of exsolved diopside parallel to (100) (Fig. 4.6). Small rounded inclusions of augite nucleii are prevalent in the upper zone of the MSZ, close to the contact with the overlying websterite layer.

Sulphide inclusions occur within unaltered cumulus pyroxene and in the unzoned portions of the plagioclase and clinopyroxene oikocrysts, and these may represent liquid droplets of magmatic sulphides that were co-precipitated and included at the time of pyroxene crystallization. These inclusions of sulphide testify to the early formation of this phase and may thus also be considered to be of cumulus status.

4.2.2 *Intercumulus phases*

Plagioclase oikocrysts form the dominant intercumulus phase. Some zoning is evident at the margins of the oikocrysts, reflecting a state of equilibrium between the plagioclase and magma during postcumulus growth. Augite oikocrysts are an important feature of the MSZ and often contain smaller orthopyroxene grains (Fig. 4.10) as compared to those enclosed in plagioclase. This implies that (i) clinopyroxene predated plagioclase in postcumulus crystallization, and (ii) post-cumulus growth of orthopyroxene has occurred in the bronzitite.

4.2.3 *Significance of Primary Textures*

Although the features discussed above are based on the study of limited samples from one drill hole intersection, similar textural features have been noted elsewhere on the Great Dyke (Evans and Buchanan, 1991; Prendergast, 1990; Wilson, 1992; Coghill and Wilson, 1993). The cumulus status of some of the

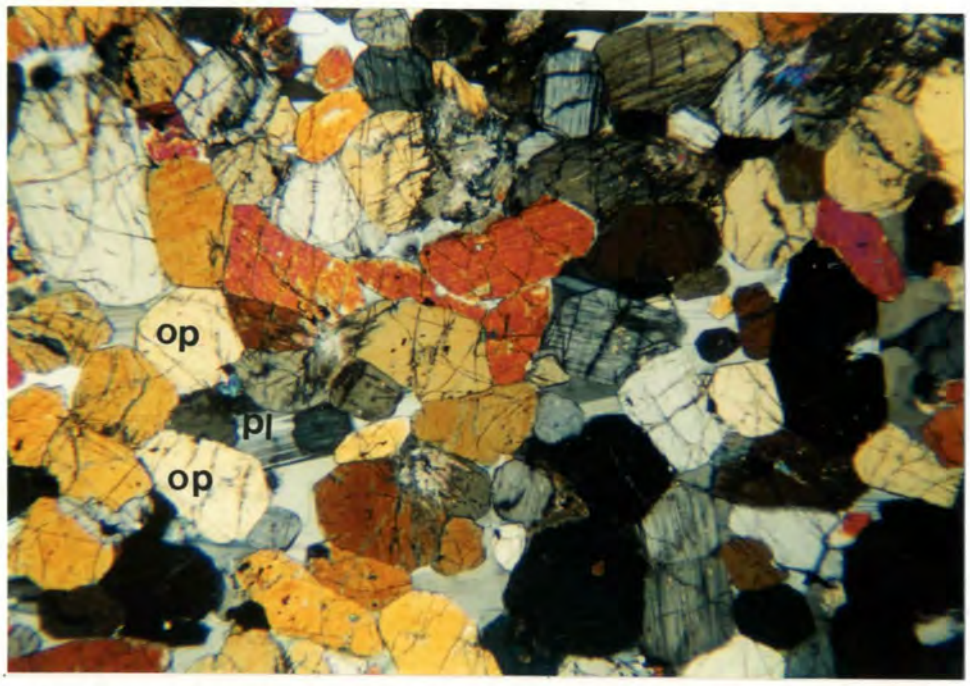

Fig.4.9 Feldspathic pyroxenite with euhedral bronzite (op) in contact with plagioclase (pl) as described in text. [Crossed polars, objective 5]

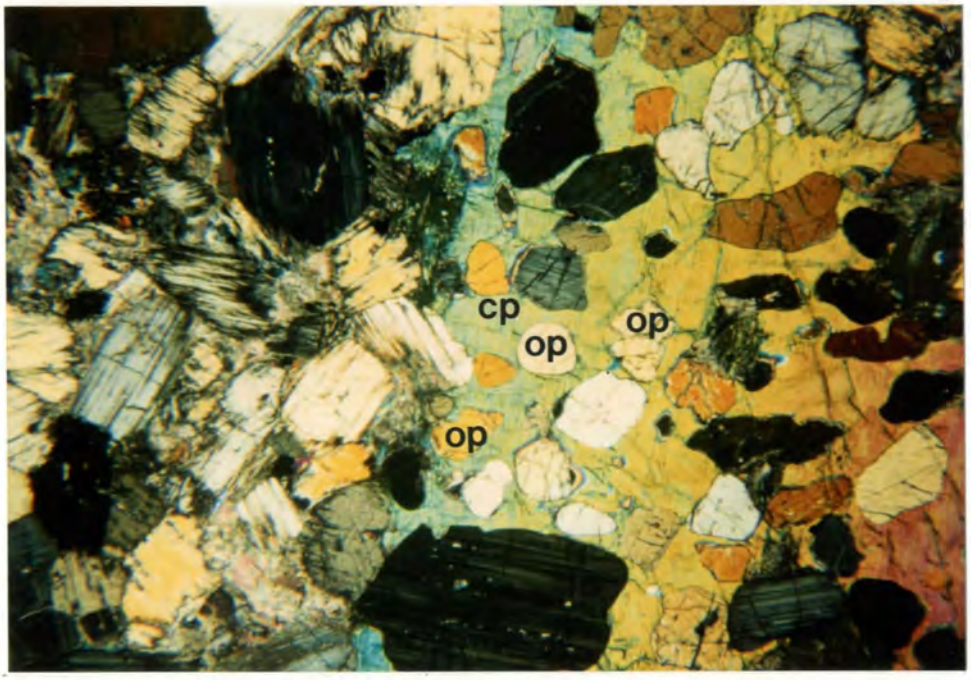

Fig.4.10 Boundary of altered zone (al) with oikocrysts (cp) showing no alteration. Note various forms of bronzite (op) as described in text. [Crossed polars, objective 5]

sulphides provides unequivocal evidence for an orthomagmatic origin of the MSZ. The inclusions of augite nuclei that are prevalent in the bronzites of the upper MSZ, reflect that the change from bronzitite into the overlying websterite layer is gradual rather than abrupt. This is consistent with fractionation.

4.3 Secondary Textures

4.3.1 *Postcumulus Phases*

Postcumulus phases embrace all the late-stage crystallization products of trapped pockets of liquid. They can also be referred to as interstitial phases and include mineral assemblages of quartz, biotite, K-feldspar, and opaques in the form of sulphides and oxides. Associated with these but less common are the accessory minerals sphene, apatite and zircon, and hornblende. The accessory minerals (sphene and zircon) are, however, not confined to the MSZ but are ubiquitous throughout the P1 layer. They assume euhedral shapes in the interstices of cumulus grains.

As already mentioned, most interstitial phases have skeletal to micrographic intergrowth textures (see Figs. 4.5 to 4.8). Primary amphibole hornblende is rare and, when present, occurs as overgrowths on pyroxenes by reaction with the hydrous component of late-stage trapped liquid. The opaque minerals form skeletal intergrowths with plagioclase biotite and altered pyroxenes.

4.3.2 *Alteration*

Alteration within the MSZ is a prominent feature which is marked by the replacement of primary silicate minerals by secondary hydrosilicates and also by the progressive obliteration of primary magmatic sulphide-silicate textures. It is important to ascertain at what stage this alteration took place. A typical largely altered zone consists of an intergrown mass of sulphides,

magnetite, biotite, tremolite and talc, plus minor chlorite, hornblende, quartz, carbonate, epidote, fine-grained secondary magnetite and apatite (Figs. 4.11). Circular and radial structures of alteration are prevalent (Figs. 4.12 and 4.13). The hydrosilicates impart a local dark discoloration that is superficially similar in appearance to a serpentinized zone.

In most cases, orthopyroxene is more altered than clinopyroxene. Bronzite is altered to tremolite and talc, whereas augite is replaced by actinolite. It is suggested that biotite and tremolite are indicative of a high temperature, late-magmatic component of the alteration assemblage. Base-metal sulphide-biotite-tremolite-magnetite intergrowths are a common feature (Fig. 4.2). Similar textures have been observed in the Wedza Subchamber (Prendergast, 1990) and in the Sebakwe Subchamber (Evans and Buchanaan, 1991). The more pervasive replacement of primary silicates and early formed hydrosilicates by fine-grained talc and chlorite (Fig. 4.14) represent a lower-temperature, sub-solidus, deuteric phase of alteration.

4.4 Secondary Processes

Three main stages of postcumulus processes can be identified from textural and petrographic observations as previously noted in the Zinca area (Sebakwe Subchamber) by Evans and Buchanan (1991). Stage 1 is represented by the early stages of postcumulus solidification which involves the crystallization of poikilitic clinopyroxene and plagioclase followed by hydrous interstitial phases (biotite, quartz, K-feldspar, etc.) The resultant orthocumulate textures with an abundance of late-magmatic hydrous minerals are evidence that a residual, volatile-enriched melt was trapped as an interstitial phase. The entrapment mechanism can be explained in terms of a greater rate of cooling or by the reduction of permeability in the crystal framework above the level of the MSZ (Evans and Buchanan, 1991).

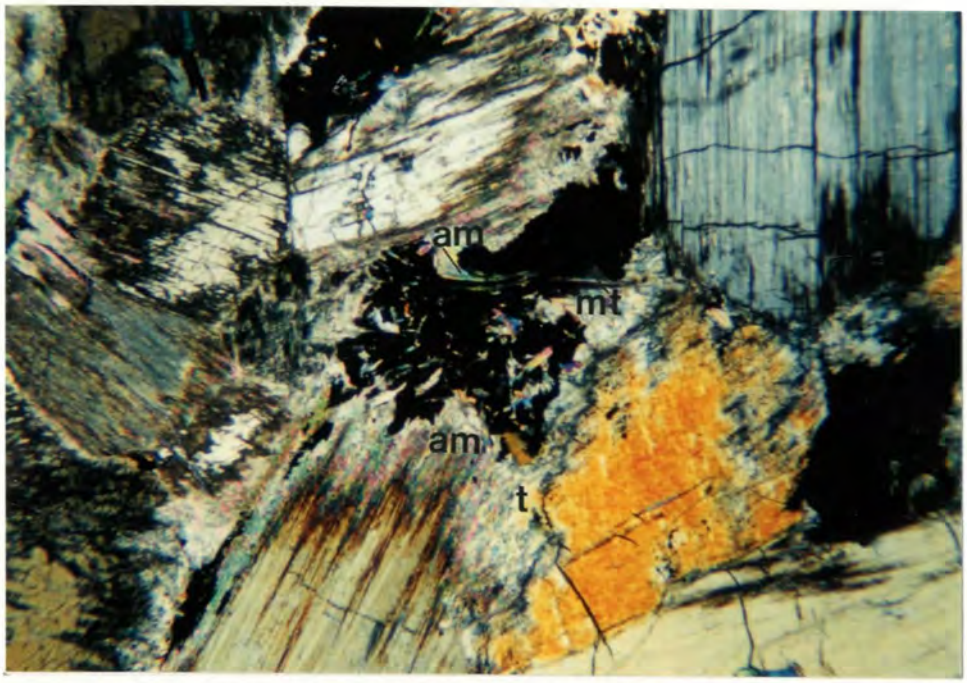

Fig.4.11 Fibrous amphibole (am), some talc (t) and secondary magnetite (mt) within altered pyroxenite of the MSZ as discussed in text.
[Crossed polars, objective 2,5]

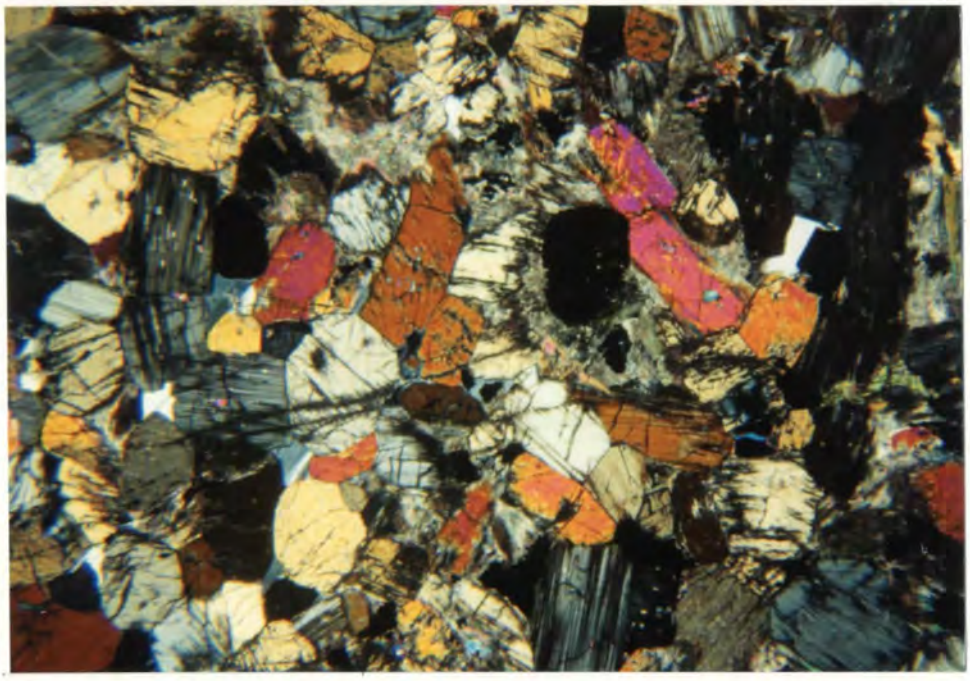

Fig.4.12 Circular structure of alteration within pyroxenite of the MSZ as discussed in text.
[Crossed polars, objective 2,5]

Stage 2 relates to sub-solidus and alteration processes. It is a complex stage as evidenced by the contact and reaction relationships between mineral grains (Section 4.2) and the ubiquitous hydrous alteration of pyroxenes to secondary amphiboles throughout the MSZ. This amphibole alteration is generally isochemical and isostructural with respect to the pyroxene host (Evans and Buchanan, 1991).

The third and final stage of postcumulus events overprints earlier textures of alteration (Figure 4.14). Fibrous amphibole and random blades of talc penetrate pyroxenes with no regard to crystallographic orientation and are better developed along and adjacent to horizontal fractures.

4.5 Significance of Secondary Textures and Processes

The secondary textures of the MSZ provide clear evidence that the original cumulate mush was subjected to substantial postcumulus modification during subsequent cooling and solidification. Although the primary mineralizing events were orthomagmatic, the presence of hydrosilicate alteration is conclusive evidence for the involvement of a high temperature volatile fluid, at least on a micro-scale, in the last stages of the development of the MSZ (Coghill and Wilson, 1993; Prendergast, 1990).
At Mimosa in the Wedza Subchamber, hydrosilicate alteration is most intense in the marginal facies of the subchamber and very limited in the axial region (Prendergast, 1990). This has been attributed to the concentration of volatiles towards the margins. In the Darwendale Subchamber the distribution of late-stage mineral assemblages is heterogeneous although it is overall much greater in the marginal facies than in the axis of the Darwendale Subchamber (Wilson, 1992). The Unki drill hole intersection used in this study is from the axial facies and clearly demonstrates that hydrosilicate alteration is not restricted to the margins of the Selukwe Subchamber, but there may be differences related to the larger subchambers. The strong association of sulphide with alteration may be attributed to reactions between highly

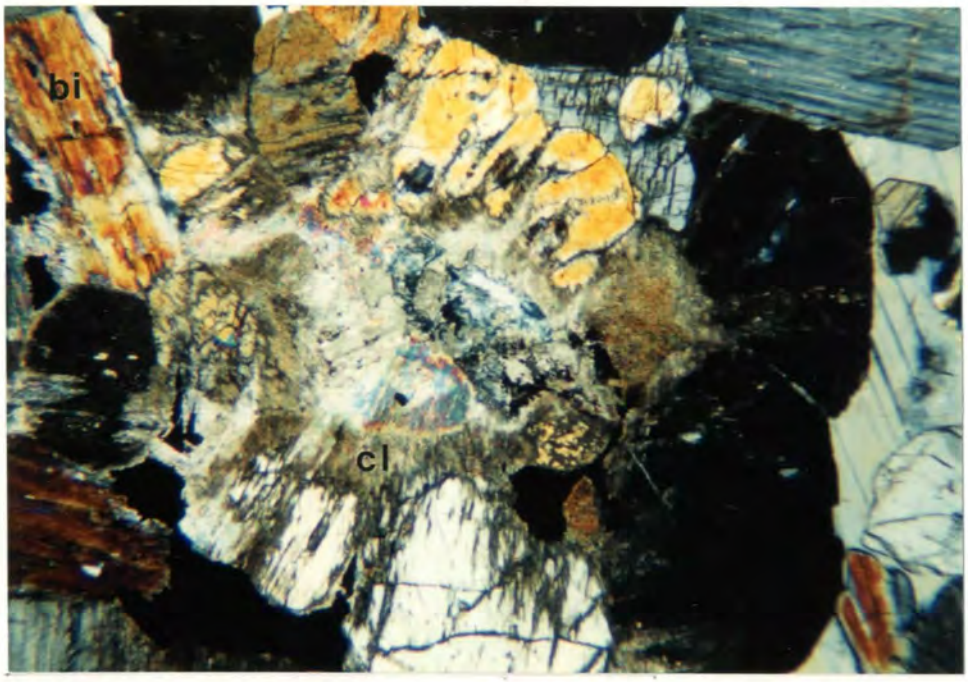

Fig.4.13 Radial alteration within pyroxenite of the MSZ (bi = biotite, cl = chlorite) [Crossed polars, objective 2,5]

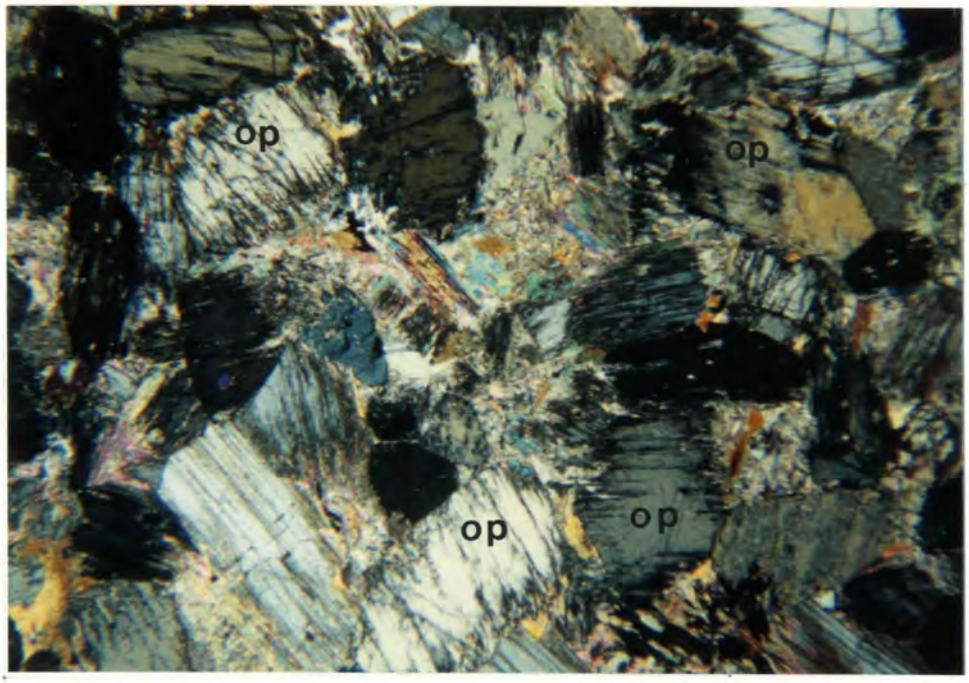

Fig.4.14 Pervasive alteration of orthopyroxene (op) in the bronzitite of the MSZ [Crossed polars, objective 2,5]

reactive sulphuric acid-enriched fluids generated from sulphide liquid and volatile late-stage interstitial liquids.

4.6 PGE Mineralogy and Occurrence within the MSZ

4.6.1 *Introductory Statement*

The knowledge of PGE mineralogy in general (see section 1.3) has advanced significantly in recent years mainly due to the application of electron microbeam techniques. The information provided under this section is based on SEM-EDS and electron microprobe analyses by Anglo American Research Laboratories (Pty) Ltd (RSA) on three MSZ drill core intersections from the Unki Area on behalf of Anglo American Corporation, Zimbabwe. The three drill holes represent the marginal zone (drill hole U4), the axial zone (drill hole MR 51) and the intermediate zone (drill hole U12) - (see Fig. 3.3 for locations). The relevant detail pertaining to these samples is given in Table 4.2. The techniques are given in appendix 2.

4.6.2 *Platinum Group Minerals (PGM): Phases and compositions*

Four principal PGM phases were identified in the four drill hole intersections (Fig. 4.15a):

(i) Arsenide (Sperrylite group) $PtAs_2$ - 61%
(ii) Tellurobismuthide (Moncheite-Maslovite group)
Pt Pd Bi Te - 30%
(iii) Sulphide Pt Pd S - 7%
(iv) Alloy Pt Fe - 2%

These results highlight the importance of tellurobismuthides as Pt- and Pd- bearing phases. Typically, Pt is associated with arsenides, tellurides and sulphides, Pd with bismuthides and sulphides, and Rh with arsenides. There is no obvious difference in the distribution of phases between the axial and marginal facies. Similar phases have been identified at Mimosa, Wedza Subchamber (Prendergast, 1990). Compared to other occurrences,

Table 4.2 Samples submitted for mineralogical examination

Drill Hole No.	Sample No.	Depth (m)	Pt (ppm)	Pd (ppm)	Cu (%)	Ni (%)
MR51	17579A	254,7	5,40	2,04	0,32	0,45
MR51	17580A	255,6	2,79	2,55	0,04	0,06
U12	17581A	211,6	1,70	0,80	0,30	0,40
U12	17582A	211,8	4,20	2,10	0,16	0,20
U12	17583A	212,5	2,50	3,30	0,14	0,21
U4	17584A	72,5	2,00	0,08	0,21	0,28
U4	17585A	72,7	4,80	2,50	0,18	0,19

Table 4.3 Estimated Abundances (%) of Discrete PGM in Unki, Kromdraai, Uitkomst, and Merensky Reef (M.R.) Deposits (Boshoff, 1993)

PGM TYPE	UNKI	KROMDRAAI	UITKOMST	M.R.
Metal	2	-	-	major
Sulphide	7	13	<1	major
Arsenide	61	56	2	minor
Antimonide	-	20	13	-
Tellurobismuthide	30	6	82	-

(Boshoff, 1993), Unki is far more similar to Kromdraai (NW Cape) than it is to the Merensky Reef because the latter has a dominant metal-sulphide phase, whereas the former is dominated by an arsenide phase analogous to Unki (Table 4.3). The dissimilarity with the Merensky Reef holds important clues to the genetic model (see chapter 7).

The base-metal sulphides (BMS) with which PGE are associated, are, (in order of abundance), pyrrhotite, pentlandite and chalcopyrite (Fig. 4.15b). Although the BMS are concentrated at or close to the top of the PGE zone, there is no apparent preference of association of PGM phases to any particular sulphide. The distribution of PGM phases through the MSZ profile has not been fully investigated. It can only be assumed that the arsenide-sulphide-telluride phases are greatest at peak Pt zones while bismuthides are in greater abundance at peak Pd zones.

4.6.3 *Occurrence, Textures and Mineral Associations*

The PGE in the MSZ at Unki have been identified in three different textural environments based on the three drill hole intersections examined i.e. U4, U12 and MR52 (Fig. 3.3).

(i) at the contacts between BMS and adjacent silicates or hydrosilicates ($\pm$80%),
(ii) wholly enclosed within BMS ($\pm$10%), and
(iii) wholly enclosed within gangue, i.e. silicates or hydrosilicates ($\pm$10%).

In the latter two cases, the PGE mostly occur near the periphery of the host grain. At the commonest site of occurrence, (i.e. the contact zone between BMS and gangue), the PGE are either (a) intergrown into the silicate and sulphide minerals, or (b) not intergrown with but in contact with the sulphide, or (c) confined to sulphide boundaries. A significant feature of these textures is the observation that the boundaries of PGE are irregular against hydrosilicates but euhedral against BMS. The presence

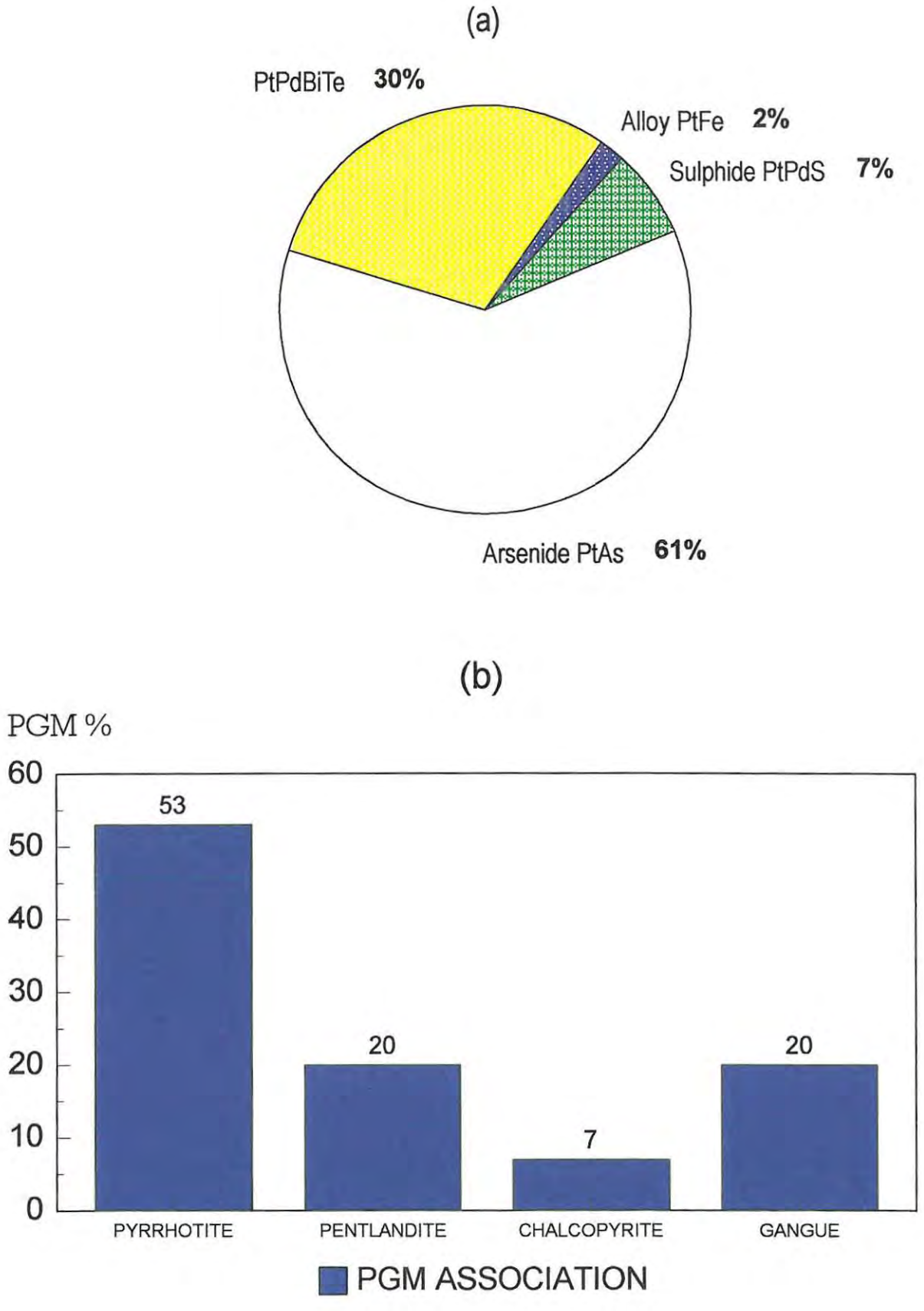

Fig. 4.15: PGM Distribution (a) and host mineral association (b) for the Unki deposit. (After Boshoff , 1993)

of BMS in veins along with talc suggests a certain degree of redistribution of sulphides. Trace amounts of chromite, ilmenite, titanium-oxide, haematite and magnetite occur in association with BMS but no PGE are linked with these oxide minerals.

Discrete PGE grains from the MSZ at Unki are in the range 5 to 30μm, with the largest up to 90μm in length. Generally, the PGE entirely enclosed within silicates are finer grained than those associated with sulphides. The variations in grain sizes and textures are to be expected in view of the fact that the BMS and PGE formed over a very wide temperature range.

4.6.4 *Mineralogical Significance on Metallurgy*

Mineralogical characteristics of the Unki deposit have important implications for the metallurgical treatment of the ore. These characteristics are as follows:

(1) The dominant BMS is pyrrhotite (Fig. 4.15b) which is known to be a slow floater. This may adversely affect recoveries and concentrate grades unless sufficient conditioning time is given, and the sulphides are not over milled.

(2) The greater percentage of the BMS is fairly coarse and should be easily liberated as they are situated at the edges of silicate minerals. Excessive milling is not necessary.

(3) The fine BMS in talc-rich areas and those entirely enclosed within silicate grains may be difficult to liberate. Firstly, the presence of talc on its own is an unfavourable factor, since talc is known to float and cause low concentrate grades. If talc flotation is suppressed, some of the PGM associated with it, if not liberated during grinding, might be lost to the tailings fraction. Secondly, while grinding may liberate the fine BMS enclosed within silicate grains, the flotation of fine-grained particles will be a crucial factor.

Chapter 5

GEOCHEMICAL CHARACTERISTICS

5.1 General statement

Geochemistry provides important information on the evolution of layered igneous successions both from the variation of major elements by virtue of the dominant mineral phases, but also the trace elements which provide information on liquid compositions and controlling mechanisms. A major limitation in the study of geochemical trends of cumulate sequences is that liquid compositions are rarely, if ever, preserved. The cumulate assemblage is, by definition, an extract from the liquid with only a relatively small component of trapped liquid (usually between 0 - 20%) (Brown, Hawkesworth, Wilson, 1992). In addition, there is a wide range of subliquidus processes that will affect the distribution of trace elements (Wilson, 1992). These include:

(1) continued growth of the cumulus crystals from the trapped liquid resulting in more evolved phase compositions than the liquidus composition;
(2) re-equilibration of the primary cumulus crystals with the trapped liquid as well as the more evolved growth component;
(3) subsolidus re-equilibration between the phases;
(4) reaction and replacement of liquidus and subliquidus phases with late-stage hydrous fluid resulting in the replacement of primary phases with secondary, usually hydrous, minerals.

All of these processes will occur to a lesser or greater extent and their evaluation is complex and inter-related. Quantitative evaluation of such processes is beyond the scope of the present study. Geochemical trends for major and trace elements of whole

rocks and minerals will be described on a general basis with qualitative inferences.

The geochemical data presented are part of a broader study currently under way and the present are restricted to the 2-metre section of the ore zone encountered in borehole MR126 (see Fig. 3.3 for location).

5.2 Major and Trace Element Geochemistry of the Unki MSZ

5.2.1 *Introduction*

Systematic sampling of the MSZ profile of drill hole MR126 drilled in the axial region (Fig. 3.3) of the Unki deposit was carried out to determine vertical controls on the major and minor element compositions in (i) whole rock and (ii) cumulus orthopyroxene. XRF analyses were carried out using facilities in the Geology Department of the University of Natal, Pietermaritzburg, South Africa. Electron microprobe work was carried out by Prof. A. H. Wilson at the University of Melbourne, Australia. The methods of sample collection and preparation, and the analytical techniques used are summarized in appendices 3 and 4. The results are presented in Table 5.1.

5.2.2 *Stratigraphic Variation of the Major Element Oxides*

Changes in magma composition of major element oxides during magmatic fractionation and crystallization can be used to elucidate the evolution of the magma. Controls on the chemical evolution include magma composition, temperature and pressure, although it can be assumed that pressure remained constant through the crystallization interval. All samples analyzed are of bronzitite constituting the ore zone over a 2 m interval and, therefore, only small compositional differences may be expected. In Figure 5.1, the major element oxides are plotted versus height. The more important observations are summarized as follows:

TABLE 5.1

MAJOR AND TRACE ELEMENT DATA SET FOR DRILL HOLE MR 126

(a) Whole Rock (WR)

	Si02	Al203	Fe20	FeO	MnO	MgO	Ca	Na2O	K2O	TiO	P2	Cr20	NiO	Tot
MR126/38	52.84	3.09	1.44	11.66	0.24	25.36	3.18	0.29	0.11	0.167	0.02	0.421	0.497	99.31
MR126/39	51.72	2.60	1.56	12.65	0.24	25.16	3.34	0.21	0.09	0.169	0.02	0.442	0.807	98.99
MR126/40	52.24	2.51	1.50	12.14	0.24	25.94	2.95	0.19	0.07	0.153	0.01	0.434	0.610	98.98
MR126/41	53.31	2.91	1.36	11.04	0.24	26.08	2.97	0.14	0.15	0.157	0.02	0.427	0.366	99.16
MR126/42	53.96	2.89	1.29	10.42	0.24	26.46	3.23	0.23	0.13	0.160	0.02	0.445	0.192	99.67
MR126/43	53.90	2.68	1.32	10.65	0.24	26.33	3.14	0.24	0.13	0.165	0.02	0.460	0.240	99.50
MR126/44	53.42	2.85	1.26	10.22	0.24	25.95	3.53	0.28	0.14	0.163	0.03	0.464	0.145	98.71
MR126/45	54.57	2.91	1.27	10.25	0.24	26.28	3.05	0.22	0.17	0.182	0.02	0.448	0.106	99.72
MR126/46	54.45	2.79	1.25	10.16	0.24	26.02	3.62	0.30	0.11	0.187	0.02	0.465	0.113	99.73
MR126/47	54.69	2.63	1.25	10.16	0.25	26.18	3.38	0.40	0.12	0.206	0.03	0.463	0.076	99.83
MR126/48	54.03	2.92	1.27	10.30	0.25	26.23	3.08	0.29	0.10	0.171	0.02	0.447	0.113	99.22

(b) Orthopyroxene (opx)

	Si02	Al203	Fe20	Fe	MnO	MgO	Ca0	Na2O	TiO2	Cr203	NiO	Total	Mg No
MR126/38	54.78	1.45	1.36	11.06	0.26	28.42	1.85	0.00	0.169	0.421	0.120	99.89	0.821
MR126/39	54.67	1.48	1.37	11.11	0.26	28.27	1.86	0.02	0.174	0.425	0.135	99.77	0.819
MR126/40	54.67	1.60	1.34	10.86	0.26	28.38	1.94	0.18	0.149	0.434	0.116	99.93	0.823
MR126/41	54.85	1.70	1.32	10.71	0.25	28.25	2.05	0.15	0.140	0.432	0.105	99.96	0.825
MR126/42	54.76	1.70	1.31	10.65	0.26	28.34	2.03	0.04	0.146	0.441	0.102	99.78	0.826
MR126/43	54.47	1.75	1.31	10.65	0.26	28.14	2.05	0.08	0.148	0.444	0.095	99.39	0.825
MR126/44	54.89	1.60	1.32	10.70	0.26	28.34	2.00	0.07	0.140	0.452	0.082	99.85	0.825
MR126/45	54.89	1.53	1.33	10.76	0.26	28.46	1.92	0.06	0.154	0.451	0.077	99.90	0.825
MR126/46	54.83	1.50	1.34	10.85	0.25	28.56	1.83	0.05	0.171	0.444	0.077	99.90	0.824
MR126/47	54.90	1.47	1.34	10.91	0.26	28.45	1.77	0.11	0.182	0.441	0.072	99.91	0.823
MR126/48	54.86	1.51	1.33	10.82	0.26	28.43	1.82	0.02	0.163	0.444	0.079	99.73	0.824

(C) Whole Rock Trace Elements

	Zr	Y	S	Zn	Cu	Ni	K	S	P	Ba
MR126/38	7.00	2.80	25.80	76.90	1706.2	3283.4	980	15758	94.0	38.6
MR126/39	8.30	2.20	17.90	78.10	2958.4	5332.0	801	28706	101.0	35.9
MR126/40	7.30	3.10	16.30	78.80	2268.2	4047.5	537	20361	48.0	28.7
MR126/41	7.70	2.40	22.70	74.00	1071.7	2307.1	1082	8706	62.0	51.1
MR126/42	6.80	2.80	21.10	72.70	533.8	1307.8	945	3699	16.0	41.3
MR126/43	6.50	2.60	16.80	72.80	672.1	1579.4	870	5113	101.0	40.1
MR126/44	7.20	3.50	18.10	72.00	357.3	1029.1	1189	2975	117.0	36.6
MR126/45	11.20	3.30	21.60	73.50	193.9	755.7	1437	1588	104.0	60.6
MR126/46	10.80	4.30	21.00	74.10	216.8	801.8	1150	2220	103.0	40.9
MR126/47	13.10	4.50	18.90	75.10	57.5	556.3	1273	645	138.0	44.5
MR126/48	10.20	3.40	22.50	75.50	232.7	830.3	959	2511	145.0	26.5

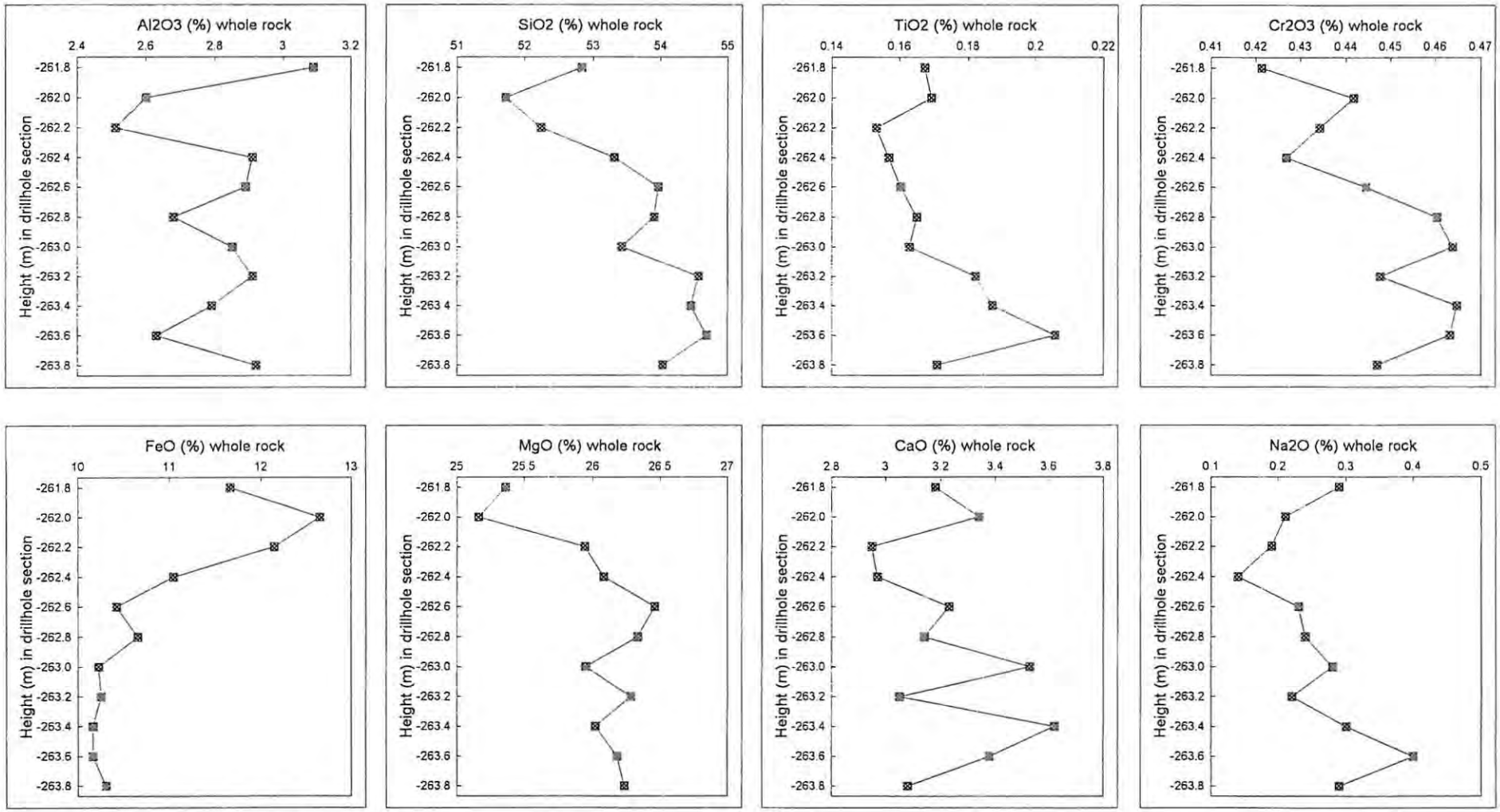

Fig. 5.1 Stratigraphic variation of the major element oxides

Al_2O_3 has a mean value of 2,80% with cyclical variations of between 2,5 and 3,1% in the succession. The minima and maxima correspond to the peak values of Pt and Ni and the PGE poor zone in the hanging wall, respectively.

SiO_2 shows a general decrease upwards through the profile which may reflect changes in the pyroxene composition or the modal amounts of primary silicate phases. The values range from 51,72% to 54,69% within an average of 53,55%. The minimum value occurs at the top of the peak Pt zone.

TiO_2 shows a gradual decrease upwards through the profile similar to SiO_2. Its values range from 0,153% to 0,206% with an average of 0,171%. As is the case with SiO_2, its lowest value occurs at the top of the peak Pt zone.

Cr_2O_3 has a general upward decreasing trend with values ranging from 0,421% to 0,465%. The average value is 0,447%. The lowest values occur just before and immediately after the peak Pt zone.

FeO (total iron) shows a sigmoidal upward increase with its maxima just above the zone corresponding to the peak values of Pt and Ni. The values are in the range 10,30% to 12,65% with an average of 10,87%.

MgO exhibits a mirror image trend to FeO and is likely to reflect changes in the composition of orthopyroxene. Its values range from 25,16% to 26,46%. The average value is 25,99%. The minimum value is at the top of the peak Pt zone.

CaO is variable but with an initial general decrease upwards, attaining its minima at a zone corresponding to the peak Pt zone. Its values range from 2,95% to 3,62%. The average value is 3,22%.

Na_2O shows a variable upward decreasing tendency attaining its lowest value just below the zone corresponding to the peak value of Pt. The values range from 0,14% to 0,40% with an average of 0,25%.

5.2.3 *Discussion on major elements*

The most important facts established from the trends shown by the major element oxides are as follows:

(i) variation of major element is controlled mainly by the cumulus phases;
(ii) the inverse correlation of MgO and FeO indicates that changes in orthopyroxene composition and/or modal proportions are responsible. This is also confirmed by SiO_2 variation which is similar to that for MgO;
(iii) TiO_2 and Na_2O are similar, probably reflecting the variation of postcumulus phases, i.e. magnetite or sphene with feldspars;
(iv) Cr_2O_3 and MgO show a general decrease upwards indicating the expected trend of normal silicate fractionation.

5.2.4. *Stratigraphic Variations of Trace Elements*

Compatible elements (Ni, Cu, S, Zn)

The compatible trace elements constitute those which would partition into sulphide i.e. the chalcophile metals. In this context, sulphide is regarded as a cumulus phase. The distribution patterns for Ni, Cu and S through the MSZ profile are broadly similar (Fig. 5.2) although each metal exhibits a unique vertical distribution. The trends for all three through the profile show an overall upward increase which is controlled by sulphide followed by a sudden fall at the top of the PGE rich zone. Zn behaves in a slightly different pattern in the lower half of the profile. From the base upwards to the mid-portion

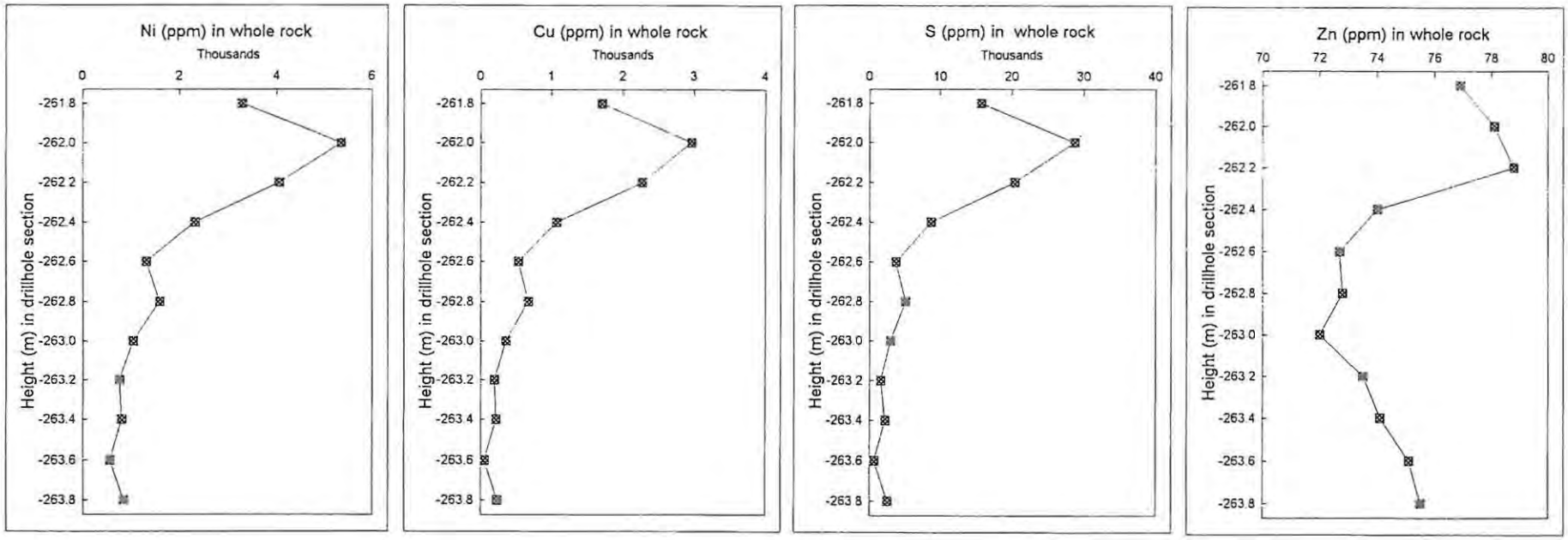

Fig. 5.2 Stratigraphic variation of compatible trace elements

of the MSZ, it shows a steady decline, stabilises, then shows a rapid upward trend up to the peak PGE/BM zone after which it drops drastically.

Incompatible elements (K, P, Y, Zr, Ba)

K shows an overall decrease upwards with pronounced small-scale variation. Two major troughs are noticeable (Fig. 5.3): the first is just after the Pd peak and the 2nd coincides with the Pt peak. The values range from 537 ppm to 1437 ppm with an average of 1020 ppm.

P shows a general decrease upwards through the lower part of the section and a rise in the upper part. This trend is not similar to that shown by K. The values range from 16 ppm to 145 ppm with an average value of 93,54 ppm.

Y shows a systematic decrease upwards in the section, but with some variation. The values are variable between 2,2 ppm and 4,5 ppm with an average of 3,2 ppm.

Zr shows a rapid general decrease and then becomes relatively constant in the main PGE Zone. It has a similar pattern to Y. The values range from 7,0 ppm to 13,1 ppm with an average of 8,73 ppm.

Ba has a trend which is almost identical in pattern to that of K but with less overall decrease upwards in the section. The average value is 40,43 ppm with a minima and maxima of 27 ppm and 61 ppm, respectively.

In summary all the incompatible elements show an overall decrease upwards through the MSZ profile.

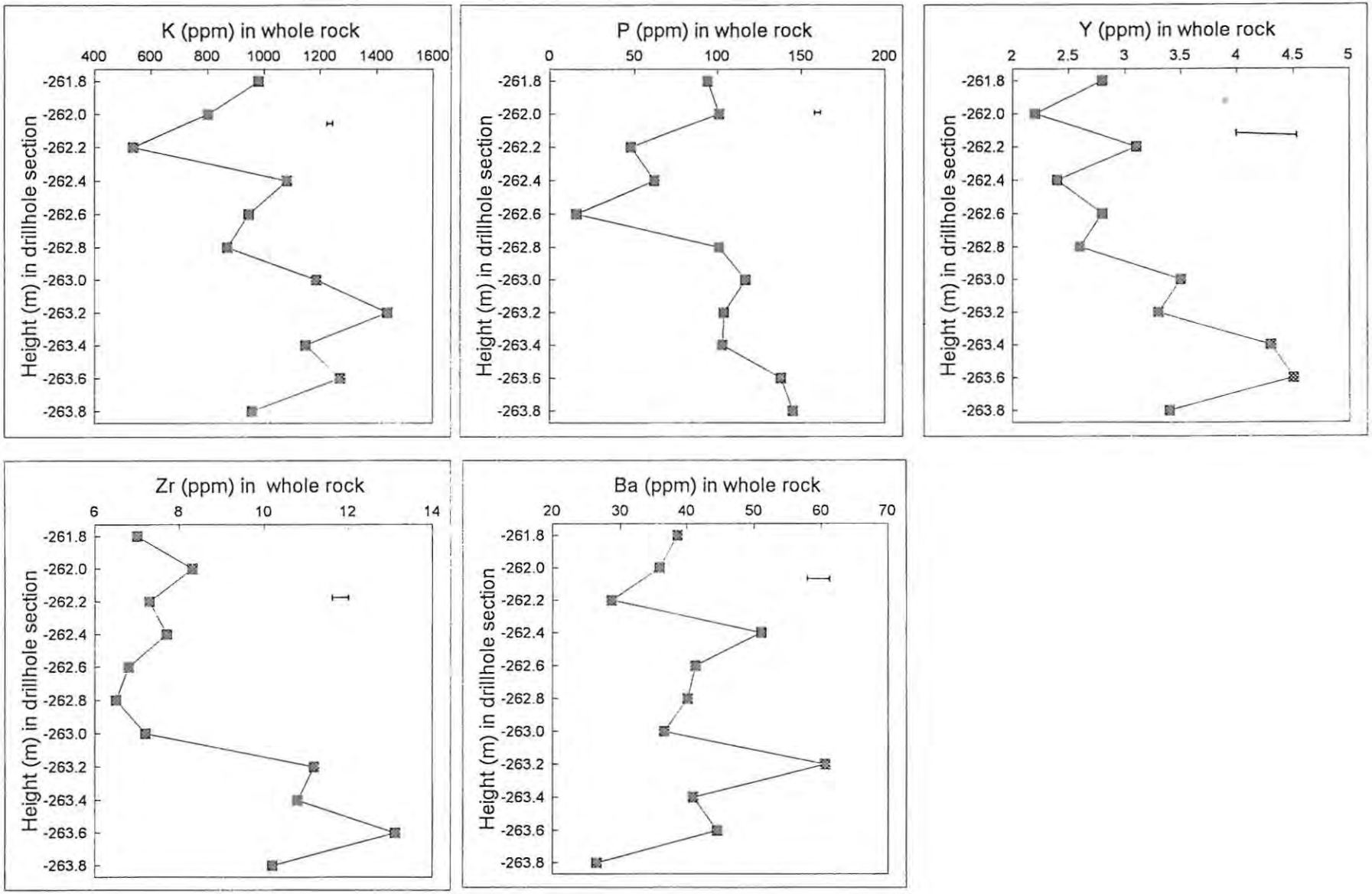

Fig. 5.3 Stratigraphic variation of incompatible trace elements
N.B. ⊢⊣ : error bar

5.2.5 *Discussion on Incompatible trace elements*

The overall trends observed for the incompatible trace elements (with the possible exception of Ba) are a decrease in concentration upwards in the succession. The amount of trapped liquid is the major control on the incompatible element content (Wilson, 1992). Therefore, these data indicate that the amount of trapped liquid decreases upwards in the succession. At the same time, smaller-scale variations show consistent patterns between trace elements (e.g. K and Ba in K-feldspar, and (Zr and P in accessory zircon and apatite) indicating that other mineralogical controls also operated.

5.2.6 *Orthopyroxene compositions in MSZ*

Compositions of orthopyroxene reflect the primary liquidus composition of the crystallizing magma, together with any postliquidus modification as a result of reaction with trapped liquid. These compositions from the MSZ intersection of drill hole MR 126 are shown in Table 5.2 and Figure 5.4.

Table 5.2 also shows the site allocation of the cations on the basis of charge balance with 6 oxygens. Abbreviations and numbers are as recommended by Morimoto (1988).

A constant ratio of $Fe^{2+}/(Fe^{2+} + Fe^{3+}) = 0.97$ is used for Great Dyke pyroxenes at this level (Wilson, pers. comm., 1995).

The analyses all confirm to quality criteria with total cations averaging 3,997 ± 0,002 and average excess charge (calculated as (Al IV + Na) - (Al VI + Cr + 2Ti)) - 0,0016 ± 0,0004.

Owing to the narrow thickness of the section studied, there are only small differences in pyroxene composition. **SiO_2, MgO and FeO** are stoichiometric components of pyroxene, but with absolute amounts that are influenced by substitution of minor or non-stoichiometric components.

Table 5.2: Compositions of bronzites (Opx) in the MSZ of drill hole MR126.

Mineral type - orthopyroxene											
Sample	126/38	126/39	126/40	126/41	126/42	126/43	126/44	126/45	MR126/46	MR126/47	MR126/48
SiO2	54.78	54.67	54.67	54.85	54.76	54.47	54.89	54.89	54.83	54.90	54.86
Al2O3	1.45	1.48	1.60	1.70	1.70	1.75	1.60	1.53	1.50	1.47	1.51
Fe2O3	0.41	0.41	0.40	0.40	0.39	0.39	0.40	0.40	0.40	0.40	0.40
FeO	11.92	11.97	11.70	11.54	11.47	11.47	11.53	11.60	11.69	11.75	11.66
MnO	0.260	0.260	0.260	0.250	0.260	0.260	0.260	0.260	0.250	0.260	0.260
MgO	28.42	28.27	28.38	28.25	28.34	28.14	28.34	28.46	28.56	28.45	28.43
CaO	1.85	1.86	1.94	2.05	2.03	2.05	2.00	1.92	1.83	1.77	1.82
Na2O	0.00	0.02	0.18	0.15	0.04	0.08	0.07	0.06	0.05	0.11	0.02
K2O	0.00	0.00	0.00	0.00	0.00	0.00	0.00	0.00	0.00	0.00	0.00
TiO2	0.1699	0.1735	0.1494	0.1400	0.1455	0.1475	0.1398	0.1537	0.1707	0.1817	0.1628
Cr2O3	0.4212	0.4251	0.4342	0.4320	0.4411	0.4439	0.4515	0.4514	0.4436	0.4412	0.4439
NiO	0.1201	0.1351	0.1157	0.1050	0.1019	0.0952	0.0815	0.0767	0.0767	0.0722	0.0788
ZnO	0.0000	0.0000	0.0000	0.0000	0.0000	0.0000	0.0000	0.0000	0.0000	0.0000	0.0000
Total	99.89	99.77	99.93	99.96	99.78	99.40	99.85	99.89	99.90	99.91	99.74
Site cations on 6 oxygens											
1Si	1.9569	1.9563	1.9524	1.9558	1.9550	1.9531	1.9583	1.9579	1.9562	1.9588	1.9595
TAl	0.0351	0.0352	0.0315	0.0343	0.0303	0.0382	0.0350	0.0342	0.0344	0.0320	0.0355
TFe3	0.0000	0.0000	0.0000	0.0000	0.0000	0.0000	0.0000	0.0000	0.0000	0.0000	0.0000
M1Al	0.0260	0.0272	0.0359	0.0372	0.0332	0.0358	0.0323	0.0301	0.0287	0.0298	0.0281
M1Ti	0.0046	0.0047	0.0040	0.0038	0.0039	0.0040	0.0038	0.0041	0.0046	0.0049	0.0044
M1Fe3	0.0110	0.0111	0.0108	0.0106	0.0106	0.0106	0.0106	0.0107	0.0108	0.0108	0.0108
M1Fe2	0.1796	0.1807	0.1755	0.1740	0.1734	0.1740	0.1744	0.1750	0.1759	0.1769	0.1762
M1Cr	0.0119	0.0120	0.0123	0.0122	0.0125	0.0126	0.0127	0.0127	0.0125	0.0124	0.0125
M1Mg	0.7635	0.7604	0.7582	0.7592	0.7634	0.7603	0.7638	0.7652	0.7654	0.7630	0.7658
M1Ni	0.0035	0.0039	0.0033	0.0030	0.0029	0.0027	0.0023	0.0022	0.0022	0.0021	0.0023
M1Zn	0.0000	0.0000	0.0000	0.0000	0.0000	0.0000	0.0000	0.0000	0.0000	0.0000	0.0000
M2Mg	0.7496	0.7473	0.7522	0.7420	0.7445	0.7435	0.7430	0.7477	0.7532	0.7498	0.7476
M2Fe2	0.1763	0.1776	0.1741	0.1701	0.1691	0.1701	0.1697	0.1710	0.1731	0.1738	0.1720
M2Mn	0.0079	0.0079	0.0079	0.0076	0.0079	0.0079	0.0079	0.0079	0.0076	0.0079	0.0079
M2Ca	0.0708	0.0713	0.0742	0.0783	0.0777	0.0788	0.0765	0.0734	0.0700	0.0677	0.0697
M2Na	0.0000	0.0014	0.0125	0.0104	0.0028	0.0056	0.0048	0.0041	0.0035	0.0076	0.0014
M2K	0.0000	0.0000	0.0000	0.0000	0.0000	0.0000	0.0000	0.0000	0.0000	0.0000	0.0000
Tot.Tet	1.9920	1.9915	1.9838	1.9901	1.9933	1.9913	1.9933	1.9921	1.9906	1.9908	1.9949
Tot.M1	1.0000	1.0000	1.0000	1.0000	1.0000	1.0000	1.0000	1.0000	1.0000	1.0000	1.0000
Tot.M2	1.0046	1.0054	1.0208	1.0084	1.0019	1.0058	1.0018	1.0041	1.0072	1.0067	0.9985
Tot.cat	3.9966	3.9969	4.0047	3.9985	3.9952	3.9971	3.9951	3.9962	3.9978	3.9975	3.9934
Exc.chg	-.0009	-.0009	-.0014	-.0015	-.0019	-.0019	-.0021	-.0020	-.0017	-.0016	-.0018
Formulae and end-members											
Mg#	0.8095	0.8080	0.8121	0.8135	0.8149	0.8138	0.8141	0.8139	0.8132	0.8118	0.8130
Ca	3.6299	3.6604	3.8166	4.0491	4.0055	4.0657	3.9451	3.7768	3.5908	3.4845	3.5868
Mg	77.5584	77.3807	77.6562	77.6088	77.7772	77.6237	77.7525	77.8656	77.9454	77.8992	77.9290
Fe	18.8117	18.9588	18.5272	18.3421	18.2173	18.3106	18.3024	18.3576	18.4637	18.6163	18.4842
Q	1.9398	1.9373	1.9342	1.9237	1.9281	1.9266	1.9273	1.9322	1.9374	1.9312	1.9312
J	0.0000	0.0028	0.0249	0.0207	0.0055	0.0111	0.0097	0.0083	0.0069	0.0152	0.0028
Wo	3.6153	3.6457	3.8012	4.0334	3.9894	4.0492	3.9292	3.7616	3.5770	3.4704	3.5723
En	77.2469	77.0690	77.3434	77.3070	77.4630	77.3086	77.4386	77.5520	77.6443	77.5853	77.6146
Fs	19.1378	19.2853	18.8553	18.6596	18.5476	18.6422	18.6323	18.6864	18.7787	18.9443	18.8131
JD1	0.0000	0.0014	0.0125	0.0104	0.0028	0.0056	0.0048	0.0041	0.0035	0.0076	0.0014
AE1	0.0000	0.0000	0.0000	0.0000	0.0000	0.0000	0.0000	0.0000	0.0000	0.0000	0.0000
CFTS1	0.0115	0.0116	0.0115	0.0114	0.0115	0.0116	0.0117	0.0117	0.0117	0.0116	0.0117
CTTS1	0.0046	0.0047	0.0040	0.0038	0.0039	0.0040	0.0038	0.0041	0.0046	0.0049	0.0044
CATS1	0.0260	0.0258	0.0234	0.0268	0.0305	0.0302	0.0275	0.0260	0.0252	0.0222	0.0267
Wo1	0.0201	0.0204	0.0234	0.0239	0.0216	0.0223	0.0226	0.0216	0.0201	0.0203	0.0193
Fs1	0.1819	0.1831	0.1787	0.1759	0.1752	0.1760	0.1760	0.1769	0.1782	0.1793	0.1780
En1	0.7582	0.7558	0.7569	0.7521	0.7554	0.7533	0.7546	0.7575	0.7604	0.7574	0.7578

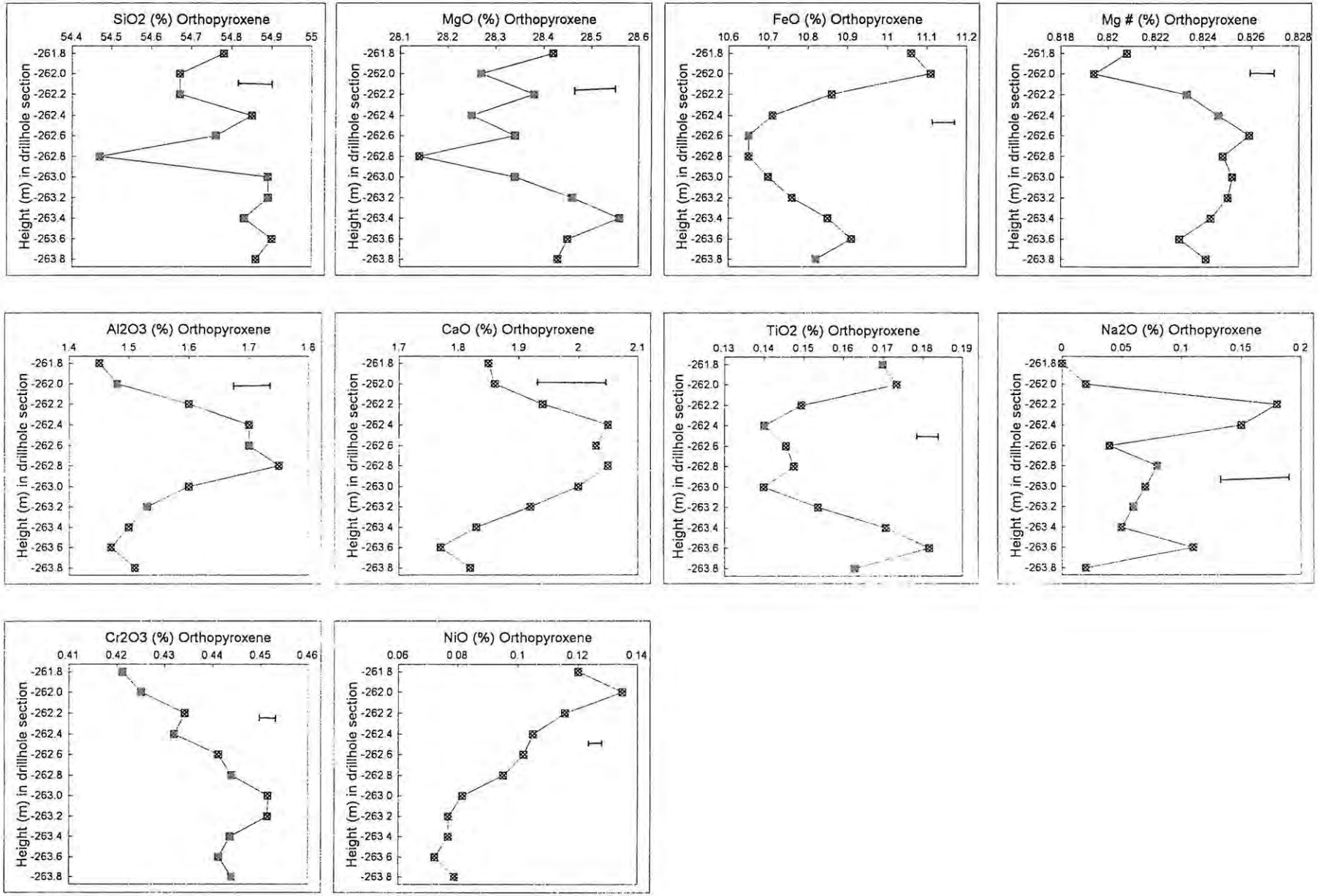

Fig. 5.4 Stratigraphic variation of element oxides in orthopyroxenes
N.B. ⊢⊣ : error bar

The stratigraphic variations in orthopyroxene compositions are plotted on Figure 5.4 from which the following is evident. **SiO_2** shows an overall slight decrease upwards in the succession. **MgO** exhibits an initial rapid decrease upwards from the base of the section and then a small, slight increase with a pattern that is broadly reflected by **FeO**. A more definitive indication of pyroxene composition is **Mg#** (i.e. Mg-number calculated as atomic **$Mg/(Mg+Fe^{2+})$**.

The **Mg#** of orthopyroxenes is one of the most important parameters used as a pointer to where dramatic changes in magma composition may have occurred. These changes may be interpreted as relating to either new influxes of magma or convective overturns in the magma body.

Mg# shows a smooth trend through the succession that is marked by an initial upward increase in values, followed by a relatively rapid decrease. The average value is 0,824 with a minima and maxima of 0,819 and 0,826, respectively.

Al_2O_3 shows a broadly similar pattern to **Mg#**, but one which is even more pronounced giving a rather bell-shaped distribution with the highest values occurring in the middle part of the section. The mean value is 1,57% with a range of between 1,45% and 1,75%.

CaO shows a trend almost identical to Al_2O_3. The values range from 1,77% to 2,05% with an average of 1,92%.

TiO_2 shows a trend which is almost the complete opposite to that of Al_2O_3 and CaO, with a marked decrease in the middle part of the succession. Variation of TiO_2 is antipathetic to Mg#. The average value is 0,158% with a range of between 0,140% and 0,182%.

Na_2O is very low and generally below 0,1%. The variation has no stratigraphic significance.

Cr_2O_3 and NiO are expected to show chemical trends which are both similar to each other and to Mg#. These data show that in the section studied, such variations are not observed. Cr_2O_3 shows a slight increase upwards at the base of the section, followed by a marked decrease in the upper part. NiO shows a continuous increase upwards in the section.

5.2.7 *Discussion on orthopyroxene geochemistry*

These variations cannot be explained by simple fractionation models and complex re-equilibration with both trapped liquid and sulphide are responsible for possible decoupling of major and minor elements. The strong inverse correlation of Mg# to S content (Figs. 5.4 & 5.2) is indicative of iron exchange between sulphide and pyroxene, while the NiO variation also indicates re-equilibration with sulphide.

Further attention will be drawn to these trends in the next section, but additional detailed evaluation and modelling of the orthopyroxene data is not within the context of this study.

A strong temperature control may also have influenced the pyroxene compositions and this is further evidenced by the plots of Al(VI) versus Al(TOT) - (Fig. 5.5) and Al(IV) versus Al(TOT). The linear correlation of these components is indicative of small but significant temperature variations over the interval studied (Morimoto, 1988).

5.3 Relation of metal profile to geochemistry

5.3.1 *Introduction*

This subsection focuses on the MSZ metal profile in relation to the silicate geochemistry. Mineral composition data from the reference drill hole MR126 are used to illustrate various points with important implications for the petrogenesis of the MSZ in the Unki area.

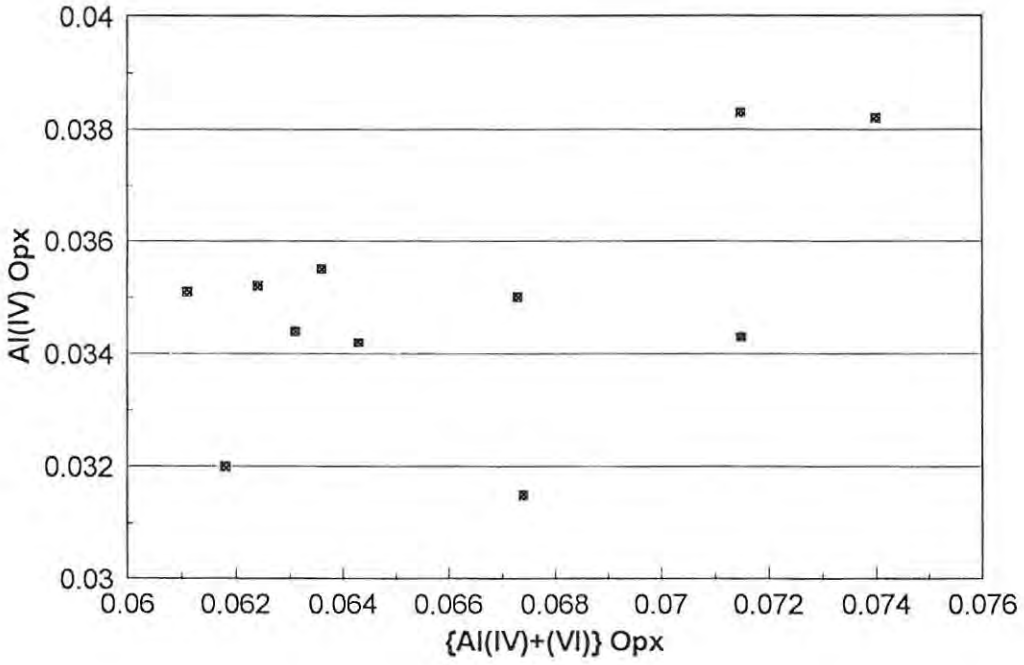

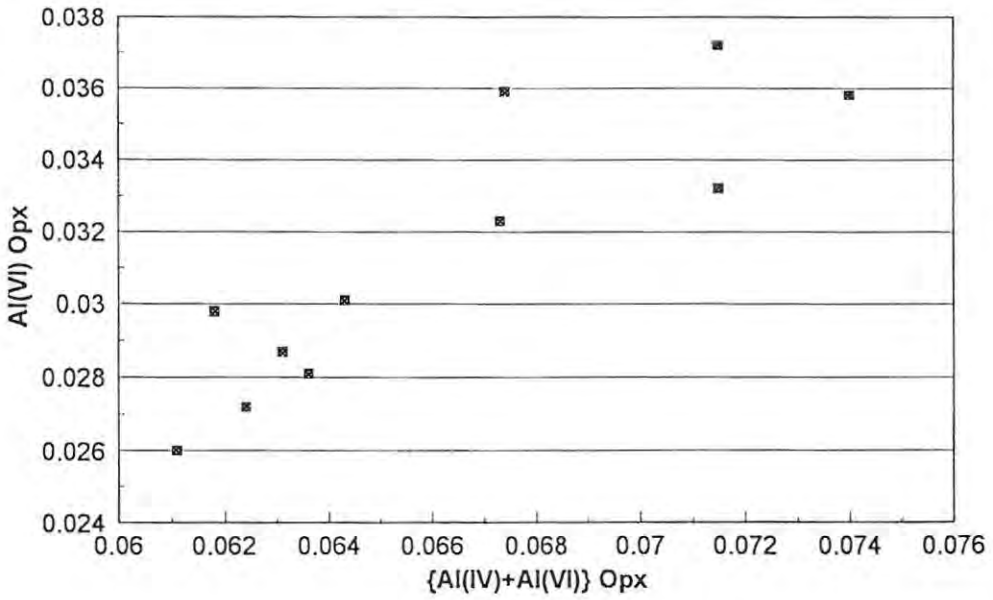

Fig 5.5 Plots of Al(IV) Opx versus Al(TOT) and Al(VI) Opx versus Al(TOT)

5.3.2 *Vertical distributions of* PGE-Ni-Cu

The vertical variations of Pt, Pd and Au of bulk rock are shown in Fig. 5.6 allowing the following observations: (a) Pt and Au peak in the upper main interval of the PGE-enriched zone, whereas Pd peaks in the mid section, (b) Peaks for Ni and Cu (for extractable sulphide - Fig. 5.7) correspond to Pt and Au peaks in bulk rock. Pt, Pd and Pd+Pt contents per unit sulphide (as a ratio to bulk Cu+Ni content in Fig. 5.7) show an initial rapid increase upwards to a zone corresponding to the peak value of Pd, followed by a gradual upward decreasing trend (Fig. 5.7). The decrease upwards is more rapid for Pd than Pt, indicating the higher partitioning of Pd into early formed sulphide.

The ratios Au/Pt, Au/Pd and Pt/Pd plotted against stratigraphic height increase upwards with Au/Pd more rapid than Au/Pt at the top of the succession (Fig. 5.8). Pt/Pd shows an initial smooth increase from the base upwards, followed by a sharp rise to the zone corresponding to the Pt peak value, thereafter there is a sharp drop to the upper limit of the PGE zone, followed by an abrupt increase. The abrupt increase beyond the top of the PGE zone corresponds to the reversal noted in the Mg# (section 5.2.6). The Au/(Pt+Pd) pattern shows an upward increasing trend similar to that of Au/Pt and Au/Pd.

Important features in silicate mineral compositions discussed in section 5.2.6 and directly linked to the metal profile geochemistry include the following:

(a) Orthopyroxene compositions abruptly becoming more iron-rich over the interval of peak PGE values followed by a reversal to more magnesian compositions upwards.

(b) Upward Fe enrichment of orthopyroxene through the succession with the maxima correlating positively with peak PGE and BM grades.

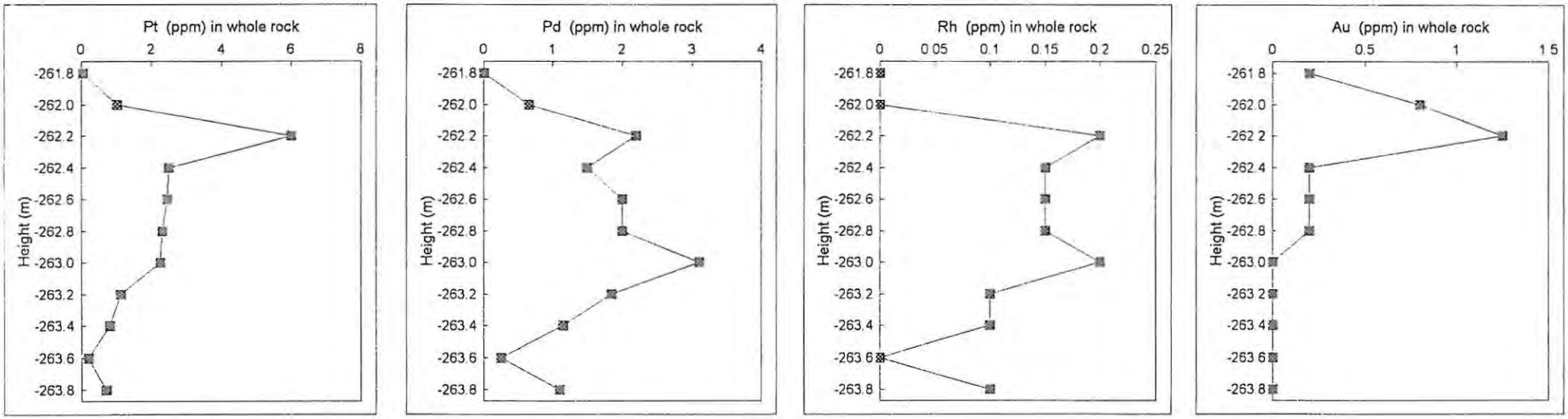

Fig. 5.6 Stratigraphic variation of major PGE in whole rock.

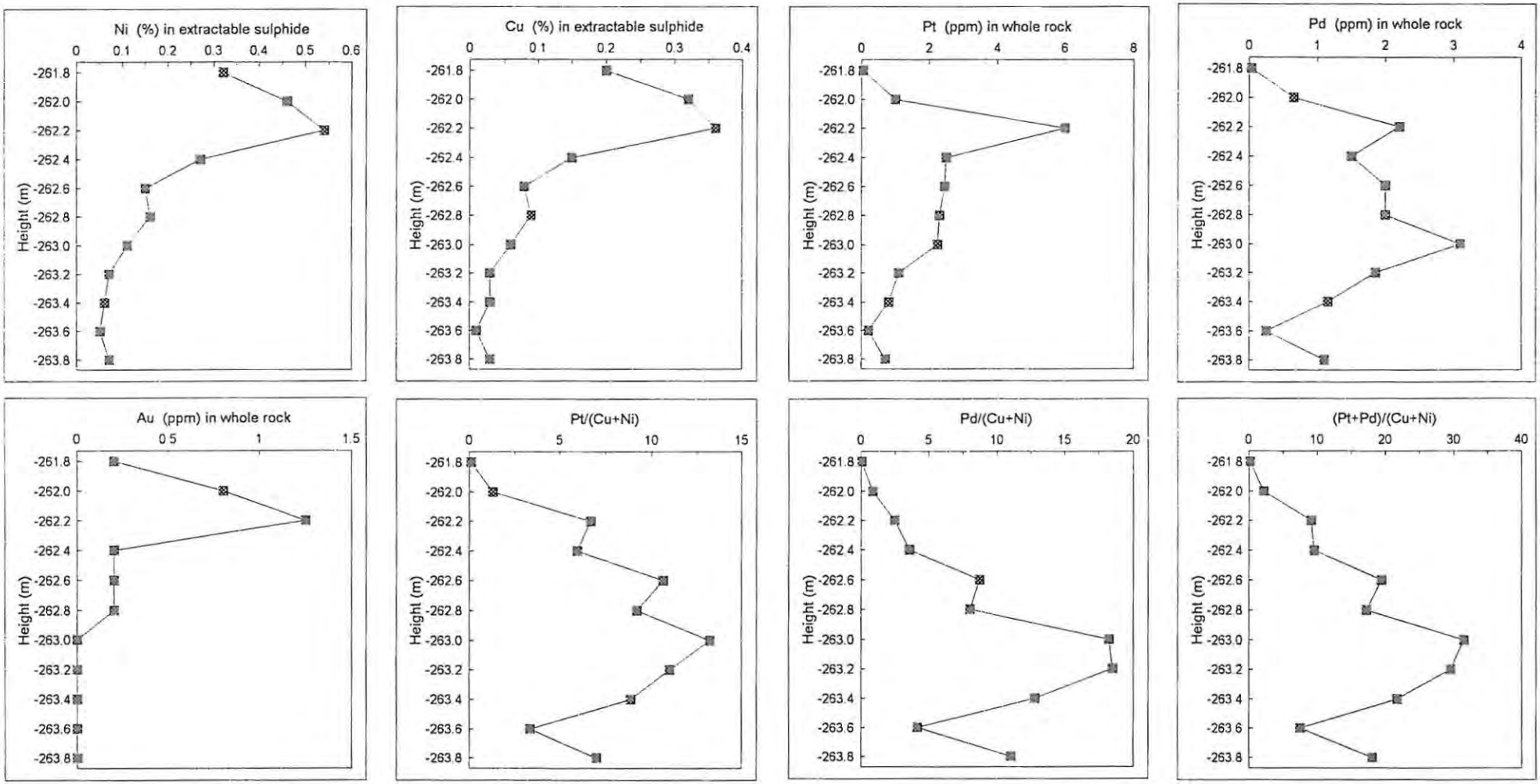

Fig 5.7 Stratigraphic variation of extractable sulphide and metal contents per unit sulphide

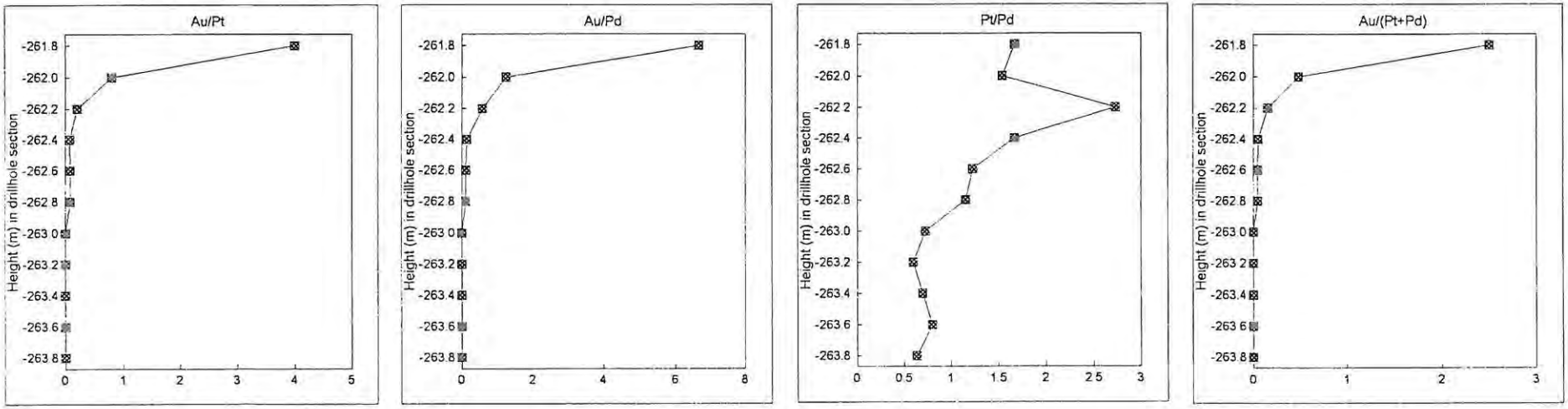

Fig 5.8 Stratigraphic variation of metal ratios.

(c) The inverse relationship of sulphide with Zr and with Pt+Pd/(Cu+Ni), Pd/(Cu+Ni) and Pt/(Cu+Ni) ratios.

(d) An apparent reversal in the Mg# near the top of the succession indicating a dramatic change in magma composition above the PGE zone.

5.4 Intepretation

The marked iron enrichment in orthopyroxene which corresponds to the enrichment in sulphide indicates that precipitation of sulphide was caused by the fractionation process with lowering of temperature in the magma. The reversal in Mg# of orthopyroxene, which in turn corresponds to the decrease in sulphide content, suggests that the termination of this zone was due to an increase in temperature associated with an influx of new magma.

The apparent inverse correlation of sulphide variation with Zr content, and also with the metal ratios, indicates that sulphide in the ore zone was in space competition with trapped silicate liquid. Thus, the origin of the ore zone is indicated to be the result of a complex interplay of chemical and physical process occurring at a critical stage in the overall fractionation of the Great Dyke magma chamber.

Chapter 6

CHARACTERIZATION AND ECONOMIC ASSESSMENT OF THE ORE ZONE

6.1 Characterization of main types of vertical profiles

Diamond drill core intersections through the MSZ from 76 drill holes in the Unki area were examined. The original sampling of the drill core had been undertaken by continuous half-core splitting with a diamond saw, sample lengths being 20cm. All analyses of the samples (for PGE, Au, Ni and Cu) were carried out by Anglo American Research Laboratories in Johannesburg, South Africa (see appendix 5 for methods).

Three distinct types of vertical distribution of PGE and BM are identifiable from the assay sections. These are represented by the drill hole sections MR 100, MR 109 and MR 113 (Fig. 3.3 for locations). In **Type 1** (as shown in drill hole MR 100, Fig. 6.1), the MSZ comprises two main subzones, a lower PGE subzone rich in Pt, Pd and other precious metals, and an upper Base Metal (BM) subzone with very low precious metal contents. In the PGE subzone, bulk base and precious metals contents increase upwards, while Pd:Pt ratios and Pd+Pt contents per unit sulphide (not shown in Fig. 6.1 but calculated on basis of bulk Cu+Ni content) decrease upwards. This is reflected by the occurrence of (a) the highest PGE grades and (b) the lowest Pd:Pt ratios and Pd+Pt contents per unit sulphide at the top of the PGE subzone (Fig. 5.7). Other noticeable important features of the Type 1 profile include (i) the coincidence of Pt and Pd peak values, (ii) the non-coincidence of Au values with those of Pt and Pd. The Type 1 profile constitutes about 40% of the MSZ intersections in the Unki area and is not restricted to any particular section of the deposit. It appears to be the dominant profile in the Wedza Subchamber (Prendergast, 1988a).

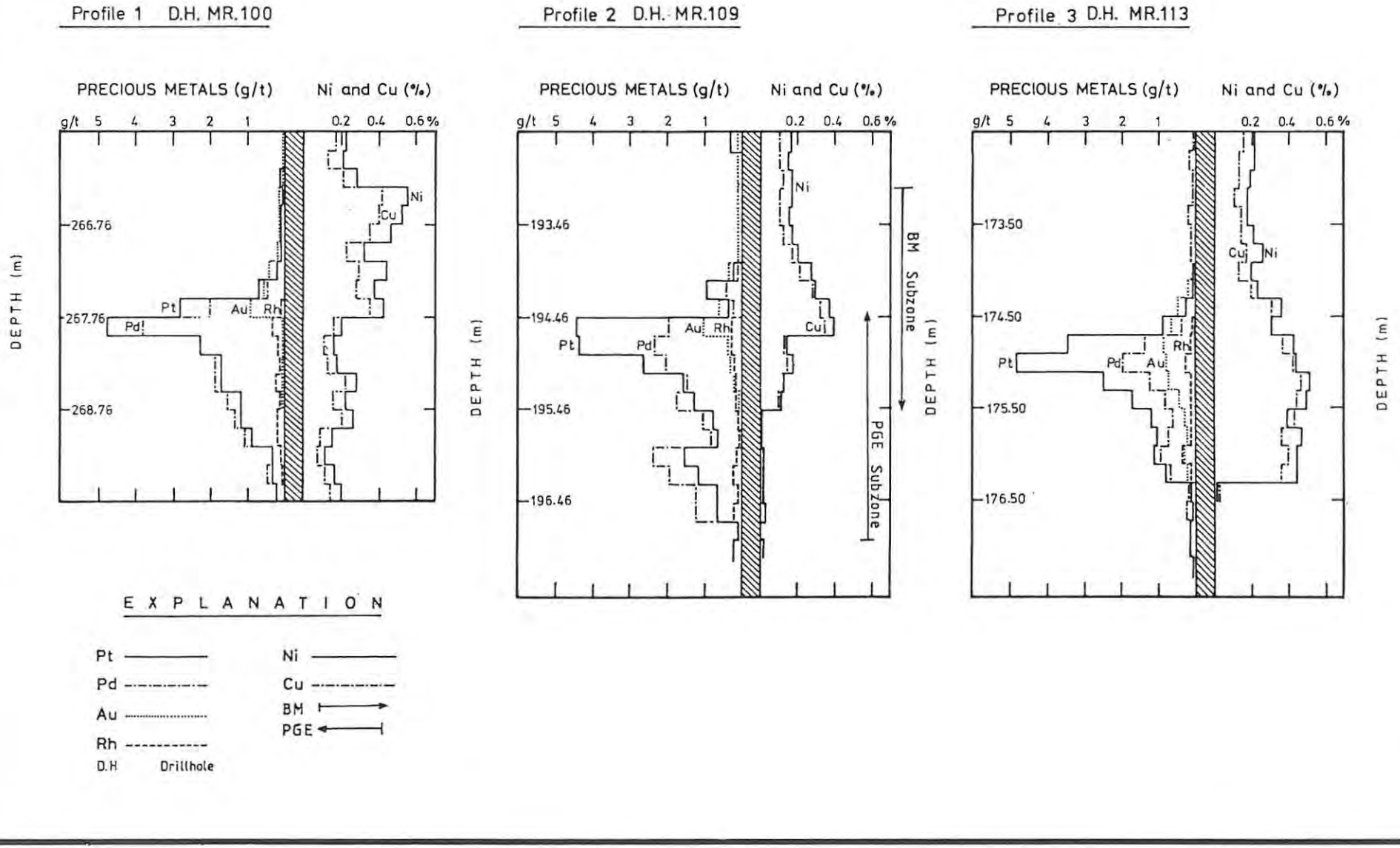

Fig 6.1 New Middleridge (Unki Project), Distribution of Metals in the Main Sulphide Zone.

Type 2 (drill hole MR 109 in Fig. 6.1) vertical profile constitutes about 55% of the MSZ intersections in the Unki area and is characterised by the coincidence of BM peak values with those of Pt and Au, and the occurrence of Pd peak values 20cm-40cm below those of Pt. Geochemically, there is an enrichment of BM in the hanging-wall of the MSZ with an overlap between the BM subzone and the PGE subzone. As in the Type 1 vertical profile, Pd:Pt ratios and Pd+Pt contents per unit sulphide decrease upwards (Fig. 5.7), and Pt, Pd and Au in sulphide drop sharply upwards into the sulphide zone. In the latter case, Pd drops more sharply than Pt, and both of them much more sharply than Au. This type comprises about 80% of the sections in the Darwendale Subchamber (Wilson and Tredoux, 1990; Wilson, pers. comm., 1995).

Type 3 (drill hole MR 113 in Fig. 6.1) vertical profile is rare, constituting between 5% and 10% of the total number of profiles examined. The PGE behaviour (Fig. 6.1) is broadly similar to that found in Type 1. The unique characteristics of Type 3 vertical profile are (i) the coincidence of the main PGE zone with the main BM interval, and (ii) the decrease upwards of bulk BM contents (Fig. 6.1). This profile type has not been reported from other subchambers.

6.2 Configuration and structure of the ore body on a mining scale

6.2.1 *Geometry*

The PGE zone dips inwards from the eastern and western flanks at an average dip of 7° with a maximum and minimum of 8° and 6° indicated on the eastern and western flanks, respectively. The slight difference in the dips may indicate some slight axial tilting. The maximum depth from surface at which the MSZ was intersected is 275m in the central axis.

Underground mapping, drilling and channel sampling at Unki shaft have shown the main PGE zone to be tabular in section but rolling/undulating along strike and down dip (Fig. 6.2). The major undulations are along strike where maximum amplitudes of up to 75cm occur over strike distances of 30m to 50m.

Contoured variations of the elevations of the hanging-wall of the PGE zone (Fig. 3.12) indicate a synclinal structure in the centre of the Unki area and the broad lateral continuity of the PGE zone with no noticeable undulations on a broader scale. The apparent synclinal structure suggests an undulating longitudinal variation in structure which may reflect feeder systems, but does not prove their existence. This synclinal structure is also apparent in a N-S section (Fig. 6.3) and is certainly not due to faulting.

6.2.2 *Significance of the Footwall Shear*

One of the most striking features of the Unki deposit is the Footwall shear which coincides with the ore body envelope in the footwall. Contoured variations of its elevations as determined in drill hole intersections (Fig. 3.9) show exactly the same pattern as that of the base of the norite (Fig. 6.3) and that of the top of the PGE zone (Fig. 3.12), implying broad similarities in lateral variation.
Mapping and sampling in the underground workings at Unki demonstrate clearly that the Footwall shear undulates sympathetically to the main metal zone.

In mining terms, the importance of the Footwall shear is two-fold. Firstly, the Footwall shear represents the only visual marker for guiding development and for stope control. Second, the blast will inevitably break preferentially along this plane of weakness. In the latter case, it would be extremely difficult to respond to variations in metal prices by reducing stope widths and moving the lower cut-off upwards.

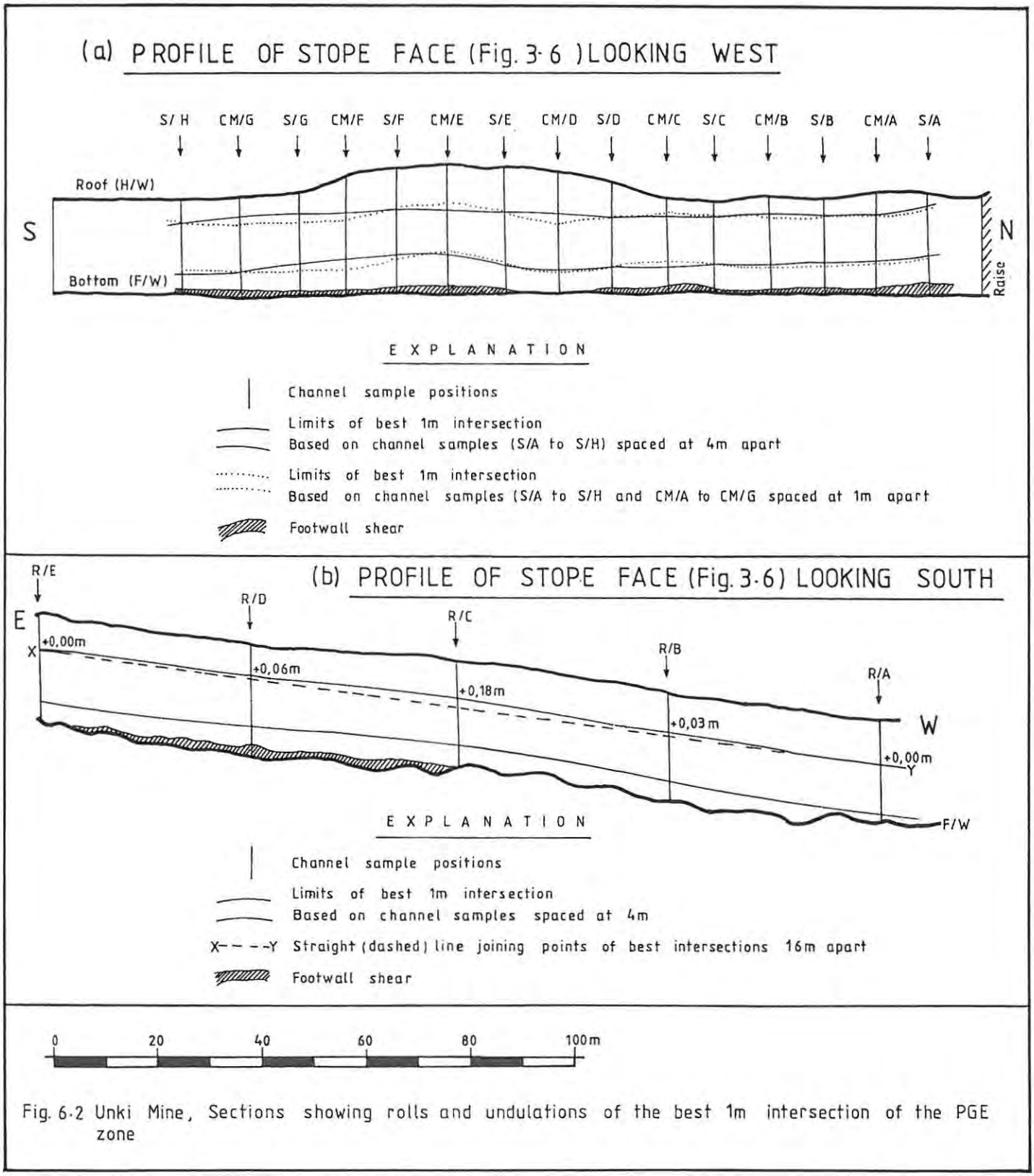

Fig. 6·2 Unki Mine, Sections showing rolls and undulations of the best 1m intersection of the PGE zone

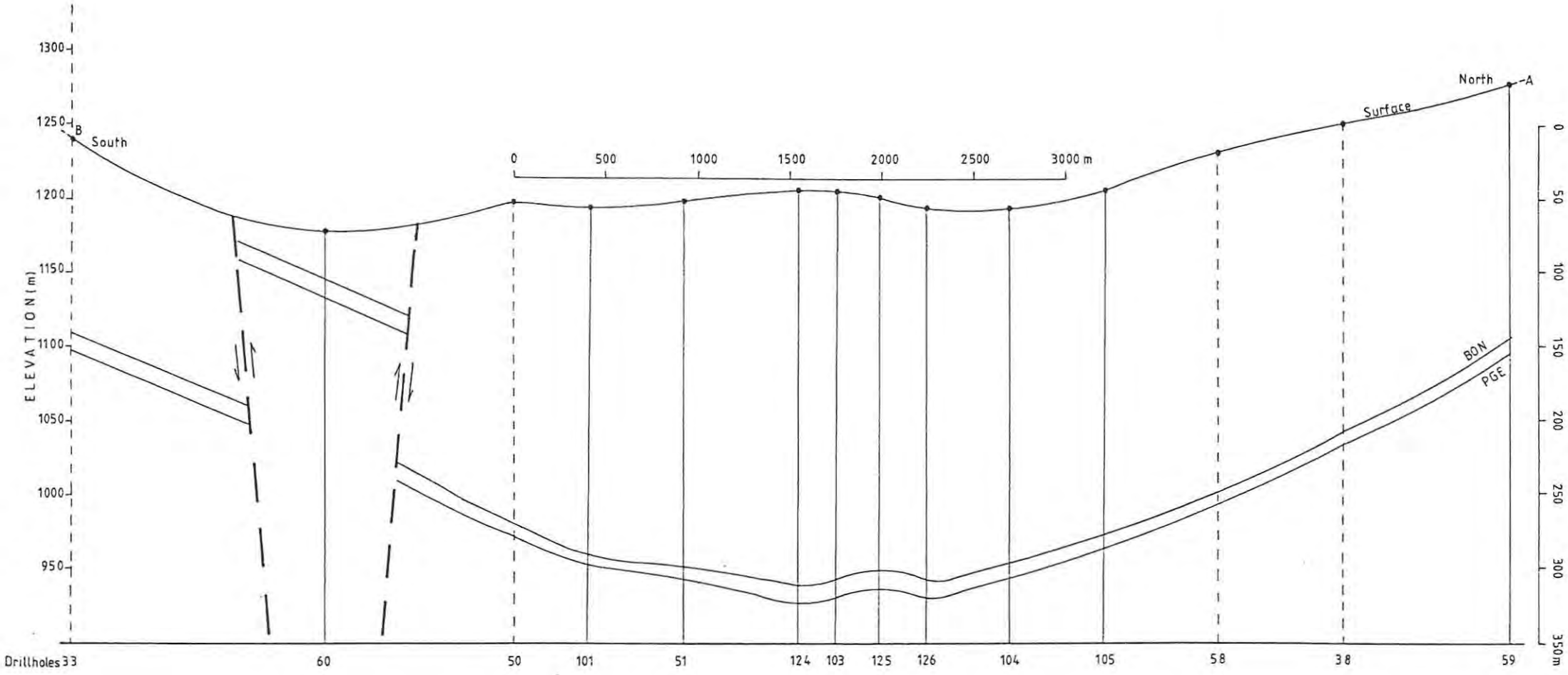

N.B. Drillholes projected to section line (A-B).

Fig 6.3 Unki N-S axial section showing topological variation of the base of norite (BON) and hanging wall of the main PGE zone.

6.2.3 *Thickness of MSZ*

Based on the average of the 76 drill hole intersections, the PGE zone of the MSZ averages about 2.10m in vertical thickness. Both the footwall and hanging-wall limits are defined by an envelope of not less than 0,4 g/t Pt against background values of 0,2 g/t Pt or less.
The most striking feature is the fact that the base of the Footwall shear is defined by minimum Pt assays of at least 0,4 g/t Pt in 95% of the cases. This leaves no doubt as to the fact that the base of the main PGE zone is demarcated by the Footwall shear. Using the ore envelope cut-off of 0,40 g/t Pt, the vertical width of the MSZ averages 2,10m. Some slight variations do exist along E-W and N-S sections but on the whole, there are no marked differences between the axis and the margins.

6.2.4 *PGE and BM grade distributions and persistence.*

The broad lateral continuity and homogeneity of the PGE zone at Unki is demonstrated in the contour plots of the hanging-wall elevations of the PGE zone, and of the base of the PGE zone which corresponds to the base of the Footwall shear (Figs. 3.12 and 3.9 respectively). As in the case with the MSZ thickness, slight variations which exist are random and not necessarily related to axial or marginal facies. The contour plots (Figs. 3.9 and 3.12) also show the absence of major structural disturbances likely to interfere with mining operations. Locally, xenoliths and intrusives may disrupt the continuity but this is volumetrically insignificant.

6.2.5. *Following the PGE-rich Zone*

So far as has been established, the geological markers denoting the position of the PGE-rich MSZ as a whole are:

1. the contact between norite and pyroxenite;
2. the contact between websterite and bronzitite; and

3. the base of sulphide distinguishing between mineralized and unmineralized bronzitite.

The norite-pyroxenite contact (BON on Fig. 3.2) is the most easily recognised but it is on average, 10m above the PGE-rich zone. It would therefore be of little practical use for the positioning of mine development.

The websterite-bronzitite contact is not readily recognisable as it is gradational. It is also a fact that the metalliferous zone, although situated at ± 1m below the contact, varies above and below this generalized limit by between 30cm and 50cm.

The base of sulphide concentrations remains the only useful geological marker that can be used visually for positioning mine development in the metalliferous zone. However, this base is in places indistinct, and irregular, and in some cases, the presence of sulphide can hardly be noticed.

The Footwall Shear is unique to Unki. It is a distinct, easily recognisable feature and offers the only reliable visual means of determining the position of the main PGE zone. Other than this, an ore zone marker that is of general application for the miners to follow, remains elusive at present.

6.2.6 *Economic evaluation of profile types.*

The MSZ is essentially a five-metal orebody with Pt as the major contributor (Fig. 6.4) plus important Pd, Rh, Au and Ni. This characteristic may provide slightly improved flexibility relative to the four-metal Bushveld ores, provided high recovery rates and cost effective extraction processes are realized.
Important factors considered to be critical in the evaluation of the MSZ profile are as follow:

1. The several metals constituting the orebody are not in fixed proportions and each has a different market price. Under these circumstances, the **monetary value method** is

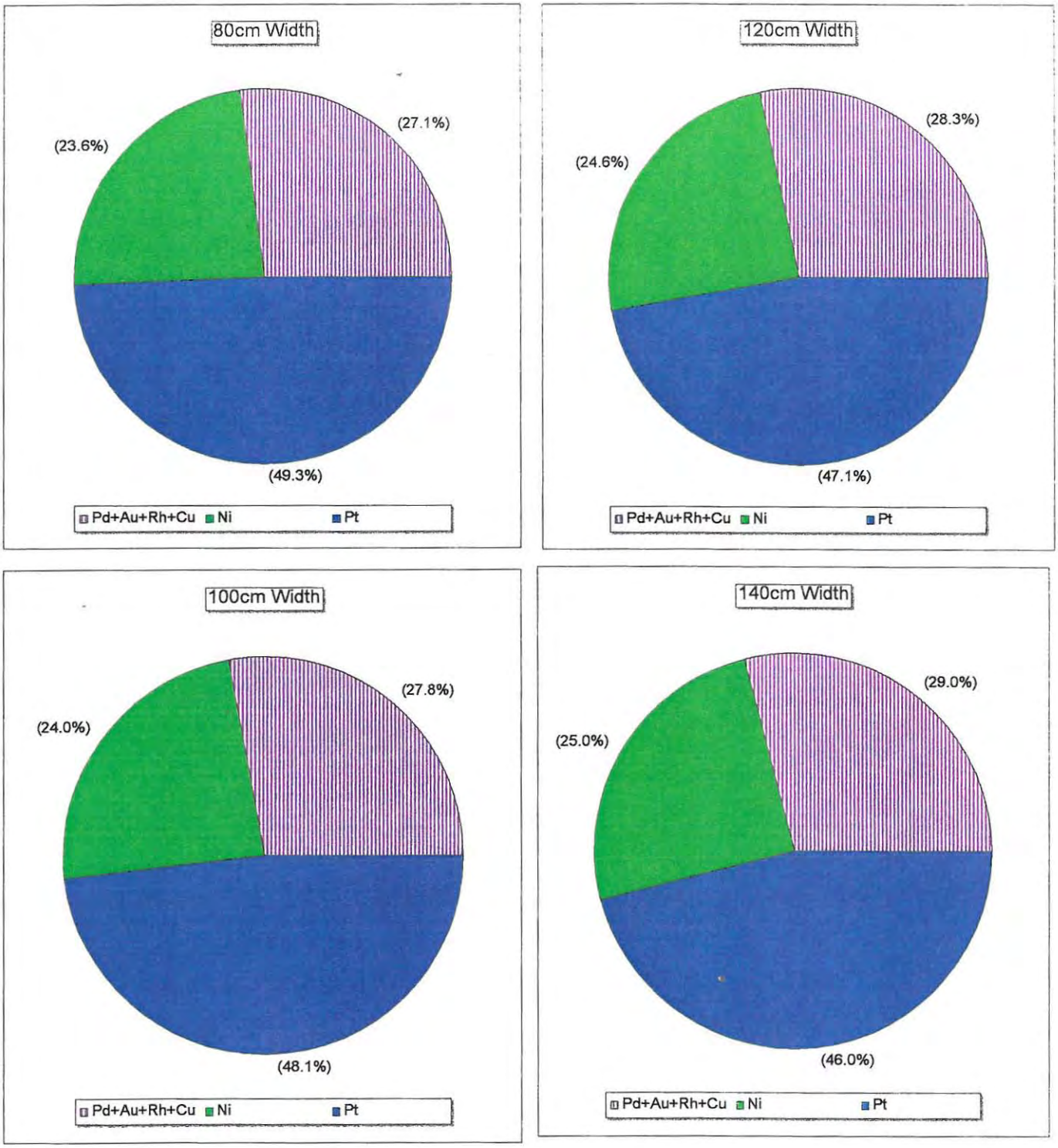

Fig 6.4 UNKI MINE: MSZ metal contributions to revenue at various widths.
(Based on the July 1995 LME prices)

considered the best method that combines the effects of these metals when evaluating the MSZ profile.

2. The grades of the PGE and BM will vary according to the stoping widths adopted. In about 40% of the cases (section 6.1) the peak values of PGE and of BM are not coincident, and a compromise based on observed grade distributions would be needed to optimize stope widths and cut-off grades.

3. The absence of a robust geological marker horizon to enable both the correlation of grade distributions between sampled profiles and the delineation of underground stope limits will render mining and grade control difficult.

4. Based on the facts that Pt and Ni peak values are not consistently in fixed proportions and that Pt is the primary component of the ore (Fig. 6.4), the best zone to be mined will have to be determined on the basis of Pt assay cut-offs. Pd cannot be used as a guide to Pt distribution since, in most cases, its peak value is 20 to 40cm below the Pt peak.

5. The gradual tailing-off of the base metals (Fig. 6.1) upwards implies that any overbreaking of rock in the hanging-wall would contain some metal. Thus, mining close to the assay footwall cut-off is more critical than in the hanging-wall.

6. Mining a restricted narrow high grade zone of the MSZ (say 1m stoping width) will be difficult because this zone, and indeed the MSZ as a whole, rolls along strike and down dip (Fig. 6.2). To define the rolls on stope faces by sampling before mining will be a costly exercise. The closer the sample spacing, the better the definition of the rolls (Fig. 6.2a). However, the phase 2 trial mining completed at Unki in April 1995 demonstrated that a mine call factor of above 80% is achievable under carefully controlled mining conditions.

A large stoping width of say 180 cm, if adopted, would bring the lower limit of the potential mineable section to the level of the base of the Footwall shear. This would obviously make the mining easy with a clear-cut visual guide and, in addition, a significant saving of assay costs would be realized. However, the Footwall shear contains significant quantities of talc which will render extraction of the metals difficult. Furthermore, metal recoveries decrease with decreasing head grades. This, compounded with the talc problem, may render mining to the natural footwall marker an unviable proposition. On the other hand, given adequate metal recovery, mining the wider, lower grade zone would allow greater latitude in positioning development and possible mechanisation for extraction on a large scale.

Chapter 7

ORE DEPOSIT MODEL FOR THE UNKI DEPOSIT

Any model to explain the petrogenetic mechanisms in the PGE-BM rich MSZ must account for the following key features observed in the Unki deposit:

1. Lateral continuity of the MSZ with fairly consistent thickness and host rock lithologies.

2. The occurrence of sulphide particles as inclusions in cumulus pyroxene.

3. The strong association of sulphide with alteration.

4. The occurrence of at least three distinctive vertical metal distributions.

As discussed in section 1.5 (chapter 1) and illustrated in Figure 1.7, there exist several possible mechanisms by which sulphide-hosted PGE mineralization may have originated. The origin of the MSZ at Unki by deposition from Cl-rich volatile fluids is ruled out on the basis of its uniformity and regularity, a fact also previously highlighted by Prendergast (1988b), and Wilson and Tredoux (1990). If hydromagmatic processes were largely responsible (in the formation of the MSZ), their characteristic random nature would culminate in irregular thicknesses of mineralisation and inconsistent stratigraphic relationships between mineralisation and host rocks.

The likely model for the PGE-enriched MSZ cannot be envisaged in the context of magma mixing processes as suggested for the Merensky Reef of the Bushveld (Naldrett et al., 1986) and J-M reef of the Stillwater Complex (Barnes and Naldrett, 1985) for two main reasons, viz: (1) in contrast to the Merensky and J-M reefs, substantial plagioclase crystallization did not occur

prior to the formation of the MSZ (Fig. 1.3), and (2) the sulphides with which the mineralisation is closely associated are concentrated in the upper part of the MSZ with a clear-cut enrichment trend from its base upwards (chapter 3.1). Under these circumstances, it is highly unlikely that magma mixing would play a major role. Instead it would appear that an understanding of the controls on sulphur solubility in silicate melts imparts important genetic clues to the MSZ mineralisation.

Fincham and Richardson (1954) showed that at low oxygen fugacities (less than 10^{-6} atm in melts studied at 1400 and 1500°C) sulphur dissolves primarily as sulphide and that the sulphur capacity (Cs) of the melt is constant for melts of the same composition. The main factors controlling S-solubility in mafic magmas are temperature, and FeO and SiO_2 contents (Campbell, 1977; Irvine, 1975). In some instances, the fugacities of S_2 and O_2 (fS_2 and fO_2) also play an important role (Buchanan and Rouse, 1984). Based on experimental evidence (Buchanan et al., 1983) and theoretical considerations (Irvine, 1975; Moore, pers. comm. 1994), Cs increases with rise in temperature and changes with composition, generally increasing with increasing FeO, MgO and CaO contents and decreasing with increasing SiO_2 and Al_2O_3. Haughton et al., (1974) were able to establish a strong correlation of sulphur content at sulphide saturation point with FeO and to a lesser extent, with TiO_2 contents.

The evidence presented in this study (chapter 5), notably the behaviour of FeO, MgO and CaO contents and that of SiO_2 and Al_2O_3, and the distribution of S within the MSZ, are consistent with a fractionation process. This fractionation leads to an abrupt compositional change of the silicate magma which is attained at the top of the PGE-rich zone and is supported by an abrupt upwards decrease in the Mg# followed by its reversal. This reversal at the top of the PGE-rich zone, reflects changes in magma composition which may be due to either new influxes of magma or convective overturn in the chamber. The reversal

occurs close to the upper limit of the bronzitite, ± 50 cm from the overlying websterite layer. Thereafter, the rapid changes in lithologies from bronzitite to websterite, where clinopyroxene is the dominant cumulus phase, appear to support a resumption of the fractionation process, bearing in mind that the crystallization of clinopyroxene (in the Great Dyke phase system) reflects a lower temperature, i.e. the crystallization order is opx --> cpx --> plag. In summary, the MSZ originated from the progressively cooling fractionating magma. The point of sulphide saturation was aided by decreasing temperature and increasing Fe content due to the fractionation of bronzite. This is consistent with previous studies (Wilson et al., 1989; Prendergast and Keays, 1989).

The presence of magmatic sulphide inclusions in cumulus pyroxenes of the MSZ show that the magma was in a state of progressive sulphide fractionation (Prendergast, 1988b; Coghill and Wilson, 1993) and that sulphur saturation of the magma was achieved at this level. Thus the majority of the sulphides are of cumulus status having formed as an immiscible phase rather than originating from the intercumulus liquid (Keays and Campbell, 1981).

The strong association of sulphide with alteration indicates that late-stage differentiate fluids interacted with the interstitial sulphides. While large-scale remobilization by hydromagmatic processes is ruled out, the reaction of fluids with sulphide certainly resulted in redistribution of the sulphide on a millimetre to centimetre scale as evidenced by the pervasive alteration noted in Figure 4.4. Where sulphides are abundant, the degree of reactivity and hence alteration, would be high. Unlike at Mimosa, where this hydromagmatic fluid activity is restricted to the marginal facies and lacking in the normal MSZ (Prendergast, 1990), the type reference drill hole (MR 126) used in this study is from the 'normal' MSZ in the axial facies.

The distribution of metals within the MSZ profile can be explained in terms of chalcophile metal behaviour which is governed by three main factors (Campbell and Naldrett, 1979; Campbell et al., 1983):

(i) The metals have high partition coefficients (D) and are thus quickly scavenged from the magma upon the formation of sulphide liquid. This explains the strong association of sulphide with PGE. Liquid sulphide acted as a collector for these metals.

(ii) The removal of the metals from the melt is directly related to the magnitudes of their D values. The D values for Ni and Cu in basaltic magma are low (Naldrett, 1981), while those of Pd, Pt and Ir are relatively higher (Naldrett, 1981). Based on these facts and the observed PGE fractionation trends (Barnes et al., 1985), the following order of removal is implied and is consistent with that reported elsewhere for the MSZ in the Great Dyke (Wilson et al., 1989; Prendergast and Keays, 1989).

Ir > Pd > Pt > Ni > Au = Cu.

This order almost perfectly satisfies the condition relating to profiles 1 and 2 (Fig. 6.1). Minor discrepancies and/or inconsistencies are attributable to secondary microscale remobilisation already described above. Profile 3 (Fig. 6.1), however, represents a complex anomalous situation and may be explained in terms of sulphur availability.

Quantitative modelling is currently under way (Wilson and Murahwi, in prep.) to demonstrate the primary origin of these profiles, but its discussion is beyond the scope of the present work.

(iii) The magma/sulphide ratio (R) as previously discussed in section 1.5 (chapter 1), is important in that both the absolute metal contents of the sulphide phase and the ratios of metals with high and low D values in the sulphide phase increase in proportion to R at equilibrium. Where R is low, the Ni contents of the sulphides will be higher than the PGE and will yield typical sulphide ores corresponding to those of the Sudbury deposit. Such a condition may not have been impossible on a localized scale during the formation of the MSZ and may have given rise to the scenario depicted in Fig. 6.1, profile 3. Where R is high, PGE concentration will be much higher and in the range of that characterising the Merensky Reef.

CHAPTER 8

SUMMARY, CONCLUSIONS AND RECOMMENDATIONS

8.1 Summary

Generalities

The MSZ in the Selukwe Subchamber is broadly similar to that of the Wedza, Sebakwe and Darwendale Subchambers. Thus, despite these subdivisions into chambers/subchambers, the primary mineralizing events throughout the Great Dyke were basically the same. However, in detail, the mineralization, lithologies, position and petrological characteristics differ between subchambers and in some cases, are variable even within the same subchamber, notably Darwendale. These variations are attributed to the differences in the thermal regimes and the resultant fluid dynamics within the subchambers. For instance, in the narrow subchambers (Wedza and Selukwe), the heat loss in the axis and margins was about the same thereby restricting major variations while in the wider subchambers (Sebakwe and Darwendale), the effect of heat loss was more pronounced along the margins than in the axis (Wilson and Prendergast, 1989).

MSZ Assay Profiles throughout the Great Dyke

The assay profiles of the MSZ at Unki consist of three types (Figure 6.1) which occur randomly throughout the Selukwe subchamber but with profile 2 dominating. The axial and marginal facies exhibit the same characteristics in terms of the MSZ thickness and grade. In the Wedza Subchamber, the typical assay profile of the MSZ consists of two sharply defined main subzones similar to the Unki profile 2 (Figure 6.1) (Prendergast 1988a).

At Hartley Prospect (Darwendale Subchamber), the dominant assay profile on the western marginal facies corresponds to the Unki profile 2 but major variations in both the MSZ thickness and grade have been observed between the axis and the margins (Wilson and Prendergast, 1989).

In all subchambers, the MSZ has been affected by later hydrous processes, regarded as late-stage magmatic (hydromagmatic) in origin. Alteration is likely to be most intense near the margins where primary textures are often completely replaced by an intergrown assemblage of sulphides, hydrosilicates, quartz, carbonate and chrome spinel, together with remnant pyroxene and plagioclase (Prendergast, 1990; Wilson and Tredoux, 1990). These variations in alteration are attributed to differences in the temperature regimes. In the axis, the temperatures were higher and compaction greater than along the margins where heat loss was faster. This resulted in -

(i) less interstitial fluids in the axis than along the margins
(ii) the lower temperatures in the margins exsolving sulphur to give more sulphidic liquids and hence, more marked alteration
(iii) greater compaction of silicate cumulates in the axial zones leading to expulsion of sulphide.

Large, norite-filled depressions interpreted as linear erosional 'washout channels' (Prendergast, 1990) which locally interrupt the MSZ towards the margins have only so far been found at Mimosa (Wedza Subchamber) and in the Darwendale area (Wilson et al., 1989).

Applicability of existing models to MSZ assay profiles

Based on the majority of the MSZ metal profiles observed at Unki, the current models on the formation of the MSZ (Prendergast, 1988b; Wilson and Tredoux, 1990; Coghill and Wilson, 1993) adequately account for the mineralization. The inconsistencies observed in the metal profiles (Figure 6.1) are indicative of

delicate conditions of adjustment in chemical and physical factors that must have prevailed during the formation of the MSZ and of how these conditions differed locally in the same magma chamber.

The strong association of PGE with sulphides in the MSZ appears to hold important genetic clues, specifically that liquid sulphide acted as a collector for these metals in a convecting magma chamber. The R factor thus appears to have played a major role in concentrating PGE. The mechanisms responsible for the attainment of a high equilibrium R value are turbulent mixing and convection. These two factors permit sulphide droplets to equilibrate with a large volume of silicate liquid (Campbell et al., 1983). There is however no evidence of magma replenishment at the base of the MSZ. This implies that all the S and chalcophile metals were derived from the hybrid magma as first noted by Prendergast (1988b).

The batch segregation model as has been proposed for the Merensky Reef (Campbell et al, 1983; Barnes et al, 1985) is not supported by the form of the vertical profiles for the PGE in the MSZ. The general trend in the order of metal enrichment of the MSZ from the base upwards is Ir > Pd > Pt > Ni > Au = Cu and implies evolution within a system of liquid layers controlled by double-diffusive processes (Prendergast, 1988b). This order of metal enrichment is enhanced if the sulphides also liquated at the floor with the chalcophile metals being removed from the overlying convecting magma in the order of their D values. The double-diffusive processes encompass in situ sulphide liquation, Rayleigh fractionation, and rapid convection within the basal liquid layer, thereby attaining a high R value. Thus, the high R value necessary for PGE enrichment was attained without the injection of new magma.

The factors which may account for the different patterns of metal profiles observed at Unki are (a) variable R values, (b) the rate of convection, (c) variations in magma metal contents, and (d)

partition coefficients coupled with the complex behaviour of chalcophile elements. In the latter case, it must be noted that PGE have different chemical properties compared with Ni and Cu which are strongly chalcophile in character. On this basis, it is quite possible that the mechanism by which the PGE are incorporated into liquid sulphide may be markedly different from that of the base metals (Wilson and Tredoux, 1990). Initially the PGE may form metallic clusters which stabilize by surface adsorption of elements such as S, As, Sb, and Te, thereby becoming activated for incorporation into sulphide melt (Lindsay, 1988). D PGE vary with changes in the fO_2/fS_2 ratio of the magma (Naldrett et al., 1986).

For the base metals, decreasing temperature and/or decreasing MgO content increases D Cu and D Ni, respectively (Rajamani and Naldrett, 1978; Campbell et al., 1979). Thus a multi-model process which takes into account the fluid dynamics of the magma system must be viewed as being responsible for the MSZ profiles observed at Unki (Wilson, pers. comm., 1995).

8.2 Conclusions

The specific conclusions pertaining to future mining operations as controlled by the geological characteristics of the Selukwe Subchamber, particularly Unki, are:

1. The sulphide concentration within the MSZ can be used as a rough guide to the PGE-rich zone, but is not sufficiently precise to be used in stope control.

2. The stopes, and the grade, will need to be controlled by assay cut-off, using Pt. Mining close to the assay footwall cut-off will be more critical than in the hanging-wall.

3. The Footwall Shear offers the only reliable means of determining the position of the PGE-rich zone. Other than this, an ore zone marker that is of general application for the miners to follow, remains elusive at present.

4. Evidence for potholes or washout channels is lacking in the MSZ at Unki.

5. The MSZ at Unki is affected by faults and joints but the throw of the majority of these is small, and contour diagrams based on 76 drill holes show no significant dislocations.

6. The MSZ is persistent and consistent throughout Unki, but in places it contains xenoliths of barren rocks. These are however, believed to be small and are most common in the western margins of the Unki area. However, while the deposit may be assumed to be laterally continuous, the dolerite dyke area (Fig.3.2) is likely to have a disrupted MSZ.

7. The success of extracting the best economic zone will depend on the ability to (a) control dilution from the footwall shear, and (b) contend with the undulations. Day-to-day grade control will have to rely on carefully controlled mining operations including strict and frequent face sampling for Pt assays, and on accurate survey control. Dilution and visual markers to the ore zone remain the critical problems to successful mining.

The following broad conclusions which may be of general application throughout the Great Dyke MSZ are made:

1. Petrological evidence suggests an orthomagmatic origin for the MSZ at Unki. This is consistent with previous findings as noted in chapter 7.

2. The PGE enrichment of the MSZ is due to fractionation processes involving double-diffusive convection rather than mixing of parental and resident magmas.

3. The termination of the PGE-rich MSZ within bronzitite was due to an increase in temperature probably associated with an influx of new magma.

8.3 Recommendations

The following recommendations are made:

1. The magnitude of the difference in alteration between the marginal and axial facies needs to be ascertained. Intense alteration will render the flotation of the ore difficult due to the high talc content.

2. Mine design must take into account the longitudinal variation in the attitude of the MSZ (Fig. 6.4). The question of whether this broad synclinal structure represents a feeder system at depth can only be resolved by extensive deep drilling in the axial region.

3. To achieve the optimum economic production rate, development must always move well ahead of production as the mining will have to rely on Pt assay cut-offs.

References

Anastasiou, P. and Seigent, F., 1972. Solid solubility of Al_2O_3 in enstatite at high temperature and 1 - 5 lab water pressure. Contrib. Mineral. Petrol., **34**, 272-287.

Barnes, S.J. and Naldrett, A.J. 1985. Geochemistry of the J-M (Howland) Reef of the Stillwater Complex, Minneapolis Adit area. I. Sulphide chemistry and sulphide - olivine equilibrium. Econ. Geol. **80**, 627 - 45.

Barnes, S.J., McIntyre, J.R., Nisbet, B.W., and Williams, C.R., 1990. Platinum Group Element Mineralisation in the Munni Munni Complex, Western Australia. Contrib. Mineral. Petrol., **42**, 141 - 64.

Bichan, R., 1969. Origin of chromite seams in the Hartley Complex of the Great Dyke. In Magmatic ore deposits, Wilson H.D.B.ed., Econ. Geol. Monogr., **4**, 95 -113.

Boshoff, F., 1993. Applied Mineralogical research on PGM and sulphide deposits. Anglo American Research Laboratories (Pty) Ltd - Confidential internal report. 20p.

Bowen, D.J., 1994. Platinum Exploration on the Great Dyke of Zimbabwe. Explor. Mining.Geol., Vol.3, No.4, 329-335.

Brown, G.C., Hawkesworth, C.J. and Wilson, R.C.L., 1992. Eds. Understanding the Earth. Cambridge University Press, New York. 551p.

Buchanan, D.L., 1979. Platinum Group metal production from the Bushveld Complex and its relationship to world markets. Bureau for Minerals Studies Report, University of the Witwatersrand, Johannesburg, 4, 31p.

Buchanan, D.L., 1988. Platinum - Group Element Exploration. Elsevier, Amsterdam, 21 - 35.

Buchanan, D.L., Nolan, J., Wilkinson, N., and de Villiers, J.P.R.,1983. An experimental investigation of sulphur solubility as a function of temperature in synthetic silicate melts. In ICAM'81 : Proceedings of the First International conference on Applied Mineralogy, Johannesburg, 1981., de Villiers, J.R.P.R. and Cawthorn P.A., eds., Spec. Publ. geol. Soc. S. Afr., 7, 383-391.

Buchanan, D.L. and Rouse, J.E., 1984. Role of contamination in the precipitation of sulphides in the Platreef of the Bushveld Complex. In Sulphide deposits in mafic and ultramafic rocks, Buchanan, D.L. and Jones, M.J., eds., The Institution of Mining and Metallurgy, London, 141-146.

Campbell, I.H., 1977. A Study of macro-rhythmic layering and cumulate processes in the Jimberlana Intrusion, Western Australia. Part 1: The upper Layered Series. J. Petrol., **18**, 183-215.

Campbell, I.H., McCall, G.J.H., and Tyrwhitt, D.S., 1970. The Jimberlana Norite, Western Australia - a smaller analogue of the Great Dyke of Rhodesia. Geol. Mag. **107**, 1-12.

Campbell, I.H., Naldrett, A.J., 1979. The influence of silicate:sulphide ratio on the geochemistry of magmatic sulphides. Econ. Geol., **76**, 1503-1506.

Campbell, I.H., Naldrett, A.J., and Barnes, S.J., 1983. A model for the origin of the platinum-rich sulphide horizons in the Bushveld and Stillwater Complexes. J. Petrol., **24**, 133-165.

Campbell, I.H., Naldrett, A.J. and Roeder, P.L., 1979. Nickel activity in silicate liquids: some preliminary results. Canadian Mineralogist, **17**, 495-506.

Campbell, I.H. and Turner, J.S., 1986. The influence of viscosity on fountains in magma chambers. J. Petrol., **27** 1-30.

Coghill, B.M. and Wilson, A.H. 1993. Platinum-group minerals in the Selukwe Subchamber, Great Dyke, Zimbabwe: implications for P.G.E. collection mechanisms and post-formational redistribution. Mineralogical Magazine **57**, 613-633.

Collender, F.D., 1986. Platinum - one of the world's most strategic metals. Trans. Instn. Min. Metall. (Sect. A.: Min. industry.), **96**, A104-A108.

Cowley, A., 1994. Platinum 1994. Johnson Matthey Ltd, London. 52p.

Cowley, A., 1995. Platinum 1995. Johnson Matthey Ltd, London. 52p.

Daltry, V.D.C. and Wilson, A.H. (in prep). Platinum - Group Mineralogy Review: I General trends and the inter PG-element chemistry of the PG-minerals and unidentified PG-phases.

Evans, D.M. and Buchanan, D.L., 1991. Application of petrographic studies to MSZ platinum-group element and base-metal mineralisation at Zinc prospect, Great Dyke, Zimbabwe. Trans. Instn. Min. Metall. (Sect. B: Appl.earth sci.), **100**, B216-26.

Fincham, C.J.B. and Richardson, F.D., 1954. The behaviour of sulphur in silicate and aluminate melts: Proc. Roy. Soc., **A223**, 40-62.

Hamilton, J., 1977. Sr isotope and trace element studies on the Great Dyke and Bushveld mafic phase and their relation to early Proterozoic magma genesis in Southern Africa . J. Petrol., **18**, 244-52.

Haughton, D.R., Roeder, P.L. and Skinner, B.J., 1974. Solubity of sulphur in mafic magmas. Econ. Geol., **69**, 451-467.

Hess, H.H., 1950. Vertical mineral variation in the Great Dyke of Southern Rhodesia. Trans. Geol. Soc. S. Afr., 53, 159-168.

Hughes, C.J., 1970. Major rhythmic layering in the ultramafic rocks of the Great Dyke of Rhodesia, with particular reference to the Sebakwe area. Geol. Soc. S. Afr. Spec. Publ., 1, 594-609.

Huppert, H.E. and Sparks, R.S., 1980. The fluid dynamics of a basaltic magma chamber replenished by influx of hot, dense, ultrabasic magma. Contr. Miner. Petrol., 75, 279-289.

Irvine, T.N., 1975. Crystallisation sequences in the Muskox Intrusion and other layered intrusions. II. Origin of chromite layers and similar deposits of other magmatic ores. Geochim. Cosmochim. Acta, 39, 991 - 1020.

Irvine, T.N., 1977. Origin of the chromite layers in the Muskox Intrusion and other stratiform intrusions: a new interpretation. Geology, 5, 273-277.

Irvine, T.N., 1979. Rocks whose composition is determined by crystal accumulation and sorting. In The evolution of the igneous rocks, Yoder, H.S., ed., Princeton, 245-306.

Jackson, E.D., 1961. Primary textures and mineral associations in the Ultramafic Zone of the Stillwater Complex, Montana. U.S. Geol. Surv. Prof. Paper., 358, 106p.

Jackson, E.D., 1970. The cyclic unit in layered intrusions - a comparison of repetitive stratigraphy in the ultramafic parts of the Stillwater, Muskox, Great Dyke, and Bushveld Complexes. Geol. Soc. S. Afr. Spec. Publ., 1, 391-424.

Keays, R.R. and Campbell, I.H., 1981. Precious metals in the Jimberlana Intrusion, Western Australia: Implications for the genesis of platiniferous ores in layered intrusions. Econ. Geol., 76, 1118-1141.

Kushiro, I., 1960. Si-Al relation in clinopyroxene from igneous rocks. AM. J. Sci., 258, 548-554.

Lightfoot, B., 1926. Platinum in Southern Rhodesia. S Rhod. Geol. Surv. Short Report, 19, 13p.

Lightfoot, B., 1927. Traverses along the Great Dyke of Southern Rhodesia. S. Rhod. Geol. Surv. Short Report, 21.

Lindsay, N.M., 1988. The processing and recovery of the platinum - group elements. Unpub. D. Phil. Thesis. University of the Witwatersrand, Johannesburg.

Macdonald, A.J.1987. Ore Deposit Models#12.The Platinum Group Element Deposits:classification and genesis Geoscience Canada, 14, 155-166.

Macdonald, A.J., 1988. Platinum -group element mineralisation and the relative importance of magmatic and deuteric processes: Field evidence from Lac des Iles deposit, Ontario, Canada. In Geo - Platinum '87, Prichard, H.M., Potts, P.J., Bowles, J.F.W., and Cribb, S.J. eds., Elsevier Applied Science, Barking, Essex, 215-236.

Morimoto, N., 1988. Nomenclature of pyroxenes. Amer. Mineral., 73, 1123-1133.

Morrison, E.R., 1974. Exclusive Prospecting Orders Nos. 1-250. Rhod. Geol. Surv. Bull., 72, 254p.

Naldrett, A.J.,1981. Platinum-group element deposits. In Platinum Group Elements: Mineralogy, Geology, Geochemistry. Cabri, L.C., ed., Can. Inst. Min. Met., Special Vol. 23, 197-232.

Naldrett, A.J., 1989. Magmatic Sulphide Deposits. Oxford University Press, Oxford, New York, 196p.

Naldrett, A.J., 1993. Magmatic Ni-Cu and PGE deposits: Short course notes, University of Zimbabwe, 1993. Geology Dept.

Naldrett, A.J., Brugmann, G.E., and Wilson, A.H., 1990. Models for the concentration of PGE in layered intrusions. Can. Mineral., **28**, 239-408.

Naldrett, A.J., Cameron, G., von Gruenewaldt, G. and Sharpe, M.R., 1987. The formation of stratiform PGE deposits in layered intrusions. In Origins of igneous layering, Parsons, I., ed., D.Reidel Publishing Company, Dordrecht, 313-398.

Naldrett, A.J., Gasparrini, E.C., Barnes, S.J., von Gruenewaldt, G. and Sharpe, M.R., 1986. The Upper Critical Zone of the Bushveld Complex and origin of Merensky-type ores. Econ. Geol., **81**, 1105-1117.

Page, N.J. Zientek, M.L., Czamanske, G.K., and Foose, M.P., 1985. Sulphide mineralisation in the Stillwater Complex and underlying rocks. In Stillwater Complex, Czamanske, G.K., and Zientek, M.L. eds. Montana Bureau of mines and Geology, Spec. Pub., **92**, 93-96.

Podmore, F. and Wilson, A.H., 1987. A reappraisal of the structure, geology and emplacement of the Great Dyke, Zimbabwe. In mafic Dyke Swarms, Halls, H.C. and Fahrig, W.F.,eds., Spec. Pap. Geol. Ass. Can., **34**, 433-444.

Prendergast, M.D. 1988a. The geology and economic potential of the PGE-rich Main Sulphide Zone of the Great Dyke, Zimbabwe. In Geo - Platinum '87. Prichard, H.M., Potts, P.J., Bowles, J.F.W., and Cribb, S.J., eds., Elsevier Applied Science, Barking, Essex, 281-302.

Prendergast, M.D., 1988b. An investigation of the stratigraphy and petrology of the Pyroxenite No. 1 layer in the Wedza Subchamber of the Great Dyke, Zimbabwe, with special reference to the characteristic features and origin of the Platinum - Group Element - bearing Main Sulphide Zone. Unpub. D. Phil. Thesis. Dept. of Geology, University of Zimbabwe.

Prendergast, M.D., 1990. Platinum - group minerals and hydrosilicate 'alteration' in Wedza-Mimosa Platinum Deposit, Great Dyke, Zimbabwe - genetic and metallurgical implications. Trans. - Inst. Min. Metall. (Sect. B: Appl. earth sci.), 99, B91-105.

Prendergast, M.D. and Keays, R., 1989. Controls of platinum - group element mineralization and the origin of the PGE-rich Main Sulphide Zone in the Wedza Subchamber of the Great Dyke, Zimbabwe: implications for the genesis of, and exploration for, stratiform PGE mineralization in layered intrusions. In Magmatic Sulphides - The Zimbabwe Volume, Prendergast M.D. and Jones, M.J., eds. The Inst. of Min. Met., London, 43-69.

Prendergast, M.D. and Wilson, A.H.1989. The Great Dyke of Zimbabwe - II: Mineralization and mineral deposits. In Magmatic Sulphides - The Zimbabwe Volume, Prendergast M.D. and Jones, M.J. eds. The Inst. of Min. Met., London, 21-42.

Rajamani, V. and Naldrett, A.J., 1978. Partitioning of Fe, Co, Ni and Cu between sulphide liquid and basaltic melts and the composition of Ni-Cu sulphide deposits. Econ. Geol., 73, 83-93.

Roeder, P.L. and Campbell, I.H., 1987. The effect of postcumulus reactions on composition of chrome - spinels from the Jimberlana Intrusion. J. Petrol., 26, 763 - 786.

Slatter, D.De L., 1980. The composition of Zimbabwean chromium ores and the derivation of chemical and physio-chemical ratings for smelting the ores to high-carbon ferrochromium. Institution of Mining Research Report, University of Zimbabwe, C193.

Slatter, D. De L., 1981. Chromium resources of Zimbabwe. Rep. Inst. Min. Res. Zimbabwe, 36, 1981, 17p.

Sparks, R.S.J. and Huppert, H.E. 1984. Density changes during the fractional crystallization of basaltic magmas: fluid dynamic implications. Contrib Mineral. Petrol. 85, 300-309.

Stowe, C.W., 1980. Wrench tectonics in the Archaean Rhodesian craton. Trans. Geol. Soc. S. Afr., 83, 193-205

Thompson, R.N., 1974. Some high pressure pyroxenes. Mineral. Mag., 39, 768-787.

Turner, J.S., and Campbell, I.H., 1986. Convection and mixing in magma chambers. Earth - Sci. Rev. 23, 255-352.

Vermark, C.F., 1976. The Merensky reef - thoughts on its environment and genesis. Econ. Geol., 71 1270-1298.

Wagner, P. A., 1929. Platinum deposit and mines of South Africa. C Struik (Pty) Ltd., Cape Town.

Wilson, A.H., 1976. The petrology and structure of the Hartley Complex of the Great Dyke, Rhodesia. PhD Thesis, University of Rhodesia.

Wilson, A.H., 1982. The geology of the Great Dyke, Zimbabwe the ultramafic rocks. J.Petrol., 23, 240-292.

Wilson, A.H., 1992. The geology of the Great Dyke, Zimbabwe: crystallization, layering, and cumulate formation in the P1 pyroxenite of Cyclic Unit 1 of the Darwendale Subchamber. J Petrol., 33, 611-663.

Wilson, A.H., 1992. Petrographic, compositional and chemical assessment of the xenolith suite in the Unki Area of the Great Dyke. AAC Zimbabwe, unpublished internal report, 7p.

Wilson, A.H., Naldrett, A.J. and Tredoux, M., 1989. Distribution and controls of platinum group element and base element mineralization in the Darwendale Subchamber of the Great Dyke, Zimbabwe. Geology, 17, 649-652.

Wilson, A.H. and Prendergast, M.D., 1989. The Great Dyke of Zimbabwe. I: Tectonic setting, stratigraphy, petrology, structure, emplacement and crystallisation. In Magmatic Sulphides - The Zimbabwe Volume, Prendergast M.D.and Jones, M.J., eds., The Institution of Mining and Metallurgy, London, 1-20.

Wilson, A.H. and Tredoux, M., 1990. Lateral and vertical distribution of platinum-group elements and petrogenetic controls on the sulphide mineralisation in the P1 pyroxenite layer of the Darwendale Subchamber of the Great Dyke, Zimbabwe. Econ. Geol. 85, 556-584.

Wilson, A.H. and Wilson, J.F., 1981. The Great 'Dyke'. In: Precambrian of the Southern Hemisphere, Hunter, D.R., ed., Amsterdam: Elsevier, 572-8.

Wilson, J.F., Jones, D. and Kramers, J.D. 1987. Mafic dyke swarms in Zimbabwe. In Mafic dyke swarms Halls, H.C. and Fahrig, W.E., eds., Spec.Pap. Geol. Ass. Can., 34, 433-444.

Streckeisen, A.L., 1973. Classification and nomenclature recommended by the IUGS subcommission in the systematics of igneous rocks. Geotimes, 18, 26-30.

Worst, B.G., 1958. The differentiation and structure of the Great Dyke of Southern Rhodesia. Tans. Geol. Soc. S. Afr. 61, 283-354.

Worst, B.G., 1960. The Great Dyke of Southern Rhodesia Bull. Geol. Surv. S. Rhodesia, 47, 234p.

Zeally, A.E.V., 1918. The occurrence of platinum in Southern Rhodesia. S. Rhod. Geol. Surv. Short Report, 3.

APPENDICES

Appendix 1: Modal analyses

A Swift Model F point counter was used for point counting on a 0,5 x 0,3 mm grid. A total of 1500 mineral counts were done per specimen.

Appendix 2: Mineralogical techniques

Polished thin sections of the ore samples were prepared in the normal fashion, carbon coated and examined using the scanning electron microscope (SEM). The Robinson detector (back scattered electron detector) was used at 30 kV with conditions of maximum aperture, zero brightness and variable contrast. Using a magnification of 100X and a detector-sample distance of 20 mm, the whole of the polished section was scanned for PGM. The high atomic number particles appear as bright white dots which can easily be identified and viewed in more detail. After identification of an individual PGM, they are individually measured, analysed qualitatively for the elements present and the mineralogical associations noted.

The SEM technique is preferable to optical microscope techniques as the grains are often very small and difficult to positively identify in incident light.

Appendix 3: Electron microprobe analyses

All analyses were performed with a CAMECA electron microprobe at 20 kV and 20 nA. The beam diameter was fixed at 10 μm. Major and trace element concentrations were determined using the Ka-lines. Counting time for each element was 20 seconds on the peak and 10 seconds for background. Analytical parameters and statistical errors are listed in Table A.3.

Table A.3: Analytical parameters and statistical errors as calculated from 90 duplicate analyses carried out on two orthopyroxene grains.

ELEMENT	CRYSTAL	STANDARD	LLD	RANGE	AVG	STD	C
Si	TAP	quartz	nd	53.47-55.33	54.70	0.274	0.501
Al	TAP	Al_2O_3	nd	0.69- 1.11	0.91	0.047	5.165
Mg	TAP	MgO	nd	27.11-28.80	28.01	0.151	0.539
Ti	PET	TiO_2	450	0.13- 0.94	0.23	0.019	8.284
Ca	PET	Woll	590	0.62- 2.20	1.03	0.039	3.812
Fe	LIF	nat.Fe_2O_3	nd	13.96-16.47	15.16	0.275	1.512
Mn	LIF	MnO	270	0.22- 0.34	0.28	0.033	12.052
Cr	LIF	Cr_2O_3	370	0.29- 0.55	0.38	0.035	9.349
Na	TAP	omphacite	240	0.00- 0.05	0.02	0.013	75.870
Ni	LIF	NiO	300	0.03- 0.07	0.05	0.009	19.164
Mg#	100*(Mg/(Mg+Fe))			75.03-78.10	76.71	0.297	0.388

N.B. woll = wollastonite

Appendix 4: XRF analyses

A PW 1404 X-ray fluorescence spectrometer was used for the determination of major and trace elements. Analyses were performed on pressed powder pellets. All the analyses were carried out using a Rhodium tube energised at 50 kV and 50 mA with the Vacuum ON.

Running conditions and instrumental settings are listed in Table A.2 together with the detection limits (ppm) of trace elements.

Table A.2: Instrumental setting for major and trace elements analyses

Element	Line	Crystal	Counter	Count Time	Detection Limit (ppm)
Si	Ka	PET	FC*	20 sec	-
Ti	Ka	LiF 200	FC	20 "	-
Al	Ka	PET	FC	20 "	-
Fe	Ka	LiF 200	FC	10 "	-
Mn	Ka	LiF 200	FC	10 "	-
Mg	Ka	PX-1	FC	10 "	-
Ca	Ka	LiF 200	FC	20 sec	-
Na	Ka	OH-1	FC	10 "	-
K	Ka	LiF 200	FC	15 "	-
P	Ka	Ge 111	FC	20 "	-
Zn	Ka	LiF 200	SC+	100 "	4
Cu	Ka	LiF 200	SC	100 "	5
Ni	Ka	LiF 200	FC	100 "	4
Co	Ka	LiF 200	FC	100 "	5
Ga	Ka	LiF 200	SC	100 "	5
Zr	Ka	LiF 200	SC	100 "	3
Y	Ka	LiF 200	SC	100 "	3
Sr	Ka	LiF 200	SC	100 "	2
Rb	Ka	LiF 200	SC	100 "	2
Pb	Lb	LiF 200	SC	100 "	5
Cr	Ka	LiF 200	FC	100 "	12
V	Ka	LiF 200	FC	100 "	10
Ba	La	LiF 200	FC	100 "	15
Sc	Ka	LiF 200	FC	100 "	8

* = Flow counter

\+ = Scintillometer

Appendix 5: Analytical Methods

1) Gold, Platinum and Palladium were determined by inductively coupled plasma emission spectrometric measurement of the prill after cupellation, using Silver as a co-collector.

2) Rhodium was determined as in note 1, but with Palladium as the co-collector.

3) Copper and Nickel were determined by Atomic Absorption spectrometry after acid digestion of the samples.

4) Reported results are the arithmetic mean of duplicate analysis.